ELECTROMAGNETIC CONTAINERLESS PROCESSING REQUIREMENTS AND RECOMMENDED FACILITY CONCEPT AND CAPABILITIES FOR SPACE LAB

FINAL REPORT

13 MAY 1974

Contract No. NAS8-29680

Prepared for

NATIONAL AERONAUTICS AND SPACE ADMINISTRATION
Process Engineering Laboratory
George C. Marshall Space Flight Center

SPACE SCIENCES LABORATORY
GENERAL ELECTRIC
SPACE DIVISION

ELECTROMAGNETIC CONTAINERLESS PROCESSING REQUIREMENTS AND RECOMMENDED FACILITY CONCEPT AND CAPABILITIES FOR SPACE LAB

FINAL REPORT

13 May 1974

Contract No. NAS8-29680

Prepared for

NATIONAL AERONAUTICS AND SPACE ADMINISTRATION
Process Engineering Laboratory
George C. Marshall Space Flight Center

Prepared by

R. T. Frost, Manager
Earth-Orbit Applications Programs

H. L. Bloom
L. J. Napaluch
E. H. Stockhoff
G. Wouch

GENERAL ELECTRIC COMPANY
Space Sciences Laboratory
P.O. Box 8555
Philadelphia, Pennsylvania 19101

TABLE OF CONTENTS

TABLE OF CONTENTS (Cont'd)

TABLE OF CONTENTS (Cont'd)

LIST OF ILLUSTRATIONS

LIST OF ILLUSTRATIONS (Cont'd)

LIST OF ILLUSTRATIONS (Cont'd)

LIST OF TABLES

ABSTRACT

Containerless melting, reaction and solidification experiments and processes which potentially can lead to new understanding of material science and production of new or improved materials in the weightless space environment are reviewed. Most of the experiments and processes discussed are amenable to the employment of electromagnetic position control and electromagnetic induction or electron beam heating and melting. The spectrum of relevant properties of materials, which determine requirements for a Space Laboratory Electromagnetic Containerless Processing Facility are reviewed. Appropriate distributions and associated coil structures are analyzed and compared on the basis of efficiency, for providing the functions of position sensing, control, and induction heating. Several coil systems are found capable of providing these functions. The simplest configurations to implement for the earliest Space Lab facility are the "baseball" and the "cusp" coils, the former being preferred with induction heating and the latter whenever electron beam heating is employed. Exchangeable modular coils of both types in appropriate sizes are recommended to achieve the maximum power efficiencies, for a wide range of specimen sizes and resistivities, in order to conserve total facility power. Total facility input powers of five kilowatts with short peak demand loads several times higher provided by storage batteries would provide capability for nearly all of the experiments and processes presently identified as potential candidates for implementation on the Space Laboratory.

SECTION 1
SUMMARY

A wide range of important materials science experiments and materials processes which depend upon melting, reaction or resolidification in the freely levitated state has been identified. These materials range from alloy systems of relatively good electrical conductivity to glasses of electrical resistivities when preheated on the order of one ohm centimeter. For these materials, application of positioning forces by means of electromagnetic fields in a Containerless Processing Facility is practical with present day technology. Ground based studies and theory indicate promising possibilities for formation of new phases and crystal structures through elimination of gravity and the influence of crucible walls. Within the resistivity range considered many promising possibilities for new types of containerless melting and solidification experiments are included. Among these are the formation of amorphous metals and semiconductors by exploitation of the undercooling made possible by containerless solidification, formation and purification of refractory metals and oxides, free of the influence of crucible contamination, formation of immiscible alloys, cermets and transition metal carbides and nitrides of high purity which are difficult to prepare by powder metallurgy.

Because the range of physical parameters of the materials, which can be processed free of the influence of containers is extremely large compared to the experience encountered with terrestrial levitation experiments, it is inappropriate to utilize, without major change, the electromagnetic levitation techniques developed over the past decades in terrestrial laboratories. The material property to which the containerless facility's physical specifications are most sensitive is the levitated specimen electrical resistivity below and at temperatures just below the molten state. This parameter has a major effect upon the specification of an optimum frequency for the electromagnetic fields used for specimen position control and eddy current heating. The efficiency for achieving required

positioning forces and induction heating of the specimen depends sensitively upon specimen resistivity and size, both of which can be considered to vary over a much greater range than can be considered in terrestrial levitation experiments. Since available electrical power in the Space Laboratory will be limited, much attention is given in the present study to optimization of facility power efficiency. It is considered inappropriate to executive Space Laboratory experiments at high power with the very poor efficiencies which are normally tolerated in terrestrial levitation experiments for small specimen samples.

In previous contract studies, several types of electromagnetic field coil systems were considered for use in a Containerless Processing Facility, each having certain engineering advantages and disadvantages. In the present study a general comparison has been made of what is believed to be all reasonable candidate coil configurations. Existing magnetic field computer programs were utilized for some of the configurations which had been previously studied in the General Electric Research and Development Laboratory. In most cases, new magnetic field computer routines were written to permit optimization of the coil winding configuration, with respect to the positioning and heating application considered herein. After optimizing each specific coil type with respect to efficacy for electromagnetic position control and eddy current heating for spherical electrically conducting specimens, a comparison was made amongst the optima so found within each coil "family." This intercomparison was made on the basis of a number of engineering criteria in addition to the achievement of high force and heating per unit power. The result of this selection is the recommendation of alternatively a "baseball" or "cusp" coil for the basic positioning function in conjunction with an orthogonally wound circular coil for specimen rotation.

The cusp coil is preferred for use with electron beam heating because of its greater "stiffness" for specimen displacements. Measurements have been made to compare eddy current heating efficiencies for both preferred coils. The induction heating efficiency is greater for the baseball when the ratio of specimen diameter to coil diameter becomes small. Since a versatile Space Laboratory

facility will require both types of heating in order to be compatible with the widest possible range of materials and since both coils are compatible with the same type of RF power amplifier and servo equipment, it is recommended that the coils be modularly replaceable elements in the facility. The requirement for easily exchangeable modular coils is indicated, in any event, by the requirement for changing coil size when significant changes in specimen size are made so as to maintain reasonable power efficiencies within the facility.

Because most of the materials process examples which have been identified are included within a range extending six decades in resistivity above that of good conductors, coil power frequencies ranging over about three decades, from 0.01 to 10 or 15 mHz will be required. Continuous frequency variation over this range is not required. Rather, one octave steps will be sufficient, leading to power amplifier requirements similar to the band switching techniques used in commercial radio transmitter gear which can, in a single unit, typically cover five or six octaves of frequency at power levels of 1 kw and above. Tuning within such bands is not required in an electromagnetic Containerless Processing Facility.

For early Space Lab applications, available power will be the principal limitation to the variety of materials which can be processed in quantities larger than experimental samples. The maximum sample diameters, for reasonable assumed Space Laboratory facility power, extend from 16 cm for the lower melting materials such as glasses and many alloy systems, to about 2 cm for the highest melting materials such as tungsten. For later manufacturing facilities, however, the system can be scaled up to commercial quantities if adapted to the use of solar heating at the focus of a large reflector.

SECTION 2
INTRODUCTION

During the late 1960's a number of conversations were held between representatives of industry and NASA officials regarding the possibilities for exploiting the weightless environment of space to carry out new types of materials processing experiments which could lead to new materials and products. Perhaps the most obvious of the suggestions was to utilize the natural tendency of all objects to float freely in a "levitated" state in a freely orbiting space vehicle. This would allow consideration of melting and solidification experiments free from the influence of crucibles and molds since the specimen integrity could be maintained by surface tension forces alone. It was apparent that many of the restrictions of terrestrial levitation techniques utilizing electromagnetic fields would be removed. In the weightless environment, electromagnetic fields could be used to remove kinetic energy from the specimen relative to the laboratory and to prevent the melt from touching nearby equipment. Since the required forces would be relatively small, containerless melting and solidification can be performed with materials having resistivities orders of magnitude above those which can be considered in terrestrial experiments. The mass of the melt processed would be limited only by the onset of hydrodynamic instabilities and heat transfer considerations. Calculations indicate that masses of many kilograms can be considered. These early ideas have been developed in some detail through NASA contract studies over the past several years. The purpose of the present report is to indicate general facility specifications capable of processing the widest range of possible important containerless processing experiments within reasonable technology constraints. An important part of the work has been to make an up-to-date summary of these experimental possibilities. An attempt has been made to consider materials based on importance in terms of new scientific data procurable and/or possible future commercial applications thereof.

BACKGROUND

Under Contracts NAS8-24683, Task 4, and NAS8-26157 with the Product Engineering and Process Technology Laboratory of the NASA/Marshall Space Flight Center, the General Electric Company carried out conceptual studies of the containerless processing of materials in space. New possibilities were examined for preparation of improved and unique materials under weightless conditions in which the influence of crucible walls can be completely eliminated. The technology for automatic handling of freely floating molten materials was studied and led to development and demonstration of servo devices which apply correction forces by means of suitably controlled electromagnetic fields to remove specimen oscillatory motion with subsequent reduction of field forces to very low quiescent levels. This work included experimental studies of both electromagnetic and optical position sensing schemes and culminated in a test package utilized for experiments in the MSFC drop tower and in a KC135 ballistic aircraft flight.

Under Contract NAS8-27228 this development work was redirected to the initial design of an electromagnetic position control system which was to be used in conjunction with the M512 Skylab facility utilizing an electron beam for melting of specimens. Most of this work was applied to solving engineering problems which arose from the severe constraints imposed by the already existing M512 hardware and from other Skylab requirements. This Skylab design effort was terminated in February 1972. Nevertheless, some useful further basic developments were made, notably in the area of design of detailed coil configurations, electro-optical position sensors, and circuitry as well as further studies of optimum candidate material systems holding most promise for initial study in the weightless environment. Much of the design effort was concentrated upon a four-coil system which showed promise for fitting within the severe volume constraints imposed by the M512 vacuum chamber. The total position control servo system was tested successfully with a neutrally buoyant specimen. As part of a termination effort, some existing laboratory breadboard hardware was

assembled into a low-power six-coil position control test unit. This unit incorporated optical position sensing with artificial light sources to simulate the luminosity of a hot specimen, and was delivered to MSFC for test and evaluation in the MSFC drop facility.

As an independently funded effort within the General Electric Space Sciences Laboratory, an improved and simplified position control servo system was developed and tested in the laboratory. This concept utilizes electromagnetic position sensing and allows consideration of some coil configurations, simpler than those studied originally, in an arrangement permitting electrical damping of specimen motion. The coupling efficiencies for RF heating and melting can, as a result, be significantly greater than those achieved with previous terrestrial levitation work. For example, a one centimeter aluminum ball was melted and superheated utilizing only 160 watts input to a hemispherical coil system.

Although some analyses of electromagnetic field production by the above-mentioned coil geometries, as well as others, are available in the literature, comparison amongst the various approaches has not been made on a general basis. In this report, a uniform method of comparison is applied covering all aspects of the coil configurations which are most important for containerless processing.

SECTION 3

CANDIDATE CONTAINERLESS MATERIALS PROCESS EXPERIMENTS AND FUTURE INDUSTRIAL APPLICATIONS

3.1 CLASSES OF MATERIALS

In earlier studies (Ref. 3-1) a number of potentially important new materials processes and products were identified. The numerous references given in the referenced report deal primarily with processes or products and not the range of materials properties which set the specifications for a Space Laboratory Containerless Processing facility. The initiation of such specifications was a main purpose of the present study. For this reason this section will summarize the classes of materials of interest and review the processes and products which have been identified based on previous NASA-funded studies, including some new examples based on user surveys performed as part of the present study. The materials of greatest interest are discussed in terms of three major groups which are

1. Alloys, intermetallic compounds and cermets
2. Transition metal carbides and nitrides
3. Glasses.

These are discussed in the following three sections.

3.2 ALLOYS, INTERMETALLIC COMPOUNDS AND CERMETS

These materials are discussed under headings referring to their possible future commercial applications.

3.2.1 NEW ELECTRONIC MATERIALS

3.2.1.1 Carbides, Nitrides, Silicides, Borides, Beryllides and Sulfides.

These materials are beginning to be used widely in various fields of modern technology because of their high melting points, hardness, chemical stability,

high temperatures of transition into the superconducting state, metallic conductivity or semiconductivity or strength at high temperatures (Ref. 3-2 through 3-6). The preparation of high purity polycrystalline solids of these materials with adequate homogeneity and grain size as well as the preparation of high purity single crystals of low defect density has been a problem. Also, it is desirable to produce these materials with better characterization of bulk samples to assist in understanding how deviations from stoichiometry, crystal structure, lattice parameters and impurity levels should be specified. Specific examples of materials, which are prime candidates, are listed as follows:

a. TaN and NbN based alloys having electrical resistivities below 10^{-6} ohm-meters. They have very small temperature dependence from cryogenic temperatures to melting point (Ref. 3-2). They have excellent corrosion resistance and may find wide use in integrated circuits and microelectronics.

b. Hexaborides such as lanthanum boride (LaB_6). These have found use as important technological materials, e.g. cathodes of high-power electronic vacuum tubes (Ref. 3-3, 3-7). Cathodes using these materials may be capable of operating in a poor vacuum of the order of 10^{-4} to 10^{-5} torr, in high field strength, and under intense ionic bombardment, with simultaneous increased emission current, so that under these adverse conditions they may still function as good thermionic emitters. Borides of the alkalai and rare earth metals are also suitable for these applications. Lanthanum boride has a high melting point of 2210°C, latent heat of evaporation of 167 kilocalories/mole and high thermionic emission parameters, i.e. an electron work function of 2.66 - 2.68 e.v. and Richardson's constant of 29 amperes/cm^2. Much longer active cathode life in high voltage electronic vacuum tubes, by as much as a factor of 10 to 15, may be achieved with these materials.

c. Carbides such as TiC, ZrC, TaC. These have identical application as the nitrides of paragraph a.

d. Amorphous metallic conducting glasses such as palladium silicon. These amorphous metallic glasses could find application in microelectronics (Ref. 3-8). Being amorphous their electrical properties are homogeneous and isotropic and may therefore replace oriented crystals presently used in microelectronics.

3.2.1.2 Amorphous Semiconductors and Semiconducting Glasses

These materials should find wide applications in electronics in future years. Due to their amorphous nature, these materials show homogeneous and isotropic electronic and optical properties. They are not as much affected by impurities as are the crystalline semiconductors. Many of these glasses exhibit the property of "switching" their conductivities from low to high and so should be useful in electronic switching and computer applications. The semiconducting glasses and amorphous semiconductors fall into three main categories. These are

a. The chalcogenide glasses, in which one or more of the elements, S, Se, or Te is combined with one or more of the elements such as metals Si, Ge, P, As, Sb, Bi, Tl and Pb,

b. The Transition-metal oxide glasses. These are glasses in which the major constituent is a transition metal oxide, such as V_2O_5 (vanadium pentoxide),

c. Amorphous germanium and silicon.

d. Recently, "diamond lattice type" glassy semiconductors, such as Cd-Ge-As have been reported and may form a fourth category.

All of these glasses may be prepared by supercooling from the melt, bypassing crystallization. Thus they are ideal candidates for containerless processing experiments. At room temperature many of these semiconducting glasses have resistivities above 10^5 ohm-meters, but at elevated temperatures and when molten, resistivities which fall below 10^{-2} ohm-meters.

3.2.1.3 Alloy Melts having a liquid miscibility gap

These are the monotectics which exhibit the phenomenon of segregation of the liquids, on earth, by virtue of density differences (Ref. 3-9). In the weightless environment this separation should not occur and a matrix of one phase with dispersion of the other phase throughout should be obtained. Unique new alloys and intermetallic compounds with unique electronic properties may be prepared from melts of monotectic composition and hypermonotectic composition (Ref. 3-10,

If thermal gradients can be adjusted across a freely floating melt, then directionally solidified composites could be produced. An example is Fe-Pb which would have unique magnetic properties. Another example is Hg-Te which forms the semiconducting intermetallic compound HgTe. Through supercooling melts of monotectic or hypermonotectic compositions, new intermetallic compounds, new alloy compositions, or amorphous materials may be formed. The chalcogenic glasses SeSb are other examples.

3.2.1.4 Tungsten-copper

This is an alloy which is totally immiscible in the liquid and solid states (Ref. 3-9). Tungsten-copper is produced commercially at the present time by liquid copper infiltration of a Tungsten skeleton. By solidifying a tungsten power dispersion in a copper melt using containerless processing, new materials could be prepared with possible unique applications to wear resistant, high temperature circuit breakers, relays and electric switches.

3.2.1.5 Eutectics

If thermal gradients can be adjusted across a freely floating melt, directionally solidified composites may be attained with unique electronic and optical properties (Ref. 3-10). Some examples are InSb-Sb for thermoelectric applications, FeSb-InSb for magnetoresistive and infrared polarizing applications, NaF-LiF for optical properties and Fe-FeS for ferromagnetic applications.

3.2.1.6 New alloys and compounds, prepared by supercooling melts

If a high degree of supercooling can be attained through containerless processing then many new materials may be prepared with unique features through solution broadening or bypassing crystallization (Ref. 3-12). One example is Ni-Ge which has been studied through SPLAT cooling.

3.2.2 SUPERCONDUCTORS

3.2.2.1 These materials have application for generation of strong magnetic fields, power transmission, flux pumps, telephone cables, etc. (Ref. 3-2, 3-9, 3-10). Many applications demand high superconducting critical temperatures, high critical magnetic field, and high critical current density. A few important examples are presented as follows:

a. $Nb_3(Al_{0.8}Ge_{0.2})$ which has the highest critical temperature, 20.8°K, of the known superconductors.

b. Nb_3Sn which has critical temperature of 18.05°K and critical magnetic field of 221 kilo-oersteds at 4.2°K.

c. (NbN-TiC) which has critical temperature of 18.0°K, maximum, and critical magnetic field of 120 kilo-oersteds, maximum, at 4.2°K.

d. $(NbN_{0.7}C_{0.3})$ which has critical temperature 17.8°K, maximum, and critical magnetic field of 132 kilo-oersteds, maximum, at 4.2°K.

e. (NbN-TiN) which has critical temperature 17.0°K and critical magnetic field greater than 140 kilo-oersteds at 4.2°K.

3.2.2.2 The processes that have been suggested for the production of these superconductors are

a. Growing superconducting materials of Nb_3Sn in a matrix of tin or vice ver by directional solidification of melts of Nb-Sn at various compositions. Nb-Sn is a monotectic, exhibiting a region of liquid immiscibility.

b. Supercooling Nb-Sn of the required composition to attempt to form Nb_3Sn as an amorphous superconductor.

c. Purification, melting, and supercooling melts of nitrides and carbides to produce new superconducting materials.

3.3 TRANSITION METAL CARBIDES AND NITRIDES

3.3.1 SERVICE PROPERTIES

Transition metal carbides and nitrides are of extreme interest and importance in modern technology (Ref. 3-2, 3-3, 3-13). At the present time their main commercial interest is due to their hardness. The carbides in this group form the basis for "cemented carbide" cutting tools and wear-resistant parts. Due to their excellent high-temperature strength and good corrosion resistance they are also used as high temperature structural materials.

There are other, more exciting, properties possessed by these materials which hold great promise for future technological applications. The transition metal nitrides are being used increasingly not only for their electrical properties in integrated circuitry but are also being studied for their superconducting properties. Niobium nitride based alloys have some of the highest superconducting critical temperatures, as discussed above. Thin-film nitrides seem to have the most potential for application in such devices as Josephson junctions. Their refractory nature and corrosion resistance results in little chemical diffusion and hence decay of the junction with time. Junctions in use today are not chemically stable after cycling a few times between room and liquid helium temperatures.

3.3.2 PROBLEMS IN PREPARATION AND APPLICABILITY OF CONTAINERLESS PROCESSING

Polycrystalline samples of carbides and nitrides are generally prepared by powder metallurgy (Ref. 3-2, 3-3, 3-13). The metal or oxide powder is reacted with carbon or nitrogen, pressed and sintered. They can also be prepared by a number of other techniques one of which is by melting the elements or metal hydrides in a protecting atmosphere or in a vacuum. To prepare very pure samples, good vacuum conditions or highly purified protective gases are generally required. In a good vacuum they can be purified from oxygen contamination by vacuum degassing.

Preparing melts of carbides and nitrides poses many problems (Ref. 3-2). Many of them have very high melting points. Tantalum Carbide has the highest melting point known for any material (about 3983°C). The melting points of the carbides are generally higher than those of the parent transition metal element while those of the nitrides are comparable. There are no crucible materials to contain these very high temperature melts.

Contamination by impurities such as oxygen has a significant effect on the properties of carbides and nitrides and, since it forms a solid solution with both carbides and nitrides, oxygen is extremely difficult to eliminate (Ref. 3-2, 3-13). Carbon deoxidation is possible by heating under vacuum conditions at elevated temperatures and with excess carbon. It appears likely that vacuum purification and melting of these very high temperature materials without a crucible such as in containerless melting in the weightless environment may enable very high purity polycrystalline or single crystal transition metal-carbides and nitrides to be produced for electrical and superconducting applications. Their metallic electrical conductivities make electromagnetic position control feasible and they can be melted by RF induction.

3.4 GLASSES (which become electrically conductive when heated):
These are discussed as follows in terms of several important potential applications with the subsequent discussion of those which appear amenable to electromagnetic position control and controlled containerless melting.

3.4.1 APPLICABILITY OF ELECTROMAGNETIC CONTAINERLESS PROCESSING
Of the glasses to be mentioned, it is likely that electromagnetic position control and induction melting can deal with only a limited number of them since they generally require preheating before release in the position control volume. They are also prime candidates for electron beam and microwave heating and melting. Of immediate importance, therefore, are oxides, whose resistivity falls below 10^{-2} ohm-meters at elevated temperatures such as ZrO_2, ThO_2, CeO_2, and Nb_2O_3,

and glasses with metallic and semiconductive particles dispersed throughout such that their electrical conductivity may be below 10^{-2} ohm-meters depending on the degree of doping.

3.4.2 MATERIALS AND PROCESSES

3.4.2.1 High index glasses for new optical systems (Ref. 3-14, 3-15)
These are prepared from melts of oxides such as CeO_2, ZrO_2, Nb_2O_5, TiO_2, etc. These glasses would be prepared by heating, melting and, possibly, superheating the crystalline oxides, and then supercooling the melt in the absence of a crucible.

3.4.2.2 Single crystal materials, presently unknown (Ref. 3-15)
These would be produced from oxides of very high melting point such as ZrO_2. One process contemplated is the production of the oxide glass and then conversion to crystalline form. This would avoid polymorphic transitions, which occur in ZrO_2 and BeO as they are cooled.

3.4.2.3 Other materials, such as $2BeO:SiO_2$ (phenacite) (Ref. 3-15) and ZrO_2: SiO_2 (zircon), in which the composition melts incongruently should also be considered for production of single crystals by conversion from the glass. They have not been produced in usable form by conventional crystal growing techniques.

3.4.2.4 "Striking glass," new light filters, Christiansen filters, passive Q switches, phototropic glasses
"Striking glass" which is also called "ruby glass" or "temperature colored glass" contains colloidally dispersed metallic or semiconductive particles (Ref. 3-14). These may be particles of gold, silver, silver halides, cadmium sulphide compounds, Cd-S-Se compounds, or copper oxide. They are made by dispersing particles with known optical and electronic properties directly in a glass. If it were possible to disperse particles of specific properties in a matrix glass

without going through batch reactions and heat treatment, then completely new types of "ruby glasses" to be used as passive Q-switches for Nd or Er lasers or as new phototropic glasses may be produced. This may be achieved by containerless processing.

Light filters such as the Christiansen filters are made by dispersing a large number of coarse, colorless particles in a homogeneous, colorless matrix (Ref. 3-14). These could be produced by dispersing a high melting point glass in a low melting glass matrix. These are of great value in optical systems.

3.5 REVIEW OF USER INTERESTS AND REQUIREMENTS

In an effort to initiate the establishment of a coherent set of processing requirements for materials of interest to the potential users, a potential user survey was carried out as part of this contract. Previous investigations had indicated the necessity of providing position control and damping for materials undergoing free suspension processing, and that this may be provided by electromagnetic forces for many substances. The previous investigations had indicated definite advantages of electromagnetic positioning over other techniques, where it can be applied. These include:

a. The capability of working either in a protective atmosphere, e.g., high vacuum or an inert gas as required.

b. The ability to use either highly efficient electron beam heating or induction heating. (Electron beam heating requires vacua of less than a few torr, an environment in which positioning techniques that require a gaseous medium cannot function.)

c. Ability to easily provide specimen rotation at controlled rates.

d. Freedom from initiation of nucleation, e.g., due to high sonic levels.

e. Freedom from highly variable surface temperature gradients, due to gas jets.

f. Freedom from necessity to control electrostatic charge on specimens over extreme variations in thermionic emission with temperature and electron beam bombardment (used for additional heating and melting).

As a preliminary guideline, therefore, the class of materials considered was limited to those for which electromagnetic forces could produce useful positioning effects. During the study, this class was shown to include a large variety of materials.

3.5.1 SURVEY OF USERS

The identification of users and their interests has been carried out by both direct dialogs with potential users and review of documented relevant studies.

Discussions were held with key individuals from a number of industrial companies such as Kawecki-Berylco, Omniferrous Engineering and Union Carbide. In addition, information obtained from discussions with such organizations as Corning Glass and the General Electric X-Ray Department during the "Study for Identification of Beneficial Uses of Space" were held.

The bulk of data, however, was extracted from publications and reports documenting space processing concepts, experiments and tests recommended by various individuals and groups involved in materials research. Major contributions to this data bank were provided from such sources as NASA's Process Engineering Lab at Marshall Space Flight Center, GE's Space Sciences Laboratory, TRW and General Dynamics (Ref. 3-9, 3-16, 3-17, 3-18). Several symposia reports and review papers also contributed the views and interests of researchers from universities and other laboratories.

As a result of these dialogs and literature reviews, a tabulation was compiled of some 18 areas of user interest. Included are specific commercial applications, such as tungsten with substantially improved service properties (such as grain structure) for x-ray targets, including potential applications and research

areas such as more uniform dispersions of eutectic and monotectic alloys. In all, the tabulated user areas of interest are representative of approximately 400 different materials and material combinations.

Several of the examples cited have been drawn from commercial applications identified by industrial users who supported the GE "Study for Identification of Beneficial Uses of Space," performed under NASA Contract NAS8-28179. However, the documented requirements are not limited to commercial user interests alone.

3.5.2 IDENTIFICATION OF MATERIALS AND PROCESSES PROBLEMS AND BENEFITS OF SPACE PROCESSING

For each of the identified materials or material combinations, representing an area of user interest, initial effort was directed at establishing the sequence of transformations through which materials would pass in progressing from raw materials, through preprocessing on the ground, space processing, and final ground processing. Raw materials, in many cases, were identified as commercial grade stock, powders, or pellets. Ground preprocessing has called for such activities as sintering, pressing, cutting to size, etc. Containerless space processing has been aimed at producing boules, spheroids, ingots and rods. Final ground processing has been identified as the production of such diverse products such as x-ray targets, petroleum pump valve-seats and valves, electronic substrates and lenses.

Where users were willing to identify specific commercial applications, the study tabulated: quantities of space processed produce which would be required per year (from 3000 kg to 160,000 kg); and estimate of values of product per year (from $3,000,000 to $170,000,000). In addition, estimates were provided for the size of the batch of each space-processed product. that would be commensurate with the size of final ground-processed product. The sizes for identified commercial applications ranged from 0.025 to 0.23 meter radius spheres, and from 0.7 to 100 kg. Since early development of space pro-

cessing for any of the identified areas will initially entail considerable theoretical and experimental work, the study also tabulated batch sizes for meaningful experimental quantities. Such sizes cover a range from 0.005 to 0.04 meter radius spheres, and 0.0025 to 1.5 kg.

The key to user interests, whether identified commercial applications, potential applications, or applied research, is the identification of problems encountered in ground processing that might be overcome by space processing. In that respect, an important step in this study has been the tabulation of such problems for each example material or combination thereof. Typically, where applicable, problems which have been noted include: contamination from crucible walls, nucleation due to from crucible walls, thermal convection in the melt, buoyancy or sedimentation contact with crucible walls, thermal convection in the melt, buoyancy or sedimentation in melts of multiple materials, limited rates and uniformity of cooling, and limited rates and uniformity of supercooling, uniformity of alloying, sampling for test without contamination of the melt.

3.5.3 SPACE PROCESSING REQUIREMENTS

The requirements for processing these materials have been determined and are given in Tables 3-1 through 3-4. The specific requirements for each such product include:

a. The method of sample insertion into the containerless processing facility. The methods considered are mechanical and electromagnetic.

b. The heating profile, including periods of maintaining required temperatures. A process to produce tungsten with enhanced service properties for medical x-ray targets, for example, requires at least two dwell periods for vacuum purification.

c. The processing environment, which might be vacuum or inert gas, and the processing facility.

d. The necessity for stirring the melt during processing.

e. The maximum temperature required. Tungsten, for example, would require a temperature of 3400°C while beryllium would require only 1300°C.

f. The necessity, where required, for preheating the material before insertion into the containerless processing facility. Many materials, such as zirconia, have too high electrical resistivities at room temperature, which precludes electromagnetic position control at room temperatures. Preheating zirconia by an electron beam or resistance oven above 2000°C, however, decreases the electrical resistivity to 10^{-2} ohm-meters and so enables preheated specimens to be positioned by electromagnetic forces in the containerless processing facilit

g. Required cooling rates. These are established either for free radiation cooling or for quenching. Typically, cooling rates of 1000°C/sec might be obtained by quench for high temperature materials such as tungsten, while 100°C/sec might be obtained for free radiation cooling. For controlled cooling, where the power is reduced slowly, rates of less than 10°C/sec may be obtained. The types of quenching considered were gas quench at 70°F, liquid at 70°F, or a cryogenic quench at much lower temperatures, such as that of liquid nitrogen.

h. Heating power required. This could vary from 1000 watts, for small specimens, to as much as 200,000 watts, which is required for a large commercial piece of beryllium with a beryllia dispersion.

i. The method of product recovery, which would be mechanical for semiconductors or glasses, and electromagnetic for relatively good conductors, such as the metals.

j. Process duration. This includes time to melt, time spent for dwell periods, time molten, and cooling time. When considering initial experimental work, much laboratory processing time can be eliminated by initially using high purity materials, thus a shorter heating cycle. In contrast, commercial grade materials require consequent longer heating cycle for final commercial process investigations.

k. Waste produced; including gaseous products, liquid products, solid products, and heat.

l. Process safety requirements. Safety considerations, for example, consider the hot product; the presence of reactive product gases - liquids or solids; the presence of particulate radiation, such as secondary electrons from electron beam heating; or electromagnetic radiation, which may be optical or RF. Tungsten for example, at 3400°C, cannot be directly observed without risk of damage to the eye.

In cases for which users identified commercial applications, the determination of space processing requirements involves two objectives. First, the requirements for manufacturing the product. Second, the requirements to perform an experiment which would produce a small quantity of the material for investigation and evaluation. Thus, a range of requirements was determined which reflect both small quantities of materials and relatively low power requirements suitable to early experiments, and the large magnitudes representative of production.

This survey is summarized in Tables 3-1 to 3-4 as previously mentioned.

FOLDOUT FRAME 1

Table 3-1. Summary of Space Processing Requirements of a Containerless Processing Facility, A

APPLICATION AREA	TUNGSTEN	TRANSPARENT METAL OXIDE GLASSES	HIGH TEMP EUTECTICS	TUNGSTEN CARBIDE	BERYLLIA DISPERSION IN BERYLLIUM
USER	GE MEDICAL SYSTEMS	CORNING	GE AIRCRAFT ENG	OMNIFEROUS ENG	KAWECKI-BERYLCO
PRODUCT STEPS (RAW MATERIALS TO CONSUMER PRODUCT)					
RAW MATERIAL(S)	COMMERCIAL GRADE TUNGSTEN	ZrO_2, CeO_2, ThO_2, Y_2O_3	TUNGSTEN, Ni (TYPICAL)	TUNGSTEN CARBIDE	BERYLLIUM & BERYLLIA
GROUND PREPROCESSED PRODUCT(S)	PRESSED, SINTERED BAR STOCK SLUGS	PRESSED, SINTERED HIGH PURITY BOULE	COMPOSITE INGOT	PRESSED, SINTERED INGOT	PRESSED, SINTERED COMPOSITE INGOT
SPACE PROCESSED PRODUCT(S)	FINE GRAINED SPHEROIDS	GLASS BOULES	EUTECTIC BOULE	POLYCRYSTALLINE BOULE	UNIFORMLY DISPERSED INGOT
FINAL GROUND PROCESSED PRODUCT(S)	3-5" FRUSTRUM X-RAY TARGETS	LENSES, WINDOWS	TURBINE BLADES	BALL & SEAT VALVES	NUCLEAR REACTOR REFLECTORS
SPACE PROCESSED PRODUCT					
MATERIAL(S)	FINE GRAINED HIGH PURITY TUNGSTEN	TRANSPARENT ZrO_2, CeO_2, ThO_2, Y_2O_3	EUTECTIC W, Ni	FINE GRAINED POLY-CRYSTALLINE TUNGSTEN CARBIDE	INGOT OF UNIFORMLY DISPERSED BERYLLIA IN BERYLLIUM
QTY. REQUIRED PER YEAR (KG)	[3,000]	?	[80,000-160,000]	[155,000] (TOTAL)	[4000] (MINIMUM)
ESTIMATED PRODUCT VALUE PER YEAR TO USER(S)*	[$5,000,000]	[$10,000,000]	[$70,000,000 - $140,000,000]	[$136,000,000 - $170,000,000]	[~$3,000,000]
BATCH OR UNIT SIZE (METERS)	.005 [.025] RADIUS SPHERE	.005 [.04] RADIUS SPHERE	.005 [~.04] RADIUS BOULE	.005 [~.03 & ~.05] RADIUS SPHERE	.01 [~.23] RADIUS BOULE
BATCH OR UNIT WEIGHT (KG)	.01 [1.25]	.003-.006 [1-3]	.006 [2-5]	.009 [.7-1.5]	.09 [100]
PRESENT PROCESSING PROBLEMS					
CONTAMINATION FROM CRUCIBLE	-	YES	-	-	YES
NUCLEATION FROM CRUCIBLE WALLS	-	YES	YES	-	YES
CONVECTION IN MELT	-	YES	YES	-	YES
BUOYANCY OR SEDIMENTATION	-	NO	YES	-	YES
FAST OR UNIFORM COOLING	-	YES	UNIFORM	-	YES
FAST OR UNIFORM SUPERCOOLING	-	YES	UNIFORM	-	YES
OTHER	UNDESIRABLE GRAIN STRUCTURE & PURITY	-	-	UNDESIRABLE GRAIN STRUCTURE PURITY	UNDESIRABLE GRAIN STRUCTURE, NON-UNIFORM DISPERSION
SPACE PROCESSING REQUIREMENTS					
PRE-HEATING (TEMP) °C	-	2000	-	-	-
INSERTION - MECHANICAL OR ELECTROMAGNETIC	EITHER	MECHANICAL	EITHER	EITHER	EITHER
HEATING RATE - °C/SEC					
HIGH	10 - 100	10 - 100	10 - 100	10 - 100	10 - 100
LOW	5 - 10	5 - 10	5 - 10	1 - 10	5 - 10
HEATING DWELLS (TEMP) °C					
FIRST DWELL	[2400 - 3200]			[2200 - 2750]	[1000]
SECOND DWELL	3420	2000-3000	1560	2900	1300
OTHER FUNCTIONS DURING HEATING					
VACUUM - N/M^2	10^{-3} OR /INERT, 10^5/	-	10^{-3}	10^{-3} OR /INERT, 10^5/	10^{-3} OR INERT, 10^5
GAS, TYPE - N/M^2		INERT, 10^5; O_2	-		
STIRRING	YES	YES	NO	YES	YES
MAXIMUM TEMPERATURE °C	3420	2000 - 3000	1560	2900	1300
COOLING RATE °C/SEC					
HIGH	/1000 (QUENCH)/	-	-	/1000 (QUENCH)/	/1000 (QUENCH)/
MEDIUM	~100 (NO QUENCH)	~100	-	~100 (NO QUENCH)	~50 (NO QUENCH)
LOW	10 (CONTROLLED)	.1-10 (CONTROLLED)	.02-.05 (CONTROLLED	10 (CONTROLLED)	5-10 (CONTROLLED)
COOLING METHOD					
RADIATION	YES	YES	YES	YES	YES
GAS (TYPE)/TEMP °C	INERT, 25 OR	-	-	INERT, 25 OR	INERT, 25 OR
LIQUID (TYPE)/TEMP °C	H_2O, 25	-	-	H_2O, 25	H_2O, 25
CRYO (TYPE)	LIQUID N_2	-	-	LIQUID N_2 (CONTROLLED)	LIQUID N_2
HEATING POWER (WATTS)	3000 - 5000 [$4.5 \times 10^4 - 5 \times 10^4$]	1000 - 2000 [$5 \times 10^4 - 6 \times 10^4$]	1000 - 2000 [$10^4 - 2 \times 10^4$]	2000 - 5000 [$10^5 - 2.5 \times 10^5$]	4000 - 5000 [$2 \times 10^5 - 4 \times 10^5$]
PRODUCT RECOVERY					
MECHANICAL RETRIEVAL	YES OR	YES	-	YES OR	YES OR
FREE SUSPENSION CONTROLS	YES	-	YES	YES	YES
OTHER (TYPE)	-	-	-	-	-
QUENCH (TYPE)	H_2O	-	-	INERT GAS (CONTROLLED)	-

PROCESS DURATION	PROD.	EXPERIMENT	PROD.	EXPERIMENT	PROD.	EXPERIMENT	PROD.	EXPERIMENT	PROD.	EXPERIMENT
TIME TO DWELL	[1-10 MIN]	1-2 MIN	[1-10 MIN]	1-2 MIN	[0.5-5 MIN]	0.5-5 MIN	[1-10 MIN]	1-2 MIN	[0.2-5 MIN]	0.2-2 MIN
TIME AT DWELL (SOLID)	[10-20 MIN]	0	0	0	0	0	[10-20 MIN]	0	[1-3 MIN]	0
TIME TO MELT & SUPERHEAT	[2-5 MIN]	0	0	0	0	0	[2-5 MIN]	0	[1-3 MIN]	0
TIME AT DWELL (MOLTEN)	[1-5 MIN]	2-4 MIN	[1-5 MIN]	2-4 MIN	[1-5 MIN]	1-5 MIN	[1-5 MIN]	2-4 MIN	[1-5 MIN]	2-4 MIN
TIME TO COOL TO RECOVERY TEMP.	[0.1-10 MIN]	2-4 MIN	[10-100 MIN]	2-4 MIN	[60-360 MIN]	60-360 MIN	[0.1-10 MIN]	2-4 MIN	[1-10 MIN]	2-4 MIN
TOTAL TIME	[~15-50 MIN]	5-10 MIN	[12-115 MIN]	5-10 MIN	[62-370 MIN]	62-370 MIN	[15-50 MIN]	5-10 MIN	[14-43 MIN]	5-10 MIN

SPACE PROCESS WASTE					
GAS (TYPE)	INERT, CO, CO_2, O_2, N_2, STEAM	INERT, O_2	-	INERT, CO, CO_2, O_2, N_2, STEAM	INERT, CO, CO_2, O_2, N_2, STEAM
LIQUID (TYPE)	H_2O	-	-	H_2O	H_2O
SOLID (TYPE)	TUNGSTEN, WO_2	OXIDES	-	WO_2, WC	-
HEAT (JOULES)	$10^6 - 3 \times 10^6$ [$6 \times 10^7 - 2 \times 10^8$]	$3 \times 10^5 - 3 \times 10^6$ [$10^8 - 3 \times 10^8$]	$4 \times 10^6 - 5 \times 10^7$ [$4 \times 10^7 - 5 \times 10^8$]	$10^6 - 2 \times 10^7$ [$10^8 - 3 \times 10^8$]	$10^6 - 3 \times 10^6$ [$2 \times 10^8 - 10^9$]
SPACE PROCESS SAFETY CONSIDERATIONS (HAZARDS)					
HOT PRODUCT (TEMP) °C	3400	2000 - 3000	1560	2900	1300
REACTIVE GAS	-	-	-	-	-
PRODUCT LIQUID	-	-	-	-	-
BY-PRODUCT SOLID	-	-	-	-	-
PARTIC. RADIATION	/ELECTRONS (LOW)/	/ELECTRONS (LOW)/	-	-	-
LASER BEAM	-	/SPECULAR REFLECTION/	-	-	-
ELECTROMAGNETIC RADIATION	YES (INCLUDE OPTICAL)	YES (INCLUDE OPTICAL)	YES (INCLUDE OPTICAL)	YES (INCLUDE OPTICAL)	YES
OTHER	-	-	-	-	TOXIC BERYLLIUM VAPOR

/ / INDICATES UNRESOLVED OPTION
* ESTIMATED SELLING PRICE OF PRODUCT BASED ON PRESENT PRICE STRUCTURE AND SALES
**ESTIMATED NUMBER OF APPLICATION AREAS, REPRESENTATIVE EXAMPLE IS SHOWN
[ ] INDICATES DATA FOR A PRODUCTION QUANTITY OFMATERIAL UNBRACKETED DATA IS FOR EXPERIMENTAL QUANTITY

FOLDOUT FRAME 2

FOLDOUT FRAME 1

Table 3-2. Summary of Space Processing Requirements of a Containerless Processing Facility, B

APPLICATION AREA	REFRACTORY METALS ALLOYS (20)** EG, MOLYBDENUM	TANTALUM-NIOBIUM-BASED ALLOYS (10)** eg NbN	CHALCOGENIDE GLASSES (30)** $TeTe$	MONOTECTIC ALLOYS (100'S) TUNGSTEN--COPPER
USER	AIRCRAFT ENGINE MANUFACTURERS	ELECTRONICS INDUSTRIES	ELECTRONICS & LASER INDUSTRIES	POWER DISTRIBUTION INDUSTRY
PRODUCT STEPS (RAW MATERIALS TO CONSUMER PRODUCT)				
RAW MATERIAL(S)	COMMERCIAL GRADE MOLYBDENUM	COMMERCIAL GRADE Nb N	CRYSTALLINE $GeTe$	COMMERCIAL TUNGSTEN COPPER
GROUND PREPROCESSED PRODUCT(S)	PRESSED, SINTERED BAR STOCK SLUGS	PRESSED, SINTERED BAR STOCK SLUGS	ROD SLUGS	LIQUID SINTERED SLUGS
SPACE PROCESSED PRODUCT(S)	FINE GRAINED SPHEROID	FINE GRAINED SPHEROID OR SINGLE CRYSTAL	GLASS BOULES	UNIFORMLY DISPERSED SPHEROID
FINAL GROUND PROCESSED PRODUCT(S)	TURBINE BLADES	WIRE OR WAFERS	WAFERS, WINDOWS	POWER EQUIPMENT CONTACTS
SPACE PROCESSED PRODUCT				
MATERIAL(S)	FINE GRAINED MOLYBDENUM DISPERSION	FINE GRAINED NbN OR NbN CRYSTALS	AMORPHOUS BOULE OF $GeTe$	INGOT OF FINELY DISPERSED COPPER IN TUNGSTEN MATRIX
QTY. REQUIRED PER YEAR (KG)	80,000 - 160,000	EXPERIMENTAL	EXPERIMENTAL	EXPERIMENTAL
ESTIMATED PRODUCT VALUE PER YEAR TO USER(S)	$70,000,000 - $140,000,000	EXPERIMENTAL	EXPERIMENTAL	EXPERIMENTAL
BATCH OR UNIT SIZE (METERS)	.005 ~.04 RADIUS BOULE	.005 BOULE	.01 RADIUS	.005 RADIUS
BATCH OR UNIT WEIGHT (KG)	.06 2-3	.0045	.0025	.006
PRESENT PROCESSING PROBLEMS				
CONTAMINATION FROM CRUCIBLE	YES	YES (VERY REACTING)	-	-
NUCLEATION FROM CRUCIBLE WALLS	YES	-	YES	-
CONVECTION IN MELT	YES	-	YES	-
BUOYANCY OR SEDIMENTATION	-	-	-	-
FAST OR UNIFORM COOLING	YES	-	YES	-
FAST OR UNIFORM SUPERCOOLING	YES	-	YES	-
OTHER	-	UNDESIRABLE PURITY GRAIN STRUCTURE	NO, GENERALLY. (SELENIUM SENSITIVE TO LIGHT)	NON-UNIFORM DISPERSION
SPACE PROCESSING REQUIREMENTS				
PRE-HEATING (TEMP) °C	-	-	600	-
INSERTION - MECHANICAL OR ELECTROMAGNETIC	EITHER	EITHER	EITHER	EITHER
HEATING RATE - °C/SEC				
HIGH	10 - 100	10 - 100	10 - 100	10 - 100
LOW	5 - 10	5 - 10	5 - 10	5 - 10
HEATING DWELLS (TEMP) °C				
(FIRST DWELL)	2400 - 2550	-	-	-
(SECOND DWELL)	2700	2300	800	1100
OTHER FUNCTIONS DURING HEATING				
VACUUM - N/M^2	10^{-3} OR	10^{-3} OR	10^{-3} OR	10^{-3} OR
GAS, TYPE - N/M^2	/INERT, 10^5/	/INERT, 10^5/	/INERT, 10^5/	/INERT, 10^5/
STIRRING	YES	YES	YES	YES
MAXIMUM TEMPERATURE °C	2700	2300	800	1100
COOLING RATE °C/SEC				
HIGH	/1000 (QUENCH)/	/1000 (QUENCH)/	-	/1000 (QUENCH)/
MEDIUM	~100 (NO QUENCH)	~100 (NO QUENCH)	-	~100 (NO QUENCH)
LOW	5-10 (CONTROLLED)	5-10 (CONTROLLED)	10	/5-10 (CONTROLLED)/
COOLING METHOD				
RADIATION	YES	YES	YES	YES
GAS (TYPE)/TEMP °C	INERT, 25	(BOULE ONLY) INERT, 25	-	INERT, 25 OR
LIQUID (TYPE)/TEMP °C	H_2O, 25	-	-	H_2O, 25
CRYO (TYPE)	-	/LIQUID He (CONTROLLED)/	-	-
HEATING POWER (WATTS)	$2 \times 10^3 - 3 \times 10^3$ $4.5 \times 10^4 - 5 \times 10^4$	$10^3 - 2 \times 10^3$	$10^3 - 2 \times 10^3$	$10^3 - 2 \times 10^3$
PRODUCT RECOVERY				
MECHANICAL RETRIEVAL	YES OR	YES OR	YES	YES OR
FREE SUSPENSION	YES	YES	-	YES
OTHER (TYPE)	-	-	-	-
QUENCH (TYPE)	H_2O	INERT GAS (CONTROLLED)	-	H_2O

PROCESS DURATION	PROD.	EXPERIMENT	EXPERIMENT	EXPERIMENT	EXPERIMENT
TIME TO DWELL	1-10 MIN	1-2 MIN	1-2 MIN	0.1-1 MIN	1-2 MIN
TIME AT DWELL (SOLID)	10-20 MIN	0	0	0	0
TIME TO MELT & SUPERHEAT	2-5 MIN	0	0	0	0
TIME AT DWELL (MOLTEN)	1-5 MIN	2-4 MIN	2-4 MIN	2-4 MIN	2-4 MIN
TIME TO COOL TO RECOVERY TEMP.	0.1-10 MIN	2-4 MIN	2-4 MIN	1-4 MIN	2-4 MIN
TOTAL TIME	15-50 MIN	5-10 MIN	5-10 MIN	4-9 MIN	5-10 MIN

SPACE PROCESS WASTE				
GAS (TYPE)	INERT, CO, CO_2, O_2, N_2, STEAM	INERT, CO, CO_2, O_2, N_2, H_2	-	INERT, CO, CO_2, O_2, N_2 STEAM
LIQUID (TYPE)	H_2O	-	-	H_2O
SOLID (TYPE)	MOLYBDENUM, MoO_2	CARBIDES	-	TUNGSTEN, WO_2, Cu
HEAT (JOULES)	$6 \times 10^5 - 2 \times 10^6$ $6 \times 10^7 - 2 \times 10^8$	$3 \times 10^5 - 10^6$	$3 \times 10^5 - 10^6$	$3 \times 10^6 - 6 \times 10^6$
SPACE PROCESS SAFETY CONSIDERATIONS (HAZARDS)				
HOT PRODUCT (TEMP) °C	2700	2300	800	1100
REACTIVE GAS	-	-	-	-
PRODUCT LIQUID	-	-	-	-
BY-PRODUCT SOLID	-	-	-	-
PARTIC. RADIATION	/ELECTRONS (LOW)/	-	/ELECTRONS (LOW)/	/ELECTRONS (LOW)/
LASER BEAM	-	-	-	-
ELECTROMAGNETIC RADIATION	YES	YES	YES	YES
OTHER	-	-	-	-

/ / INDICATES UNRESOLVED OPTION
* ESTIMATED SELLING PRICE OF PRODUCT BASED ON PRESENT PRICE STRUCTURE AND SALES
**ESTIMATED NUMBER OF APPLICATION AREAS, REPRESENTATIVE EXAMPLE IS SHOWN
{ | INDICATES DATA FOR A PRODUCTION QUANTITY OFMATERIAL. UNBRACKETED DATA IS FOR EXPERIMENTAL QUANTITY

FOLDOUT FRAME 2

Table 3-3. Summary of Space Processing Requirements of a Containerless Processing Facility, C

APPLICATION AREA	SUPERALLOYS WITH DISPERSED RARE EARTH OXIDES (15-20)** TITANIUM-LANTHANUM	UNIFORM DISPERSIONS OF SEMICONDUCTIVE/ PHOTOCONDUCTIVE PARTICLES IN GLASS (20-40)** SILVER CHLORIDE IN HIGH SILICATE GLASS	MAGNETORESISTIVE AND INFRARED EUTECTICS (4)** IRON ANTIMONIDE-INDIUM ANTIMONIDE	SUPERCONDUCTING MONOTECTICS (5)** NIOBIUM TIN-TIN	RARE EARTH BORIDES (5)** LANTHANUM BORIDE
USER OR USES	GAS TURBINE COMPONENTS, NUCLEAR REACTOR CONTROL RODS	STRIKING GLASS	INFRARED POLARIZATION LENSES, ELECTRONIC COMPONENTS	ELECTRICAL EQUIPMENT	HIGH POWER CATHODES
PRODUCT STEPS (RAW MATERIALS TO CONSUMER PRODUCT)					
RAW MATERIAL(S)	TITANIUM, LANTHANUM OXIDE	HIGH SILICATES & SILVER CHLORIDE	IRON ANTIMONIDE & INDIUM ANTIMONIDE	NIOBIUM & TIN	LANTHANUM HEXABORIDE
GROUND PREPROCESSED PRODUCT(S)	PRESSED, SINTERED INGOT	TABLET OF COMMERCIAL SILICATE GLASS POWDER SILVER CHLORIDE POWDER	BILLET	SINTERED COMPOSITE INGOT	PRESSED, SINTERED INGOT
SPACE PROCESSED PRODUCT(S)	UNIFORM DISPERSION INGOT	UNIFORM DISPERSION BOULE	EUTECTIC BOULE	MONOTECTIC BOULE	POLYCRYSTALLINE BOULE
FINAL GROUND PROCESSED PRODUCT(S)	GAS TURBINE COMPONENTS	LIGHT FILTERS	POLARIZATION LENSES	ELECTRICAL COMPONENTS	CATHODES
SPACE PROCESSED PRODUCT					
MATERIAL(S)	INGOT OF UNIFORMLY DISPERSED LANTHANUM OXIDE IN TITANIUM	BOULE OF FINELY DISPERSED SILVER CHLORIDE IN SILICATE GLASS	BOULE OF LAMELAR IN Sb-FeSb	BOULE OF LAMELAR NbSn-Sn	BOULE OF POLYCRYSTALLINE LaB_6
QTY REQUIRED PER YR (KG)	[80,000 - 160,000]	EXPERIMENTAL	EXPERIMENTAL	EXPERIMENTAL	EXPERIMENTAL
ESTIMATED PRODUCT VALUE PER YEAR TO USER(S)*	[$70,000,000 - $140,000,000]	EXPERIMENTAL	EXPERIMENTAL	EXPERIMENTAL	EXPERIMENTAL
BATCH OR UNIT SIZE (METERS)	.005 [.04] RADIUS SPHERE	.04 RADIUS SPHERE	.04 RADIUS SPHERE	.02 RADIUS SPHERE	.02 RADIUS BOULE
BATCH OR UNIT WEIGHT (KG)	.003 [1.3]	1.3	1.5	0.3	.16
PRESENT PROCESSING PROBLEMS					
CONTAMINATION FROM CRUCIBLE	-	YES	-	-	-
NUCLEATION FROM CRUCIBLE WALLS	-	YES	YES	YES	-
CONVECTION IN MELT	-	YES	YES	YES	-
BUOYANCY OR SEDIMENTATION	YES	YES	YES	YES	YES
FAST OR UNIFORM COOLING	-	-	UNIFORM	UNIFORM	-
FAST OR UNIFORM SUPERCOOLING	-	YES	-	-	-
OTHER	NON-UNIFORM DISPERSION	NON-UNIFORM DISPERSION	-	-	UNDESIRABLE GRAIN STRUCTURE & PURITY
SPACE PROCESSING REQUIREMENTS					
PRE-HEATING (TEMP) °C	-	1300	-	-	-
INSERTION - MECHANICAL OR ELECTROMAGNETIC	EITHER	EITHER	EITHER	EITHER	EITHER
HEATING RATE - °C/SEC HIGH	10 - 100	10 - 100	10 - 100	10 - 100	10 - 100
LOW	5 - 10	5 - 10	5 - 10	5 - 10	5 - 10
HEATING DWELLS TEMPERATURE - °C (FIRST DWELL)	1700	-	-	-	-
(SECOND DWELL)	2000	1500	~ 1200	900	2300
OTHER FUNCTIONS DURING HEATING					
VACUUM - N/M^2	$< 10^{-3}$ OR	$<10^{-3}$	$< 10^{-3}$ OR	$< 10^{-3}$ OR	$< 10^{-3}$ OR
GAS, TYPE - N/M^2	/INERT, 10^5/	INERT, 10^5 ; 0_2	/INERT, 10^5/	/INERT, 10^5/	/ INERT, 10^5 /
STIRRING	YES	YES	YES	YES	YES
MAXIMUM TEMPERATURE °C	2000	1500	1200	900	2300
COOLING RATE °C/SEC HIGH	/1000 (QUENCH)/	-	-	-	-
MEDIUM	~ 50 (NO QUENCH)	25 - 50	~ 20	~ 20	~ 50
LOW	5 - 10 (CONTROLLED)	1 - 10 (CONTROLLED)	2 - 5 (CONTROLLED)	2 - 5 (CONTROLLED)	1 - 10 (CONTROLLED)
COOLING METHOD RADIATION	YES	YES	YES	YES	YES
GAS (TYPE) TEMP°C	INERT, 25 OR	-	-	-	INERT, 25
LIQUID (TYPE) TEMP°C	H_2O, 25	-	-	-	-
CRYO (TYPE)	-	-	-	-	-
HEATING POWER (WATTS)	2000 - 3000 [$5x10^4$]	$10^4 - 2x10^4$	$10^4 - 2x10^4$	$10^3 - 5x10^3$	$5x10^3 - 10^4$
PRODUCT RECOVERY MECHANICAL RETRIEVAL	YES OR	YES	YES OR	YES OR	YES OR
FREE SUSPENSION CONTROL	YES	-	YES	YES	YES
OTHER (TYPE)	-	-	-	-	-
QUENCH (TYPE)	INERT GAS	-	-	-	-
PROCESS DURATION	PROD. EXPERIMENT	EXPERIMENT	EXPERIMENT	EXPERIMENT	EXPERIMENT
TIME TO DWELL	0.2-4 MIN 0.2-2 MIN	2-5 MINUTES	2-5 MINUTES	2-5 MINUTES	0.2-2 MINUTES
TIME AT DWELL (SOLID)	10-20 MIN 0	0	0	0	0
TIME TO MELT & SUPERHEAT	2-4 MIN 0	0	0	0	0
TIME AT DWELL (MOLTEN)	1-5 MIN 2-4 MIN	1-5 MINUTES	1-5 MINUTES	1-5 MINUTES	2-4 MINUTES
TIME TO COOL TO RECOVERY TEMP.	0.1-5 MIN 2-4 MIN	2-5 MINUTES	2-5 MINUTES	2-5 MINUTES	2-4 MINUTES
TOTAL TIME	14-38 MIN 5-10 MIN	5-15 MINUTES	5-15 MINUTES	5-15 MINUTES	5-10 MINUTES
SPACE PROCESS WASTE					
GAS (TYPE)	INERT, CO, CO_2 H_2, STEAM	INERT, O_2, SiO_2 Si SUBORIDES	INERT	INERT	INERT, CO, CO_2, O_2, N_2, H_2
LIQUID (TYPE)	H_2O Z	-	-	-	-
SOLID (TYPE)	Ti, TiO_2, LaO_2	OXIDES	Sn, Fe, In	Sb, Sn	BORIDES, SUB-BROIDES
HEAT (JOULES)	$6x10^5 - 2x10^6$ $6x10^7 - 10^8$	$3x10^6 - 2x10^7$	$3x10^6 - 2x10^7$	$3x10^5 - 5x10^6$	$2x10^6 - 10^7$
SPACE PROCESS SAFETY CONSIDERATIONS (HAZARDS)					
HOT PRODUCT (TEMP) °C	2000	1500	TO 1200	900	2300
REACTIVE GAS	-	-	-	-	-
PRODUCT LIQUID	-	-	-	-	-
BY-PRODUCT SOLID	-	-	-	-	-
PARTIC, RADIATION	-	/ELECTRONS (LOW)/	-	/ELECTRONS (LOW)/	-
LASER BEAM	-	/SPECULAR REFLECTION/	-	-	-
ELECTROMAGNETIC RADIATION	YES (INCL OPTICAL)	YES	YES	YES	YES (INCL OPTICAL)
OTHER	-	-	-	-	TOXIC BORIDE VAPORS

/ / INDICATES UNRESOLVED OPTION
* ESTIMATED SELLING PRICE OF PRODUCT BASED ON PRESENT PRICE STRUCTURE AND SALES
** ESTIMATED NUMBER OF APPLICATION AREAS, REPRESENTATIVE EXAMPLE IS SHOWN
[ ] INDICATES DATA FOR A PRODUCTION QUANTITY OFMATERIAL. UNBRACKETED DATA IS FOR EXPERIMENTAL QUANTITY

FOLDOUT FRAME

FOLDOUT FRAME 2

Table 3-4. Summary of Space Processing Requirements of a Containerless Processing Facility, D

APPLICATION AREA	REFRACTORY SILICIDES (10)** MOLYBDENUM DISILICIDE	UNIFORM DISPERSION OF PHOTOCHROMIC PARTICLES IN GLASS (20)** SiO_2 GLASS WITH EUROPIUM AND/OR CERIUM	AMORPHOUS METALLIC CONDUCTORS (10)** PALLADIUM SILICON	FERROMAGNETIC EUTECTICS (10)** IRON–IRON SULPHIDE
USER OR USES	HIGH–TEMP CORROSION RESIST, ELECTRONIC SUBSTRATES	PHOTOTROPIC WINDOWS	ELECTRONIC SUBSTRATES	MAGNETIC APPLICATIONS
PRODUCT STEPS (RAW MATERIALS TO CONSUMER PRODUCT)				
RAW MATERIAL(S)	$MoSi_2$	SILICATE GLASS AND EUROPIUM AND/OR CERIUM	CRYSTALLINE PALLADIUM SILICON	IRON – IRON SULPHIDE COMPOSITE
GROUND PREPROCESSED PRODUCT(S)	PRESSED, SINTERED INGOT	TABLETS OF GLASS POWDER AND Eu OR Ce	POLYCRYSTALLINE INGOT	COMPOSITE INGOT
SPACE PROCESSED PRODUCT(S)	POLYCRYSTALLINE BOULE	AMORPHOUS BOULE	AMORPHOUS BOULE	LAMELAR INGOT
FINAL GROUND PROCESSED PRODUCT(S)	ELECTRICAL COMPONENTS	PHOTOTROPIC WINDOWS	ELECTRONIC COMPONENTS	MAGNETIC COMPONENTS
SPACE PROCESSED PRODUCT				
MATERIAL(S)	BOULE OF POLYCRYSTALLINE $MoSi_2$	BOULE OF AMOPHOUS SiO_2 GLASS WITH DISPERSED EUROPIUM AND CERIUM	BOULE OF AMORPHOUS PALLADIUM SILICON	INGOT OF LAMELAR Fe–FeS
QTY REQUIRED PER YR (KG)	EXPERIMENTAL	EXPERIMENTAL	EXPERIMENTAL	EXPERIMENTAL
ESTIMATED PRODUCT VALUE PER YEAR TO USER(S)*	EXPERIMENTAL	EXPERIMENTAL	EXPERIMENTAL	EXPERIMENTAL
BATCH OR UNIT SIZE (METERS)	0.02 RADIUS BOULE	0.02 RADIUS SPHERE	0.02 RADIUS SPHERE	0.02 RADIUS BOULE
BATCH OR UNIT WEIGHT (KG)	0.32	0.1 – 0.4	0.32	.31/M
PRESENT PROCESSING PROBLEMS				
CONTAMINATION FROM CRUCIBLE	–	YES	NO	NO
NUCLEATION FROM CRUCIBLE WALLS	–	YES	YES	NO
CONVECTION IN MELT	–	YES	YES	YES
BUOYANCY OR SEDIMENTATION	YES	YES	NO	YES
FAST OR UNIFORM COOLING	–	YES	UNIFORM	YES
FAST OR UNIFORM SUPERCOOLING	–	YES	UNIFORM	–
OTHER	UNDESIRABLE GRAIN STRUCTURE AND PURITY	UNIFORM DISPERSION	–	–
SPACE PROCESSING REQUIREMENTS				
PRE–HEATING (TEMP) °C	–	1300	–	–
INSERTION – MECHANICAL OR ELECTROMAGNETIC	EITHER	EITHER	EITHER	EITHER
HEATING RATE – °C/SEC				
HIGH	10 – 100	10 – 100	10 – 100	10 – 100
LOW	5 – 10	5 – 10	5 – 10	5 – 10
HEATING DWELLS TEMPERATURE – °C				
(FIRST DWELL)	–	–	–	–
(SECOND DWELL)	2200	1500	960	988°C
OTHER FUNCTIONS DURING HEATING				
VACUUM – N/M^2	$<10^{-3}$ OR	–	$<10^{-3}$ OR	$<10^{-3}$ OR
GAS TYPE – N/M^2	/INERT, 10^5/	INERT, 10^5: O_2	/INERT, 10^5/	/INERT, 10^5/
STIRRING	YES	YES	YES	NO
MAXIMUM TEMPERATURE °C	2200	1500	960	988
COOLING RATE °C/SEC				
HIGH	–	–	–	–
MEDIUM	~50	~25	~20	–
LOW	1 – 10 (CONTROLLED)	1 – 10 (CONTROLLED)	1 – 10 (CONTROLLED)	0.01 – 0.03 (CONTROLLED)
COOLING METHOD RADIATION	YES	YES	YES	YES
GAS (TYPE) TEMP °C	INERT, 25	–	INERT, 25	–
LIQUID (TYPE) TEMP °C	–	–	–	–
CRYO (TYPE)	–	–	–	–
HEATING POWER (WATTS)	$5 \times 10^3 - 10^4$	$2 \times 10^3 - 5 \times 10^3$	$10^3 - 5 \times 10^3$	$10^3 - 5 \times 10^3$
PRODUCT RECOVERY MECHANICAL RETRIEVAL	YES OR	YES OR	YES OR	YES OR
FREE SUSPENSION CONTROL	YES	YES	YES	YES
OTHER (TYPE)	–	–	–	–
QUENCH (TYPE)	–	–	–	–
PROCESS DURATION	EXPERIMENT	EXPERIMENT	EXPERIMENT	EXPERIMENT
TIME TO DWELL TEMP	0.2–2 MINUTES	2–5 MINUTES	0.1–5 MINUTES	0.1–3 MINUTES
TIME AT DWELL (SOLID)	0	0	0	0
TIME TO MELT: SUPERHEAT	0	0	0	0
TIME AT DWELL (MOLTEN)	2–4 MINUTES	1–5 MINUTES	1–5 MINUTES	1–5 MINUTES
TIME TO COOL TO RECOVERY TEMP	2–4 MINUTES	2–5 MINUTES	2–5 MINUTES	1–3 HOURS
TOTAL TIME	5–10 MINUTES	5–15 MINUTES	3–15 MINUTES	121–188 MINUTES
SPACE PROCESS WASTE				
GAS (TYPE)	INERT, CO, CO_2, O_2, N_2, H_2	INERT, O_2, Si_2O_2, Si SUBOXIDES Ce_2O_2, Eu_2O	INERT	–
LIQUID (TYPE)	–	–	–	–
SOLID (TYPE)	$MoSi_2$, OTHER SILICIDES OF Mo	OXIDES, Ce, Eu	PoSi	Fe, S, FeS
HEAT (JOULES) (KW)	$2 \times 10^6 - 8 \times 10^6$	$8 \times 10^5 - 8 \times 10^6$	$2 \times 10^5 - 5 \times 10^6$	$8 \times 10^6 - 6 \times 10^7$
SPACE PROCESS SAFETY CONSIDERATIONS (HASARDS)				
HOT PRODUCT (TEMP) °C	2200 ° C	1500	960	988
REACTIVE GAS	–	–	–	–
PRODUCT LIQUID	–	–	–	–
BY–PRODUCT SOLID	–	–	–	–
PARTIC. RADIATION	/ELECTRONS (LOW)/	ELECTRONS (LOW)	–	–
LASER BEAM	–	SPECULAR REFLECTION	–	–
ELECTROGAGNETIC RADIATION	YES (INCL OPTICAL)	YES (INCL OPTICAL)	YES	YES
OTHER	–	–	–	–

/ / INDICATES UNRESOLVED OPTION
* ESTIMATED SELLING PRICE OF PRODUCT BASED ON PRESENT PRICE STRUCTURE AND SALES
** ESTIMATED NUMBER OF APPLICATION AREAS, REPRESENTATIVE EXAMPLE IS SHOWN
| | INDICATES DATA FOR A PRODUCTION QUANTITY OFMATERIAL UNBRACKETED DATA IS FOR EXPERIMENTAL QUANTITY

FOLDOUT FRAME 1

FOLDOUT FRAME 2

3.6 REFERENCES

3-1 Free Suspension Processing Systems for Space Manufacturing, General Electric Company, Final Report Contract NAS8-26157, June 15, 1971.

3-2 Toth, Louis E., Transition Metal Carbides and Nitrides, Academic Press, N.Y. & London, 1971.

3-3 Samsonov, G. V., Refractory Transition Metal Compounds, High Temperature Cermets, Academic Press, N.Y. & London, 1971.

3-4 Margrave, J. L., Treverton, J. A. and Wilson, P. W., "The Use of Levitation in Inorganic Synthesis," High Temperature Science, 3, pp 163-167, March, 1971.

3-5 Roberts, O. C., Robertson, D. G. C. and Jenkins, A. E., "The Electromagnetic Levitation of Liquid Metal Sulfides and Their Reaction in Oxygen," Trans. AIME, 245, pp 2413-2420, Nov., 1969.

3-6 Nelson, L. S., "Techniques for Studying Liquids and Solids at Extreme Temperatures," Advances in High Temperature Chemistry, 4, ed. by Leroy Eyring, Academic Press, N.Y. & London, 1971.

3-7 Mandle, H. H. and Mandle, R. M., "Uses and Applications," Progress in the Science and Technology of the Rare Earths, 2, pp pp 190-297, ed. by Leroy Eyring, Pergamon Press, 1966.

3-8 Mott, N. F. and Davis, E. A., Electronic Processes in Non-Crystalline Materials, Clarendon Press, Oxford, 1971

3-9 Wuenscher, H. F., "Manufacturing in Space," Astronautics and Aeronautics, 10, p. 42, Sept. 1972.

3-10 Wechsler, A. E., "Spherical Forming and Composite Casting in Zero-G," Space Processing and Manufacturing, NASA Pub. ME-69-1, 1969.

3-11 Reger, J. L., "Reduced Gravity Processing of Homogenized Immiscible Metal Alloys," Space Processing and Manufacturing, NASA Pub. ME-69-1, 1969.

3-12 Frost, R. T., "Techniques and Examples of Zero-g Melting and Solidification Processes," Unique Manufacturing Processes in Space Environment, NASA Pub. ME-70-1, April, 1970.

3-13 Machlin, I., Begley, R. J. and Weisest, E. D., Refractory Metal Alloys, Metallurgy and Technology, Plenum Press, N. Y., 1968.

3-14 Deeg, E. W., "Glass Preparation in Space," Space Processing and Manufacturing, NASA Pub. ME-69-1, 1969.

3-15 Happe, R. A., "Possibilities for Producing New Glasses in Space," Space Processing and Manufacturing, NASA Pub. ME-69-1, 1969.

3-16 Space Processing and Manufacturing, George C. Marshall Space Flight Center, NASA Pub. ME-69-1, October 21, 1969.

3-17 Requirements and Concepts for Materials Science and Manufacturing in Space Payload Equipment Study, TRW, July, 1973.

3-18 Space Processes for Extended Low-G Testing, Final Report for Contract NAS8-28615, Convair Aerospace Division of General Dynamics, June 15, 1973.

SECTION 4

FACILITY PROCESS REQUIREMENTS AND RANGE OF MATERIALS PARAMETERS

4.1 CARDINAL MATERIAL PROPERTIES

Certain cardinal properties of materials determine the type of containerless processing facility required to perform the desired processes with such materials. Their electrical resistivity and variation with temperature determine the effectiveness of electromagnetic position control, electromagnetic spinning, induction heating, and electromagnetic stirring. The coefficient of secondary electron emission determines the feasibility for electron beam melting of the freely suspended material, without providing grounding for the piece. The maximum temperature to which the material must be heated, its dimensions and its total emissivity determine the minimum required heating power, while its specific heat and latent heat of fusion as well as amount of available power are required to estimate the melting time.

The important material parameters for the specific application examples were compiled and the results illustrated graphically with respect to the number of identified cases versus their resistivities (in the range of 10^{-8} to 10^{-2} ohm meters) as illustrated by Figure 4-1, which is a histogram of the numbers of candidate cases falling within a specific range of electrical resistivity. Also identified in this histogram are the general ranges which include examples, already discussed, of carbides, borides, nitrides, silicides, beryllides, sulfides, and oxides of metals (when heated), chalcogenide* glasses (pre-heated), pure metals, alloys of metals, and semiconductors (some require heating). The overwhelming number of cases of these materials considered fell within the range of resistivity illustrated and are thus suitable for processing in an electromagnetic containerless system.

*Glasses formed by combinations of the chalogens, S, Se, Te, with one or more elements, such as As, Ge, Si, Te, Pb, Sb, Bi, etc.

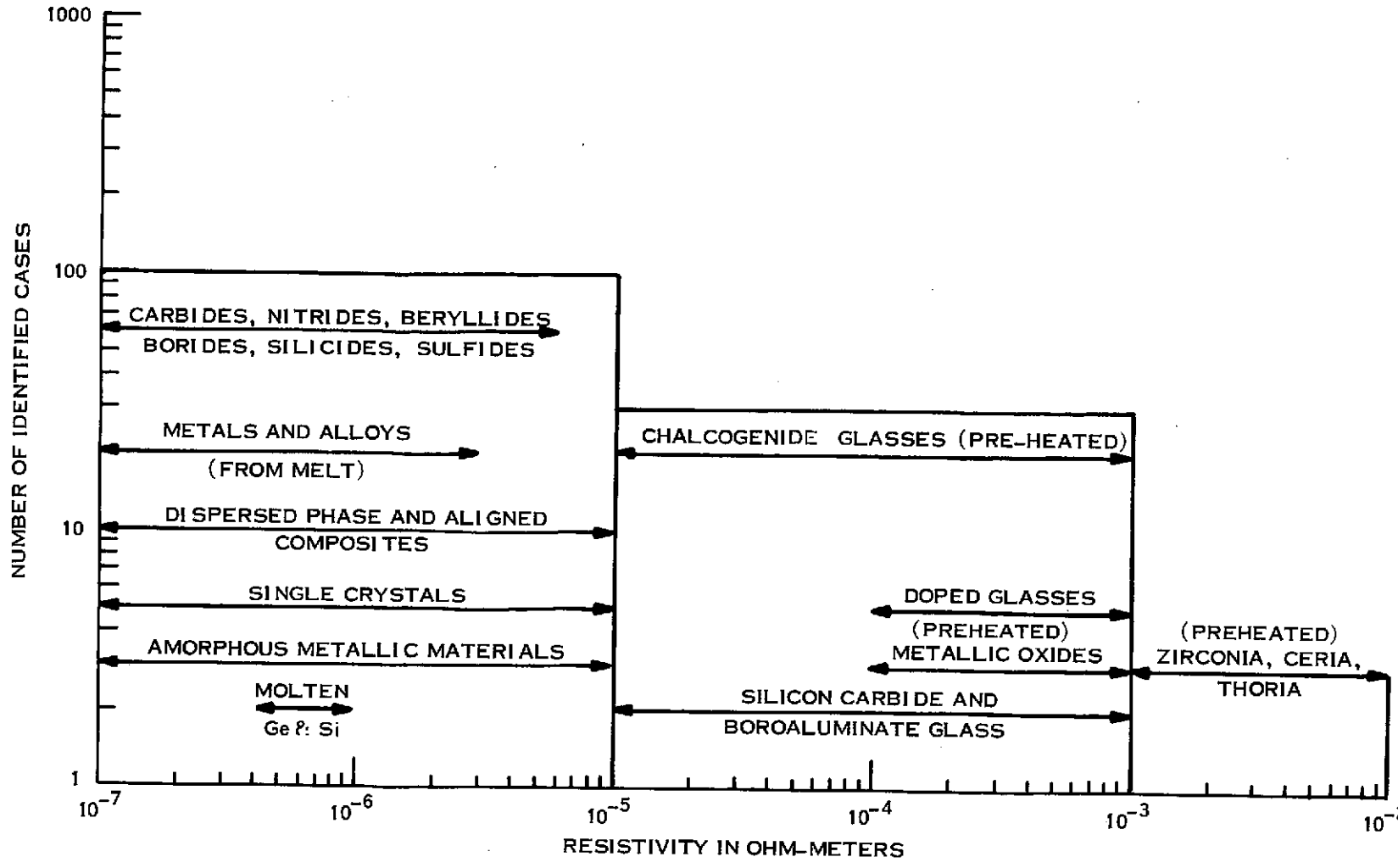

Figure 4-1. Numbers of Identified Candidate Materials with Various Ranges of Electrical Resistivity

Also considered was the number of examples for which the "second crossover point,"* in secondary electron coefficient versus energy, lies in various ranges from 0.5 kev to 20 kev.

Electron beam heating can be considered for materials for which the "second crossover point" is no less than two or three kilovolts. From Figure 4-2 it is evident that most of the cases considered have a "second crossover point" at electron energies which allow use of electron beam heating in conjunction with or as an alternate to RF induction heating. In addition to electrical resistivity and secondary electron emission coefficient, environmental gas purity requirements, possibilities of bubble formation in the melt and possible consequent requirements for removal by specimen spin and surface tension are considered. The ratio of density to surface tension determines the maximum specimen rotation speeds which can be tolerated for gas bubble removal without causing excessive deformation of the molten specimen. Density is also important in determining the relative accelerations that will be caused by application of positioning forces.

4.2 KINETICS OF SPECIMEN HEATING AND MELTING AND HEATING POWER REQUIREMENTS

4.2.1 KINETICS OF HEATING AND MELTING

It is important to know the power required to heat a specimen to the melting point and to melt it in a specified period of time. To estimate the time to melt a spherical specimen with a given amount of power coupled into it, for heating and melting, the following equation was developed:

*The "second crossover point" is defined as that electron energy at which the total secondary electron emission falls below unity, precluding electron beam melting of free specimens with electrons of greater energy.

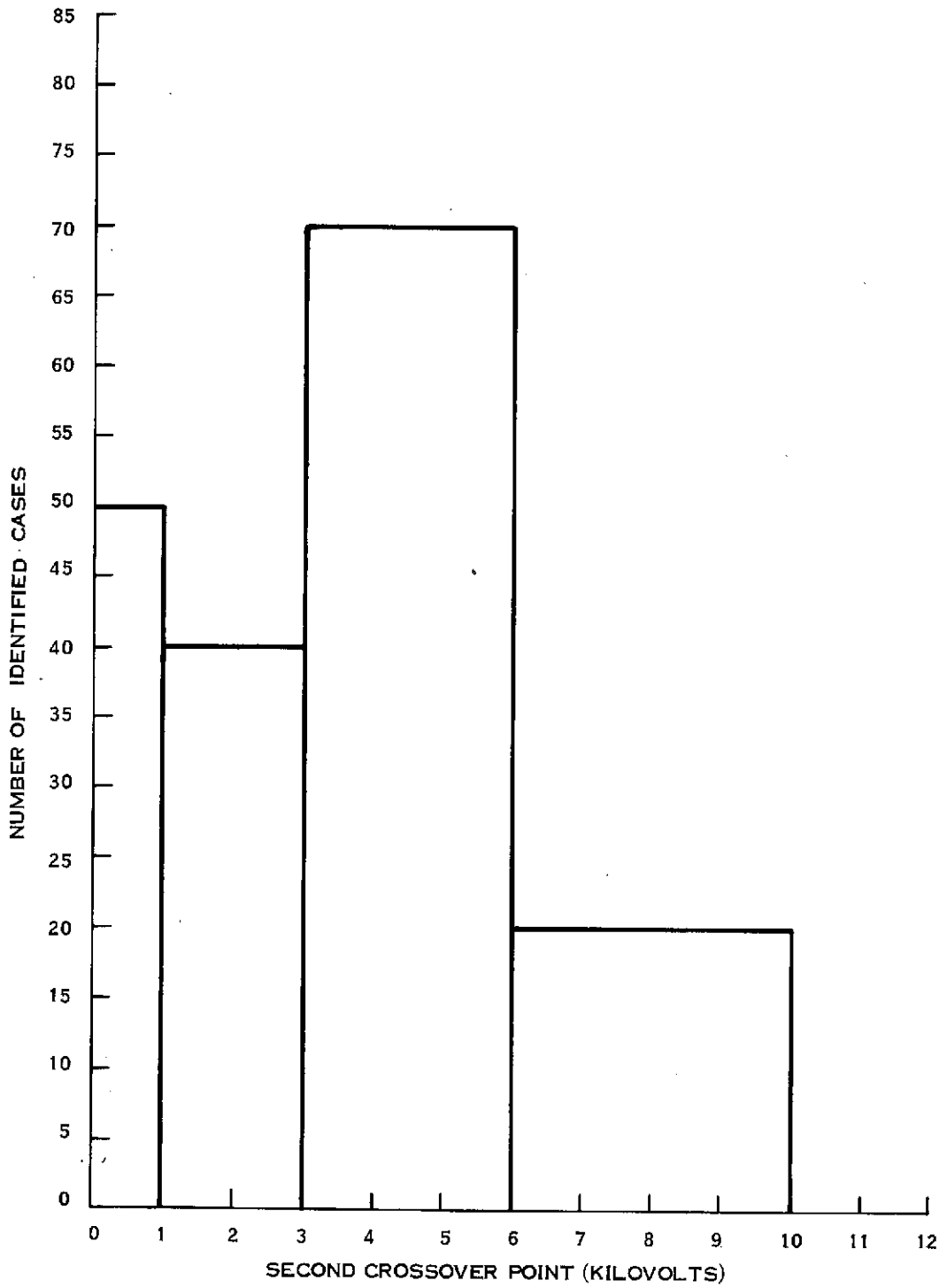

Figure 4-2. Numbers of Candidate Materials Arranged According to Second Crossover Point in Electron Emission

$$t = \frac{\beta}{2\alpha}\left\{\tan^{-1}(\alpha T_m) + \tanh^{-1}(\alpha T_m)\right\} \qquad (4.2.1\text{-}1)$$

$$-\frac{\beta}{2\alpha}\left\{\tan^{-1}(\alpha T_1) + \tanh^{-1}(\alpha T_1)\right\}$$

$$+\frac{mL}{N - A\sigma\epsilon T_m^4}$$

Wherein:

T_1	denotes	the initial temperature
T_m	"	the melting point of the material
L	"	the latent heat of fusion
m	"	the mass of the body
c	"	the specific heat of the material
N	"	the power supplied for heating
A	"	the surface area of the body
ϵ	"	the emissivity of the material
σ	"	Stefan-Boltzmann constant

$$\beta = \frac{mc}{N}$$

$$\alpha = \left(\frac{A\epsilon\sigma}{N}\right)^{1/4}$$

The foregoing equation was developed by considering a power balance equation,

$$N - A\sigma\epsilon T^4 = mc\frac{dT}{dt} \qquad (4.2.1\text{-}2)$$

for heating. It implies that the power supplied for heating minus the losses, due to radiation, equals the actual power absorbed by the material as it is heated. This equation can be put into another form,

$$dt = \frac{\beta}{\alpha} \left\{ \frac{d\mu}{(1-\mu^4)} \right\} \qquad (4.2.1\text{-}3)$$

with $\mu = \alpha T$. This gives the two bracketed terms on the right hand side of Equation 4.2.1-1 when integrated between some initial temperature T_1 and the melting temperature T_m.

Having heated to the melting temperature T_m an additional amount of heat, mL, must be supplied to melt it. The time necessary to supply this heat is: $t_m = \frac{mL}{N - A\sigma\epsilon T_m^4}$. The total time to melt a specimen, then, from an initial temperature T_1 is $t_1 + t_m$ thus giving Equation 4.2.1-1, where t_1 is the time to heat the specimen to the melting temperature, T_m, obtained in the foregoing.

The basic physical assumptions used to develop the equation include the body heated uniformly so that it experiences a nearly uniform temperature rise throughout its volume and that the power supplied to the body is constant. Considerations of heat flow have been neglected. For small specimens for which heat can be transferred rapidly throughout the specimen, this is a good assumption and so the equation 4.2.1.1 is a good estimate.

It is clear that to melt the specimen, the power supplied, N, must be greater than the power radiated at the melting temperature, $A\epsilon\sigma T_m^4$. For values of $N \approx A\epsilon\sigma T_m^4$, it will take extremely long time to melt the specimen.

Limited computations were carried out for a number of metals with melting points up to that of iron (1810°K) and reported in Ref. 4-1. When the power available for heating is greatly in excess of that required to furnish radiation losses at the melting temperature, the time for melting is inversely proportional to the total heating power. Figure 4-3 shows a typical relation for one centimeter radius metal spheres and the departure from this inverse relationship

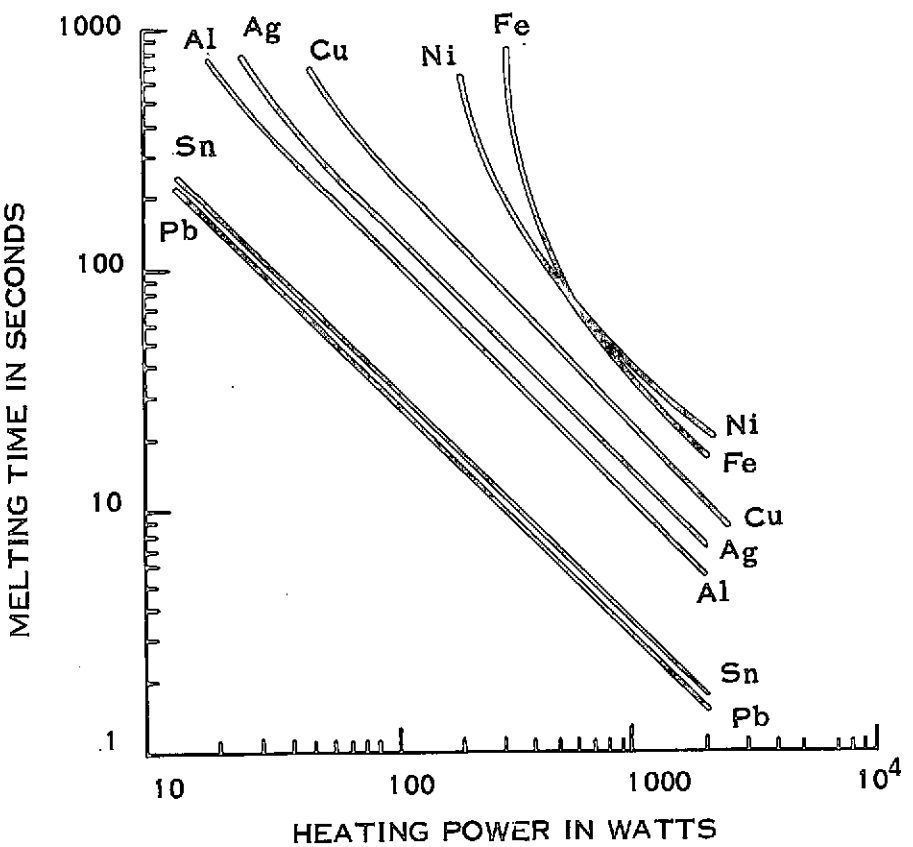

Figure 4-3. Melting Time Versus Heating Power for a Sphere of 1 cm Radius

when the heating power is only slightly in excess of that required to furnish specimen radiation loss. A computer program was written to obtain these curves and the runs for a one centimeter radius sphere were hand checked. Unfortunately, because of the many parameters involved in Eq. 4.2.1-1, it is necessary to perform new calculations for each specimen size and for other materials parameters. A survey of other cases for the refractory metals has been performed. These results were, that for high melting point materials, such as the refractories, heating powers only slightly in excess of those required to furnish radiation loss are required to reduce heating and melting times to reasonable values, of the order of a minute. For this reason the total heating power assumed in the engineering capability studies of Section 6 assume a total heating and melting power 20 percent greater than that required to furnish surface radiation losses at the melting point. For a lower melting point and larger specimen the quantity of latent heat which must be furnished for melting becomes larger, relative to the total radiated energy, for reasonable processing times. However, for these cases the heating power limitations will generally be less important for early experiments with specimens of size less than the maximum which can be handled with given facility power. Examination of the typical time requirements for maximum power for the processes discussed previously in Section 3.5, indicates that the maximum power specified, for any given material process, is generally required for periods of time measured only in minutes. For this reason, it is natural to assume such peak powers will be furnished by storage batteries capable of several times the maximum average power available to the Space Lab Containerless Processing Facility. This approach, which has already been utilized in the M512 Skylab experiments, thus allows consideration of processes whose peak power requirements are considerably in excess of average facility power capabilities. It has been suggested that a minimum power of 5 KW be considered for the facility. For this reason 5 KW was the minimum peak power in the facility capability estimates of Section 6.

4.2.2 COOLING TO SOLIDIFICATION TEMPERATURE AND TIME REQUIRED FOR SOLIDIFICATION

These questions have been discussed numerically in Ref. 4-1 including the effects on onset of solidification at temperatures well below the normal solidification point. Because of the absence of crucible walls to furnish sites for heterogeneous nucleation in the melt, the subcooling phenomenon is expected to be encountered relatively frequently. Extreme subcoolings may be observed in many cases of interest (and in fact provides one of the principal motivations for the containerless experiments), and procedures for computing upper and lower bounds on time for solidification are given in Ref. 4-1.

4.3 HEATING METHODS

In this report, much emphasis is placed upon RF induction heating which in many cases represents the simplest and most convenient heating method. In the earliest experiments, the requirement for a conservative approach in selecting the size of the field producing coils indicates use of only moderate electromagnetic coupling which, in turn, results in only moderate heating efficiencies. For this reason electron beam heating should be considered in some of these earliest experiments in which heating efficiencies of 50 percent would be desirable. Electron beam heating is also indicated for specimens of lower resistivity for which induction heating efficiency is very small.

The following two sections discuss the relative domain of applicability of these heating methods. It will be seen that the two techniques tend to be complementary, so that between them essentially all of the important examples of containerless processing discussed in Section 3 can be encompassed.

4.3.1 RF INDUCTION HEATING

Radio frequency or eddy current heating is widely used in industry for commercial processes in which it can provide high heating efficiencies when the

work coil is inductively tightly coupled to the specimen. This form of heating and melting is also favored in many materials process experiments and has been widely used in terrestrial levitation experiments in which a radio frequency field is used simultaneously for both levitation and melting. It is therefore natural to consider extending these techniques to containerless processing experiments in space for which the radio frequency generating equipment would already be available for specimen position control in the facility. An important new degree of freedom can be achieved in the space environment in which the translational forces provided by the electromagnetic system are no longer required to equal the specimen weight on earth. Since only very small forces need be provided, the positioning and heating functions can be, to a large extent, separated. The heating of the specimen is proportional to the square of the magnetic field intensity, H^2, and the translational force is roughly proportional to the gradient of H^2. Thus there is considerable latitude in the relative adjustment of these parameters by suitable coil design even at a fixed frequency. Since the frequency dependence of specimen heating and specimen translational forces are generally different, considerable flexibility is also available in adjusting the frequency to vary heating efficiency while at the same time achieving adequate positioning forces.

Another new requirement in the application of these radio frequency techniques in a Containerless Processing Facility for space is the achievement of greater power efficiencies. Levitation techniques to date have been characterized by relatively low power efficiencies with RF power sources of several tens of kilowatts being used for the treatment of specimens in the one centimeter diameter size range.

4.3.1.1 Absorbed Power

In this section the basic equation for the total joule heating in the specimen due to induced eddy currents in the specimen is discussed. It is assumed that

the specimen is introduced into a sinusoidally alternating magnetic field of intensity H_s which was relatively uniform prior to the introduction of the specimen. The total power absorbed by the specimen of radius a and electrical resistivity ρ_e is

$$N = 3\pi a \rho_e H^2 F_1(x), \qquad \text{(MKS)} \tag{4.3.1-1}$$

$F_1(x)$ is a function of x, the latter being the ratio of sphere radius to electromagnetic skin depth in the specimen. The units employed here are the meter-kilogram-second (MKS). These are the usual units employed in this report. However, for some calculations it is more convenient to employ centimeter-gram-second (CGS) or Gauss units.* In these units, formula (4.3.1-1) becomes

$$N = \frac{3 \cdot 10^9}{16\pi} a \rho_e B^2 F_1(x), \qquad \text{(CGS)}, \tag{4.3.1-2}$$

where a is in cm, ρ_e in Ω-cm, B in gauss and N in ergs-sec^{-1}. If N in the latter formula is reckoned in watts,

$$N = 5.9\, a \rho_e H^2 F_1(x), \qquad \text{(mixed units)} \tag{4.3.1-3}$$

The function $F_1(x)$ is derived by Smythe (Ref. 4-2) and Fromm and Jehn (Ref. 4-3) and is given by

$$F_1(x) = \left\{ \frac{x(\sinh 2x + \sin 2x) - \cosh 2x + \cos 2x}{\cosh 2x - \cos 2x} \right\} \tag{4.3.1-5}$$

*MKS and Gauss units will be used without prejudice in this report, due to the fact that many of the magnetic field computations that are available employ the latter units.

for very large x, $F_1(x) \rightarrow x$. Simple approximations to $F_1(x)$ for large and small x are shown in Figures 4-4 and 4-5, taken from Ref. 4-1. These figures also compare these approximations to exact computations of the function. Since the values of $F_1(x)$ drop precipitiously for x values less than the order of unity, the desire for high power efficiency requires that the facility frequency be so adjusted as to achieve values of x on the order of unity or greater. It should be pointed out that it is misleading to assume that the specimen heating will rise without limit in a practical facility as x is increased. It must be realized that Figure 4-5 gives the specimen heating variation if the magnetic intensity, H, could be maintained as the facility frequency is raised (as x is increased). However, for a facility operating at a fixed current and hence H level, the copper losses in the work coil will increase as the square root of the frequency for high frequencies due to the decrease of skin depth in copper. As is discussed in Section 5.3.10 these considerations indicate maximum power transfer to the specimen for values of x in the neighborhood of 3.

In the large x approximation, $F_1(x) \rightarrow x$, Eq. (4.3.1-1) can be written as

$$N = \frac{3\pi a \rho_e B^2}{\mu^2} \frac{R_2}{\delta} \qquad (4.3.1\text{-}5)$$

where μ is the permeability of free space ($\mu = 4\pi \cdot 10^{-7}$ MKS).

Since the skin depth δ is given by

$$\delta = \sqrt{\frac{2\rho}{\mu\omega}} \quad \text{(MKS)}$$

H becomes

$$N = \frac{3\pi}{2} \frac{\delta\left(\sqrt{\omega} B^2\right)}{\mu} a^2 \quad \text{for } x \gg 1 \qquad (4.3.1\text{-}6)$$

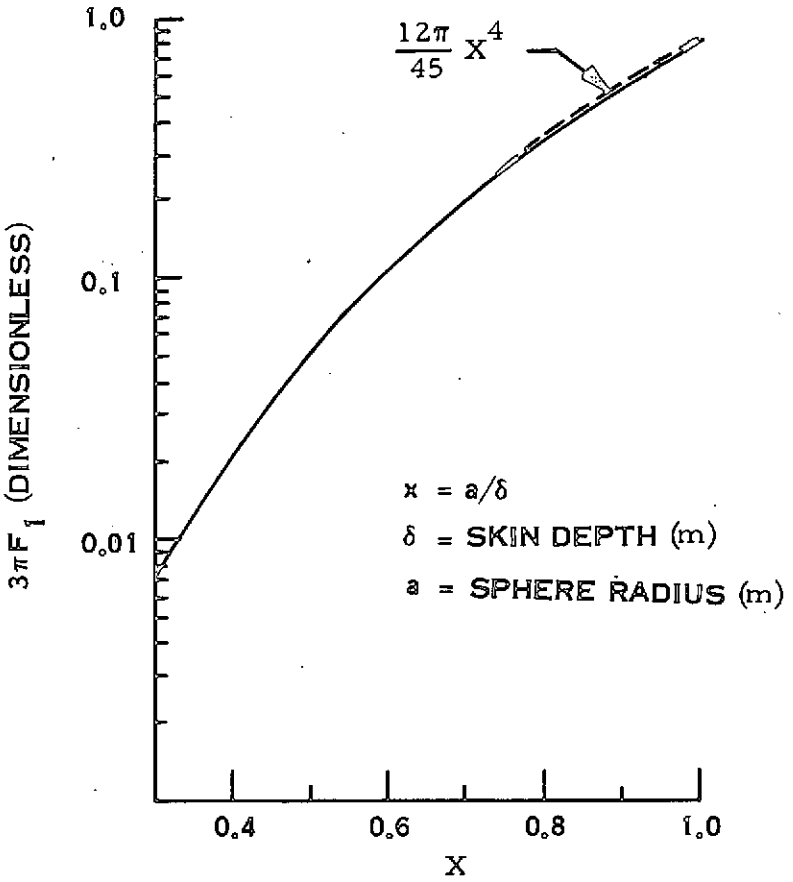

Figure 4-4. Eddy Current Heating Function, Small x

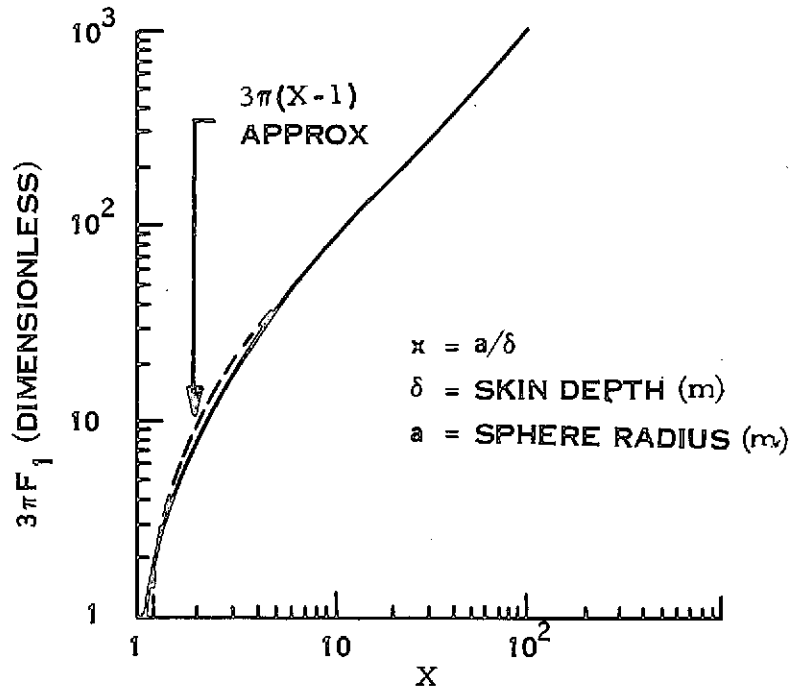

Figure 4-5. Eddy Current Heating Function, Large x

Letting $(\delta)(\sqrt{\omega}B^2) = K_3$, using the surface area A of the sphere, $A = 4\pi a^2$, and setting $\mu_o = 4\pi x 10^{-7}$ henry/meter, we may write this as

$$N = \frac{3x10^7}{32\pi} (\sqrt{\omega}B^2) A = 3x10^5 K_3 A \qquad (4.3.1\text{-}7)$$

The parameter $K_3 = \delta(\sqrt{\omega}B^2)$ is a product of the material parameter skin depth and the engineering parameter $(\sqrt{\omega}B^2)$.

It is interesting to note that for reasonable changes in specimen size in a given facility, the total heating is proportional to the total surface area A of the specimen. Of course, the radiant heat loss from the specimen is also proportional to A.

4.3.1.2 Range of Electromagnetic Skin Depths for Materials of Interest

Because the most important material parameter in determining the facility specifications is the electromagnetic skin depth, we here give a summary of this parameter over the wide range of specimen resistivities which may be considered for an electromagnetic Containerless Processing Facility. Figure 4-6 shows the variation of electromagnetic skin depth δ as a function of frequency for various resistivities. Because of the wide range considered, the straight lines have been chosen to correspond to constant resistivities, each differing from the other by two orders of magnitude (factors 10^2). Also indicated by the arrows and labels are the ranges of specimen resistivities discussed in Section 4.1. It can be seen that electromagnetic skin depths of one centimeter or less (x values of unity or greater for reasonable size specimens) can be achieved for frequencies no higher than 20 MHz. Employment of microwave induction does not appear to be necessary for the range of materials and processes which are considered here.

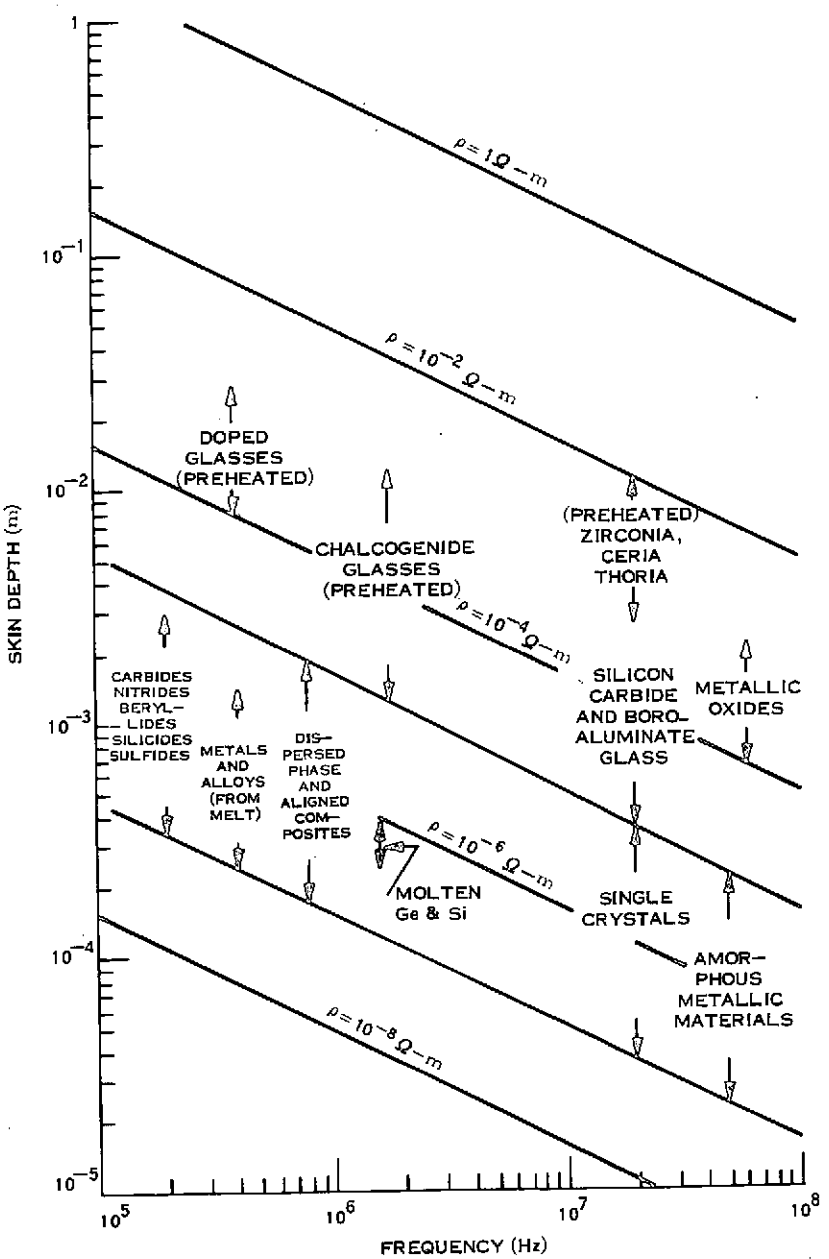

Figure 4-6. Electromagnetic Skin Depth Versus Frequency and Resistivity

For very high resistivity specimens such as cold glass, alternate position control techniques, such as standing sound waves in gas filled cavities, can be considered. Here it is anticipated that alternate methods of heating other than the RF or electron beam techniques considered in this report must be employed. The work coils required for the former would undoubtedly interfere with the standing sound wave pattern. Electron beam melting, at the required electron energies, would not be applicable due to electron scattering from the working gas in the sonic system and radiant heating may be required. However, microwave induction by cavities or resonators having no "work coils," would not interfere with the acoustic method in the range of resistivities for which it is warranted. It should be noted that many of the experiments and processes identified in Section 3.5 call for controlled gas environments at pressures too low to be practicable for the sonic positioning technique. Other experiments and processes adaptable to sonic position control are being studied in other laboratories (see Ref. 4-4 & 4-5).

The above considerations indicate that eddy current induction heating of both good and relatively poor conductors is feasible provided magnetic fields of adequate intensity can be provided over a frequency range up to 10 or 20 MHz, the higher frequencies being employed for the poorer conductors in order to achieve x values above the "knee" of the heating function curve, $F_1(x)$.

4.3.2 ELECTRON BEAM HEATING AND MELTING

There is a large class of material examples which can be electron beam heated and melted in the levitated condition, without the need for grounding of the material. This possibility arises from the circumstance that the total secondary electron emission coefficient can exceed unity for these materials if proper selection is made of electron beam energy. The electrostatic potential of the levitated material will automatically adjust itself to that value, in the range of a few tens of volts positive, which causes an adjustment of the net number of low energy secondaries emitted such that the total electron flux leaving the specimen equals the total flux of electrons in the impinging beam.

4.3.2.1 Basic Problem

The potential of a levitated solid, when bombarded by an electron beam, is determined by the number of electrons entering the solid as compared to the number of electrons leaving the solid (Ref. 4-6, 4-7, 4-8). If more electrons enter than leave, the body will charge negatively, while if more electrons leave than enter, the body will charge positively. If the potential of the body becomes too high, then there will be electrical discharges between the body and lower potential portions of the system. The current to and from the levitated specimen will be composed of true secondary electrons, charged ions, inelastic and elastic scattered beam electrons and, when the specimen temperature achieves sufficiently high values, thermionic emission (Ref. 4-8) and charged ions. If the specimen potential rises slightly, due to the total secondary emission coefficient exceeding unity, a large proportion of the low energy secondary electrons will be stopped in a space charge region surrounding the specimen and returned to the specimen.

For many materials, thermionic electron emission will become adequate to maintain a zero net electron flux prior to achievement of melting temperatures. Initial grounding of the cold specimen can then be effected by mounting the unmelted specimen on a grounded, possibly retractable, "sting" of the same material to reduce contamination. For this very large class of materials, charge balance on the specimen will be maintained with a specimen charge only on the order of an electron volt or so.

4.3.2.2 Secondary Electron Emission and Backscattering of Electrons

Experimentally it is virtually impossible to separate secondary electron emission and backscattering of electrons. These are usually lumped together and called secondary electron emission. Thus there are three groups of secondary electrons emitted from the surface of a body. These are:

a. Primary electrons reflected elastically

b. Primary electrons reflected inelastically

c. True secondary electrons.

True secondary electrons are electrons ejected from the solid as a result of bombardment by the primary electrons. Most of them have energies of a few electron volts, this energy being nearly independent of the energy of the incident primaries. An excellent review of the theory of secondary electron emission can be found in references 4-7 & 4-8. Primary electrons reflected elastically have the same energies as the primaries incident on the body. Inelastically reflected electrons and true secondary electrons cannot be rigorously distinguished because both have a continuous energy spectrum. However, since true secondary electrons are mainly slow electrons, electrons with energies lower than 50 e. V. (electron-volts) are arbitrarily identified as true secondary electrons (Ref. 4-7). The rest are identified as reflected electrons. This distinction is meaningful for primary electrons with energies in the kilovolt regime.

The total coefficient σ of secondary electron emission is equal to the ratio of the number of all secondary electrons emitted and reflected by the body to the number of primary electrons incident on it during the same time. It is given by

$$\sigma = r + \eta + \delta \qquad (4.3.2\text{-}1)$$

where r is the coefficient of elastic reflection of electrons, η the coefficient of inelastic reflection of electrons, and δ the coefficient of true secondary electron emission. It is important to recognize that when considering the potential of a levitated solid it is the total coefficient of secondary emission that must be used. There has been much confusion in the literature on this point.

Each of the three coefficients r, η, and δ (and consequently, σ) depends primarily upon the nature of the material and the energy of the primary electrons. The geometry of impingement of the electron beam is also important (e.g., normal or oblique incidence). However, for the applications discussed here the beam will impinge nearly normally upon an approximately spherical specimen and this factor is not considered an important variable.

The nature of the specimen is extremely important when considering secondary electron emission. Figures 4-7 and 4-8 show curves of the total secondary emission coefficient versus primary electron beam energy for a number of metals, semiconductors and dielectrics. Figure 4-8 illustrates the difference that can be observed in platinum between the coefficient of total secondary emission, σ, and the coefficient of "true" secondary emission, δ. Platinum has a high coefficient of inelastic reflection, η. Differences between σ and δ will be appreciable for many substances where η and r are large. Tungsten is another such substance. Figure 4-9 shows the variation of η with primary electron energy for a number of metals.

From Figures 4-7 and 4-8, it is at once evident that there may be two crossover points where σ is unity. To the left of the first crossover point, $\sigma<1$, and when bombarded with electrons with primary energy $E_p < E_1$, the levitated solid will charge negatively until arcing occurs or it reaches the potential of the electron gun cathode and the electron beam cannot reach the levitated solid. To the right of the second crossover point, the levitated solid will charge negatively until the potential between the levitated solid and the electron gun cathode is such that $\sigma = 1$ and the primary electron energy is reduced to E_2. When the bombarding energy is anywhere within the range between the two crossover points, the net electron flux will become momentarily a flux of electrons leaving the specimen. Very quickly, however, the potential of the specimen will build up positively until a certain fraction of the emitted secondary electrons are returned to the specimen. Since most of these secondarie

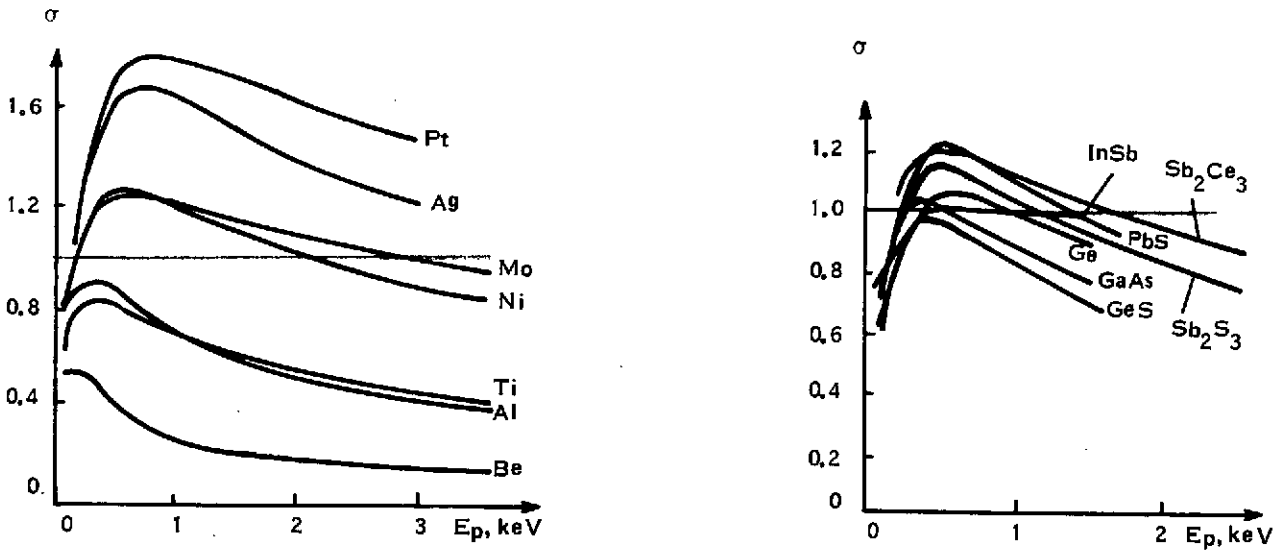

Figure 4-7. Secondary Electron Emission Coefficients as a Function of Energy for Several Materials

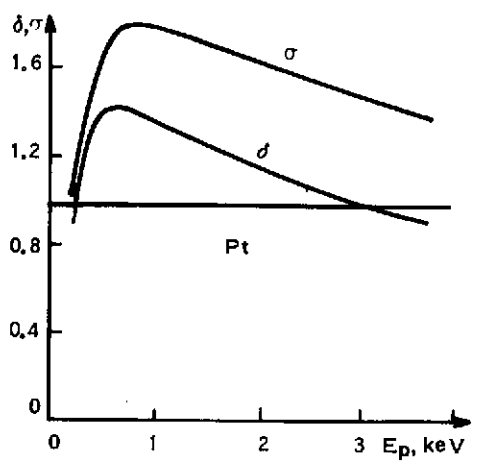

Figure 4-8. True and Total Electron Emission Coefficients as a Function of Energy for Platinum

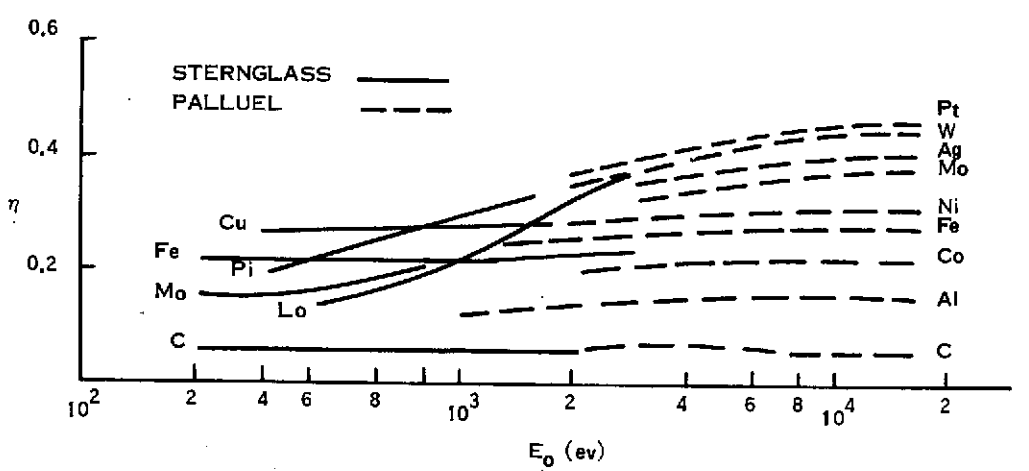

Figure 4-9. Coefficient of Inelastic Reflection versus Beam Energy for Several Materials

possess energies of only a few volts to tens of volts, only a slight adjustment of specimen potential is required. The specimen potential will automatically adjust itself to that precise value such that the net electric current leaving the specimen is reduced to zero. In practice it will generally be desirable to utilize bombarding energies towards the upper end of the energy interval between the two crossover points because of the greater ease of focussing at the higher energies.

It is clear that an immediate division among materials can be made according to coefficient of total secondary emission. When the second crossover point is high enough for efficient electron beam heating, then a levitated solid can be heated and melted by electron bombardment. When it is not or if σ never reaches unity, electron beam heating and melting can still be used for high melting materials where the thermionic emission becomes sufficient prior to melting. As mentioned above this would require mounting of these specimens upon a conducting sting prior to melting.

The state of the surface is generally very important in secondary emission. A rough surface may inhibit secondary electrons from leaving. Adsorbed layers of gases and oxide coatings may enhance secondary emission, depending upon the layer depth and primary energy. Thus contaminated material to be purified by electron beam heating and melting may have enhanced secondary emission over the purified substance. Stock tungsten, before degassing, for example, may have a second crossover point beyond 5 KeV. As the metal is purified this will shift downward to about 3.8 KeV.

4.3.2.3 Material Classes for Electron Beam Heating and Melting

The categorization of materials into candidates and non-candidates for electron beam heating while levitated depends largely on the electron beam techniques that can be employed in the environment of the levitation chamber. Primary electron energies as low as 2 KeV have been employed in zone refining to

melt a wide variety of conductors, semiconductors, and insulators (Ref. 4-9, 4-10). A wide variety of electron beam techniques such as the annular filament, the transverse gun, and the Pierce gun are available. Beam currents as high as 5 amperes for primary electron energies of 2 Ke have been employed in 10 kilowatt facilities (Ref. 4-10). In general, it is the environmental conditions in the chamber that determines whether electron beam melting of levitated solids is feasible. These factors,

a. The proximity of the gun to the material being heated,

b. The degassing rate of the material,

c. The vapor pressure of the material,

d. Interference with the electron beam by electromagnetic fields from the electromagnetic position control system,

e. The second crossover point of the material to be melted and its variation with temperature,

must be considered.

The first four of these factors must be examined further in the light of current engineering techniques. Focussing systems have been designed even for annular filaments in which the filament does not have a direct, unobstructed line of sight to the target and hence arcing and gun poisoning does not occur. The last factor is the material parameter dictating what primary electron energies can be employed in the facility without deleterious charge buildup.

Those materials which have second crossover points above 3 KeV are the best candidates for electron beam heating and melting while in the levitated state. This list includes:

a. The metals Iridium, Osmium, Platinum, Rhenium, Palladium, Silver, Gold, Rhodium, Tungsten, Tantalum, Molybdenum, Bismuth, Cadmium, Lead and Tin.

b. Alloys of these metals and alloys of these metals with other metals in which these metals predominate.

c. Metallic oxides such as Al_2O_3, MgO, ZrO_2, ThO_2, CeO_2, TiO_2.

There are many other materials such as many sulphides, phosphors, and alkalai halides which can also be considered. However, these materials have not as yet been identified as candidates for electromagnetic containerless processing.

Materials which are also candidates for low accelerating voltage electron beam heating and melting while levitated are those whose second crossover points lie between 1 and 3 Ke V. For these materials the engineering considerations discussed are critical. These include:

a. The metals Copper, Nickel, Iron, Hafnium, Cobalt, and Niobium.

b. Alloys of these metals and alloys of these metals with prime candidate metals.

c. Compound Semiconductors such as an Indium-Antimonide, Sb_2Ce_3, Lead-Sulfide, Sb_2S_3, $BiCs_3$, Bi_2C_s, and GeCs.

d. Semiconducting glasses such as the chalcogenide glasses.

e. Amorphous metallic glasses such as PdSi.

The various materials which have been identified in Section 3 of this report as being of great interest with respect to containerless processing in space have been examined with respect to their secondary electron emission coefficients. Figure 4-2 of Section 4.1 shows the number of interesting cases which have been identified arranged according to the occurrence of their second crossover point in four groups. Over half of the materials identified have second crossover points in excess of 3 Ke V.

Finally, there are those materials not considered to be candidates for electron beam melting while levitated. These either have no second crossover points or have them below 1 Ke V. These are:

a. The alkalai metals, Titanium, Aluminum, Zirconium, Scandium, Vanadium, Beryllium, Yttrium, the rare earth metals, Barium, and Radium.

b. The elemental semiconductors Germanium and Silicon.

c. Some compound semiconductors such as Gallium Arsenide, GeS and others.

d. Carbides, Nitrides, and Borides in general.

e. Carbon forms such as graphite.

There are exceptions among the carbides, borides, and nitrides which require further study. In general, however, the materials listed will require a grounding path until the temperature becomes high enough for thermionic emission to provide this role. In those cases for which melting occurs at a lower temperature, electron beam melting cannot be considered for the levitated specimens. Examination of the resistivity data of the previous sections indicates, however, that most of these exceptions are easily heated by RF induction. It should be pointed out that in early experiments with containerless processing, a conservative approach must be taken to provide sufficient free space between the specimen and work coils. For this reason induction heating efficiencies, as discussed in Section 6, would tend to be lower than electron beam heating efficiency for many materials.

4.4 ENVIRONMENTAL GAS REQUIREMENTS

4.4.1 DEGASSING REACTIONS AND PURITY REQUIREMENTS

Degassing of metals in the solid state and the liquid state is employed to significantly reduce the interstitial impurities which cause embrittlement, high ductile-to-brittle transition temperatures, and other effects detrimental to the service properties of the metal (Ref. 4-11, 4-12). The pertinent factors to consider in achieving significant purification are

a. The residual gases and their partial pressures in the chamber

b. The temperature at which degassing is performed

c. The throughput of the vacuum system

d. The degassing reactions in terms of the reactants, products, chemical equilibria at the degassing temperature, product partial pressures, and reaction kinetics

e. The dwell time at the degassing temperatures

f. The vapor pressure of the metal.

The residual gases present in vacuum systems are, generally, H_2O, O_2, N_2, CO, CO_2, H_2, and CH_4. These gases originate from system leaks, outgassing of the hot furnace surfaces, the pumping system, and the metal being heated. The pressure of each of these gases is dependent upon the furnace history and the test conditions. During the heating-outgassing cycle, the total pressure of these gases will increase to a maximum value and then decrease to a value characteristic of the pumping system. In order to perform certain processes, then, such as decarburization, the partial pressures of residual gases, such as O_2 in this case, must be adjusted to favor the degassing reactions.

Careful consideration must be given to the use of an inert gas during degassing. A major disadvantage of the use of an inert gas is the great difficulty

of measuring precisely the concentrations of the active impurity gases (Ref. 4-11, 4-12). With permissible partial pressures for degassing reactions at the level of 10^{-4} torr or less, the allowable concentrations of impurity gases in an inert gas at one atmosphere pressure will range from fractional parts per million to 10^{-5} parts per million or less. Thus the allowable impurity concentrations in the inert gas may be so low as to prevent precise measurement and to impose purity restrictions on the inert gas which are not attainable by present technology. Another disadvantage is that the presence of the inert gas will lower the reaction rate between the metal and the active gas impurity. Impurity gas must collide with and must diffuse through the inert gases to reach the metal surface. Thus the surface collision rate at a given pressure of an active gas at the metal surface is lower in an inert gas than in a vacuum. When active gases are used, as for example in decarburization, this may prolong the degassing dwell. For these reasons degassing is usually performed in a vacuum of the required partial pressures of active residual gases.

The critical knowledge gaps which must be filled, usually by experimental research, are:

a. Dwell temperatures for solid state degassing

b. Environmental conditions maintained during the process

c. Dwell times required for solid state degassing

d. Dwell times while molten

e. Dwell environment while molten.

With higher temperatures achievable in the solid state due to the lack of the necessity for supporting the solid in the weightless state, the prolonged dwell times employed in solid state degassing on the earth may be significantly reduced in the weightless environment. A short dwell time after melting, with some superheating, may result in evaporation of such minor constituents as phosphorous

and potassium. This will depend upon the vapor pressure of the metal versus the vapor pressure of the minor constituent at this temperature. It is clear, then, that the advent of processing in the weightless environment will require modification of degassing processes normally performed on the earth to take advantage of the lack of necessity for support or containment of the metal.

4.4.2 GLASSES - CONTROLLED ATMOSPHERE REQUIREMENTS

Careful consideration must be given to the use of an atmosphere in the preparation of new glasses in space. For the preparation of glasses in space it seems likely that high vacuum will be detrimental to the production of many glasses (Ref. 4-13) owing to

a. Acceleration of evaporation and decomposition of the compounds being considered, and

b. Bubble formation due to outgassing of products such as oxygen.

It is most likely that the production of many glasses such as zirconia, alumina, silica, etc., will require an embient pressure ranging from a low vacuum (above 10^{-3} torr) to one atmosphere pressure. However the atmospheres considered should be those designed to prevent degassing and volatilization of oxides. An oxygen atmosphere might be used to prepare many glasses (Ref. 4-13). Adjustments of the partial pressures of active gases to the point at which degassing and volatilization cease will be a prime requirement. As an example, BeO tends to form polymeric vapor species as (BeO)n, where n = 2, 3, 4, 5, 6. Even a small partial pressure of O_2 will suppress this incongruent vaporization.

Thus the requirement to prevent degassing, volatization of oxides, and bubble formation does not preclude the technique of "low" vacuum melting to prepare new glasses. It is necessary, however, to examine the specific

system and determine the partial pressures of active gases required to prevent degassing. An inert atmosphere or a mixture of inert gas and active gases may be considered. It is suggested that by carefully adjusting the partial pressures of active gases, many glasses could be prepared under low vacuum conditions. This would permit the employment of such efficient techniques for melting as electron beam melting. These techniques may be used with glasses whose resistivities when preheated are low enough (1 ohm-cm) to allow electromagnetic position control, since secondary electron emission coefficients tend to exceed unity at suitable beam energies.

4.4.3 SUMMARY

In summary, then, the application of vacuum technology to the processing of many materials has significant advantages. Particular processes where vacuum technology is significant are melting, brazing, sintering, annealing, welding, single crystal growth, and purification and grain refinement. Even in areas such as the production of new glasses, vacuum technology is applicable, providing attention is given to the partial pressures of active gases to prevent degassing, volatization of oxides, and bubble formation. The advantage of processing such materials as glasses in low vacuum may be the employment of efficient heating methods such as electron beam melting and the elimination of hot furnace walls which could contaminate the melt.

4.5 BUBBLE FORMATION IN MOLTEN SPECIMENS

It has been suggested that removal of gas bubbles from levitated molten specimens can be accomplished by providing spin to the specimen. The gas bubbles would then migrate towards the rotation axis under the influence of the resultant centripetal force. The agglomeration of these gas bubbles along the rotation axis should then lead to their escape from the rotating mass at the axis of rotation at sufficiently high rotational velocities. The specimen's rate of rotation could then be decreased and the mass would regain a spherical form.

The purpose of this section is to indicate to what extent this requirement for rotation can be avoided for a wide range of processes by proper preparation prior to containerless processing.

The formation of a gas bubble in a liquid metal is extremely difficult. This is shown in Reference 4-14. Assume a bubble of radius, r, in the melt. If P_1 is the external gas pressure on the liquid, and P_2 the hydrostatic pressure on the bubble, due to the surface tension, γ, at the external surface of the liquid, we obtain the pressure inside the gas bubble as

$$P = P_1 + P_2 + \frac{2\gamma}{r} \qquad (4.5\text{-}1)$$

When a gas bubble is first formed inside a melt, it is extremely small and the pressure inside the gas bubble is enormous. Consider a gas bubble of radius $r = 10^{-5}$ centimeter. Using (4.5-1) and a value of γ of 1000 dynes/cm, which is consistent with measured values of the surface tension of iron doped with carbon and oxygen, the pressure $P = 2 \times 10^8$ dynes/cm^2 or about 2000 atmospheres. Thus the required pressure for the formation of bubbles must be greater than 200 atmospheres and, because such vapor pressures will not normally exist in a melt, the formation of gas bubbles inside the melt is practically impossible from the standpoint of homogeneous bubble nucleation.

During processing on earth, bubbles may be nucleated heterogeneously at crucible walls, on impurities in the liquid, and at the boundary of solidifying metal. In the weightless environment the crucible walls can be eliminated and with high purity materials there are few sites for bubble nucleation. Thus the formation of bubbles in a liquid metal containing dissolved gases is practically impossible provided there are no insoluble impurities and no crucible walls, which is the case in the weightless environment. When dealing with a solid metal having interstitial impurities such as carbon and oxygen, the solubility of these interstitials increases when the solid is melted and these impurities

will remain dissolved. Since it is, for all practical purposes, impossible to nucleate bubbles homogeneously in the liquid, bubbles of CO, CO_2, etc. will not form and grow. Consequently all degassing will take place at the liquid-vacuum interface during vacuum degassing.

It is suggested that by proper sample preparation and degassing in a high vacuum in the solid state at elevated temperatures, many specimens can be prepared for processing in space without gas pockets. It is expected that the worst problems will be encountered in samples formed by hot pressing and sintering as is done for materials such as tungsten. Special consideration must be given to these specimens so that when melting begins spattering and gas bursts are minimized. Rotation of the resultant melts to remove residual gas bubbles is certainly worth considering in such cases. A discussion of these basic requirements in terms of provision of a spin-up capability in the Containerless Processing Facility is discussed in the next section.

4.6 SPIN CONTROL REQUIREMENTS

This section examines the physical requirements on the electromagnetic Containerless Facility when specimen rotation is required. The imparting of controlled angular rotation rates to freely floating specimens has been suggested as a means for gas bubble removal, as discussed above. It has also been suggested that some useful oblate spheroidal forms might be formed in this manner. We shall first discuss briefly the physics of rotational deformation and subsequently indicate the electromagnetic field requirements for providing this spin capability.

4.6.1 ROTATIONAL DEFORMATION OF A FLUID SPHERE

A liquid drop rotating about its vertical axis in a medium less dense than the liquid is shown in Figure 4-10. Lamb's classical work and Chandrasekhar (Ref. 4-15, 4-16) have both treated this problem for the drop in a weightless

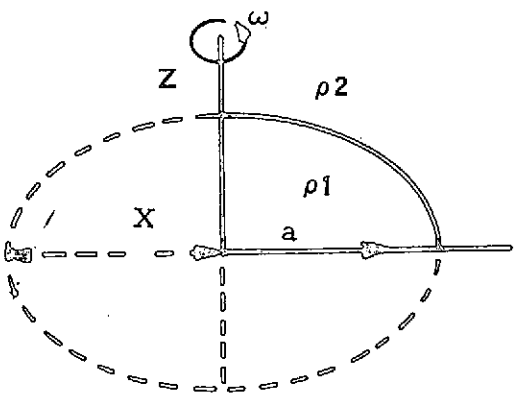

Figure 4-10. Drop Rotating About Vertical Axis

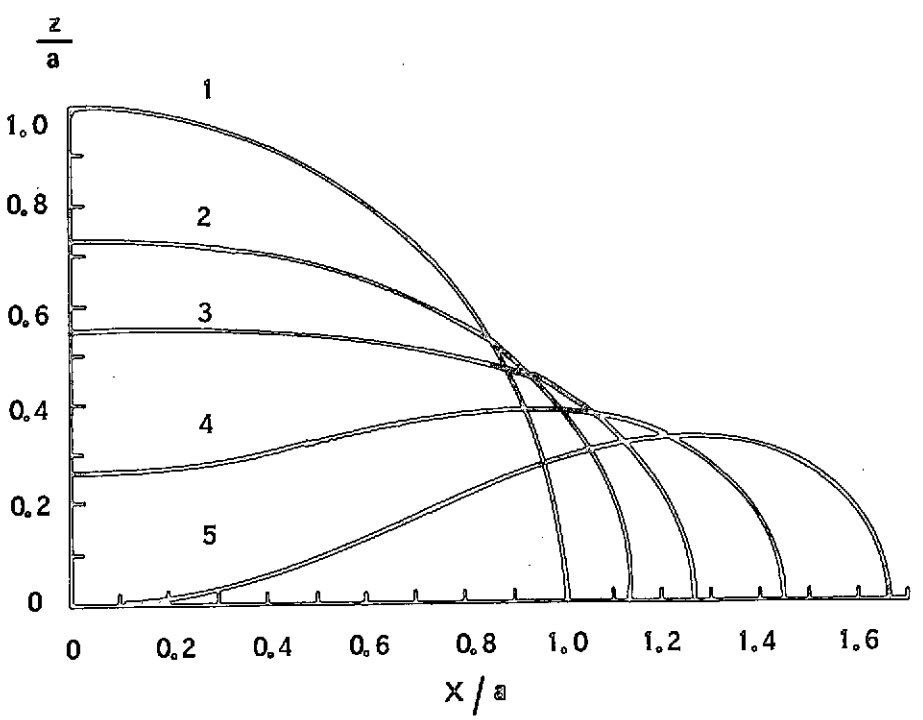

Figure 4-11. Profiles of Rotating Drop

environment. The governing parameter is the shape factor, Σ, defined by

$$\Sigma = \frac{(\rho_1 - \rho_2)\alpha^2 a^3}{8\gamma} \quad , \text{ with } \rho_1 > \rho_2 \, , \qquad (4.6.1\text{-}1)$$

where ρ_1 is the density of the liquid, ρ_2 is the density of the surrounding medium, α is the angular frequency of rotation about the vertical axis, a is the spherical radius, and γ is the surface tension. Figure 4-11 shows drop profiles for five values of Σ. At $\Sigma = 1$, the drop assumes a pronounced oblate spheroidal form. Beyond $\Sigma = 1$, increased thinning of the center continues until at $\Sigma = 2.3291$ the drop assumes a ring shape. It is clear that beyond $\Sigma = 1$, the problem of position control will become complex and perturbations may cause instabilities which will cause the drop to break up as Σ increases beyond $\Sigma = 1$. For these reasons, $\Sigma = 1$ is chosen as a practical limiting rotation speed α. Then

$$\alpha = \sqrt{\frac{8\gamma}{\rho_1 a^3}} \qquad \text{for } \Sigma = 1 \text{ and } \rho_1 >> \rho_2. \qquad (4.6.1\text{-}1)$$

Figure 4-12 shows this relationship between specimen equatorial radius R and the material parameter γ/ρ. This parameter, the ratio of surface tension to density varies over a range of about one order of magnitude for all of the materials considered in this study. By way of illustration, we may consider two cases which probably represent extreme values for the ratio γ/ρ. For Beryllium this ratio is close to the upper limit shown of 0.8 and for Mercury this ratio is 0.05. We see from Figure 4-12 that rotational speeds corresponding to the deformation into the oblate spheroid described by curve #2 in Figure 4-11 vary from a fraction of a Hertz to about 100 Hertz for the extreme range of sizes, densities and surface tensions considered.

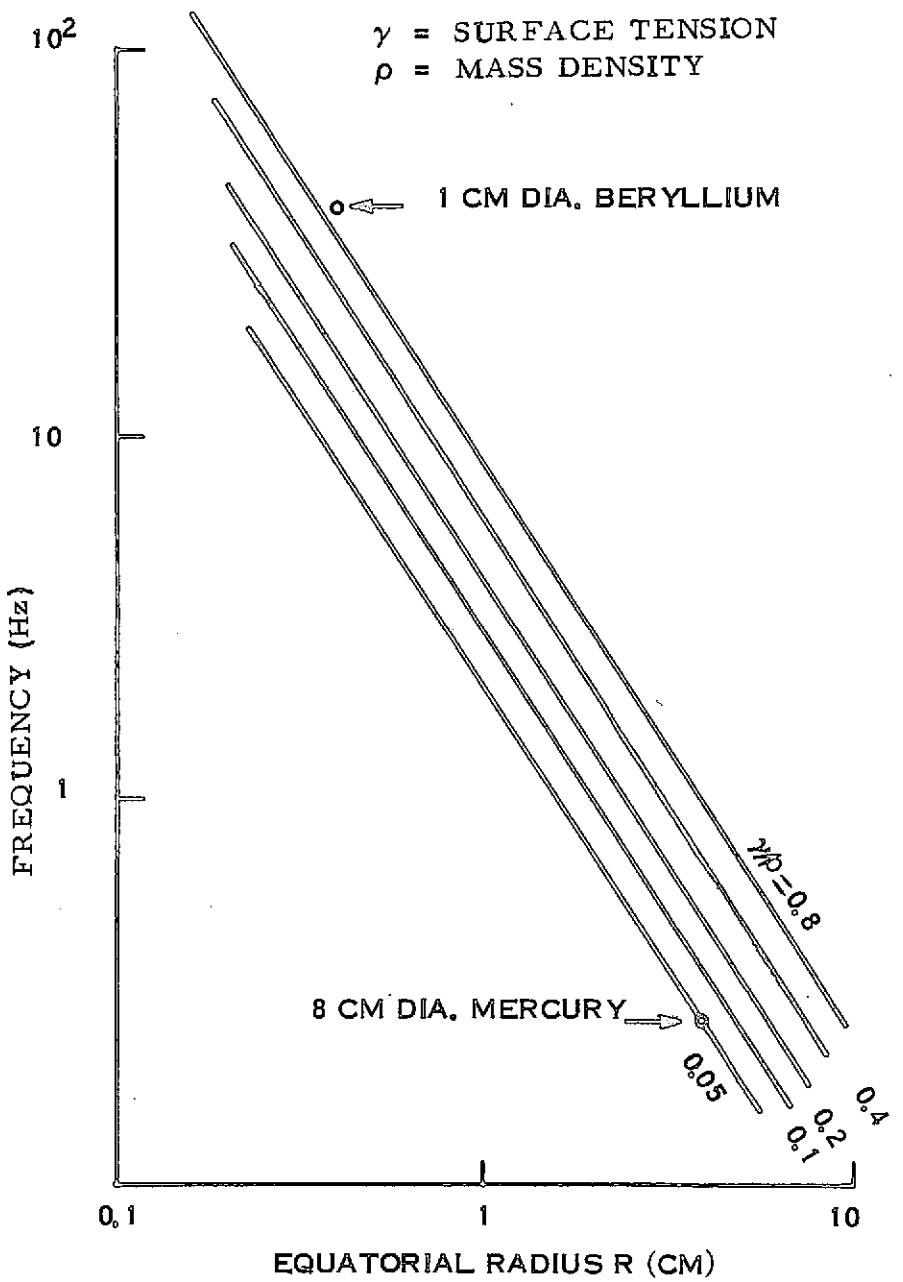

Figure 4-12. Rotational Frequency Required to Achieve 12 Percent Increase in Equatorial Radius ($\Sigma = 1$)
Various Material Properties

4.6.2 MAGNETIC FIELD REQUIREMENTS FOR CONTROLLED SPIN

Since the most desirable type of rotation control would utilize the synchronous motor principle by which the specimen can be brought as near as desired to the synchronous speed by simply waiting long enough and monitoring of rotation speed is not required, this scheme is considered first. The desired rotational speeds are low ($< 10^2$ cycles per second) and the electromagnetic skin depth in even the best conductors will be large compared to the specimen radius. We may thus use a simple expression for the torque q imparted to the specimen by the field of strength B which is rotating at uniform angle of velocity ω. This expression is

$$q = \frac{2\pi}{15} \cdot \frac{\omega-\alpha}{\rho_e} a^5 B^2 \qquad \text{(MKS)} \qquad (4.6.2\text{-}1)$$

where ρ_e is the electrical resistivity, a the radius and α the angular speed of the specimen. The moment of inertia I of a sphere having a mass density ρ is

$$I = \frac{8\pi}{15} \rho a^5 \qquad (4.6.2\text{-}2)$$

The specimen angular acceleration $d\alpha/dt$ is the ratio of torque to moment of inertia q/I.

$$\frac{d}{dt}(\alpha-\omega) = \frac{q}{I}$$

Since the rotational speed ω of the field is assumed constant, we may equally well write

$$\frac{d}{dt}(\alpha-\omega) = \frac{B^2}{4\rho\rho_e}(\omega-\alpha)$$

or

$$\frac{d}{dt}(\alpha-\omega) = -\frac{1}{\tau}(\alpha-\omega) \qquad (4.6.2\text{-}3)$$

where $\tau = \frac{4\rho\rho_e}{B^2}$. The solution is $\alpha - \omega = (\alpha-\omega)_0 e^{-t/\tau}$. The initial value of the difference in angular frequencies $(\alpha-\omega)_0$ can be normally taken to be $-\omega$ (specimen initially at rest). In this case we obtain

$$\alpha = \omega(1-e^{-t/\tau}). \qquad (4.6.2\text{-}4)$$

A reasonable value to assume for rotation speed, α, which will give reasonable centrifugal fields and deformation without approaching the instabilities encountered at higher speeds has already been discussed and illustrated in Figure 4-11. It is interesting to note from Eq. 4.6.2-4 that the time constant for spin-up, τ, does not depend upon the specimen radius, a, under the conditions assumed, but depends only upon the ratio $\rho\rho_e/B^2$. If we consider materials of a given density ρ, the time constant is proportional to ρ_e/B^2. This relationship is shown in Figure 4-13. The values of spin-up time constant for any material of density ρ can be found by interpolation on this graph. For average material densities of several grams per cubic centimeter and assuming a spin-up time constant of hundreds of seconds would be permissible, it may be seen that the required magnetic field intensities vary from 10 gauss or so for good conductors to 1000 gauss for materials with resistivities four decades higher than the good conductors.

If the synchronous type of spin control is abandoned one can get much higher spin-up torques at a given magnetic field strength by causing the magnetic field to rotate at frequencies higher than that desired for the specimen. Eq. 4.6.2-3 shows that the angular acceleration of the specimen will be proportional to the frequency ω at which the magnetic field rotates. We may thus utilize rotating magnetic fields in the kilohertz region using lower intensity fields than required for the synchronous motor approach provided specimen rotational speed is monitored. For spin-up times of the order of many seconds or more, specimen oblateness can be used as a sufficiently accurate gage of the rate of specimen rotation and the spin-up field may then be turned off at the desired speed.

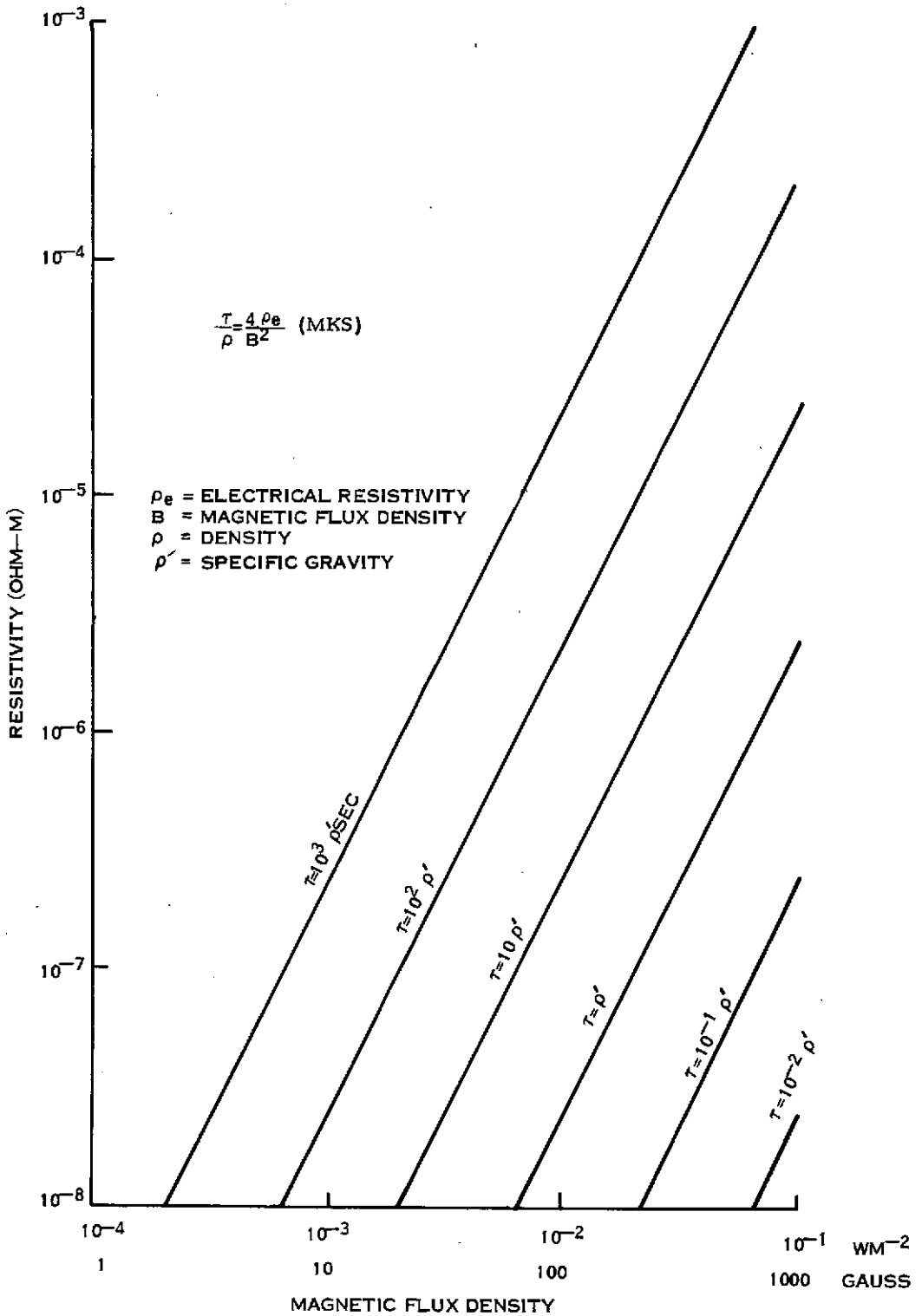

Figure 4-13. Specimen Resistivity vs. Field Strength for Several Values of τ, the e-Folding Time for Spin-up to Synchronous Speed

4.7 POSITIONING FORCE REQUIREMENTS

In this section the requirements for position control forces to be applied to the specimen being processed in the Containerless Facility will be considered. These control forces need be only large enough to overcome residual accelerations of the Space Laboratory facility relative to a coordinate system in free fall and relative to forces on the specimen resulting from electrostatic charges on the specimen, differential outgassing or vaporization from the specimen and forces due to impingement of an electron beam if this heating method is employed. We shall discuss each of these requirements in turn.

4.7.1 RESIDUAL ACCELERATIONS OF THE SPACE LABORATORY FACILITY

Calculations and experience with earth orbiting satellites of long lifetime indicate that accelerations due to atmospheric drag, slow facility rotations and differences in location from the geodesic point in the satellite are on the order of 10^{-4}g or less under normal circumstances. The geodesic point in the satellite lies very close to the center of the mass of the vehicle. It is considered that high rotational velocities of the vehicle will be avoided during operation of the Containerless Processing Facility. The largest accelerations of the facility will be due to astronaut body motions, assuming that pumping of vehicle fluids or operation of thrusters is inhibited during material processing. If we consider the total Space Lab as consisting of a mass M representing the combined mass of all equipment and any astronauts who are relatively quiescent and a second mass m representing an astronaut who has given himself an acceleration $\vec{a}$ relative to the center of mass of the total system M + m, the vehicle and Containerless Processing Facility will undergo an acceleration $\vec{A}$ relative to this combined center of mass given by

$$M\vec{A} = -m\vec{a}. \qquad (4.7.1\text{-}1)$$

A reasonable upper limit for astronaut body acceleration for locomotion is probably of the order of 0.1 g since higher accelerations would correspond to rather violent motions. The total vehicle and equipment mass will exceed the astronaut's mass by more than two orders of magnitude and we can conclude that the resultant facility acceleration $\vec{A}$ will be less than 10^{-3} g. $\vec{A}$ can approach such a value only during the very short time of initiation of astronaut's locomotion maneuvers. When the astronaut reaches his desired location in the vehicle or has otherwise negated his velocity relative to the vehicle, both $\vec{a}$ and $\vec{A}$ will acquire values opposite to those during initiation of the maneuver. A typical time profile of vehicle and facility acceleration due to body motion will thus resemble one of the sketches.

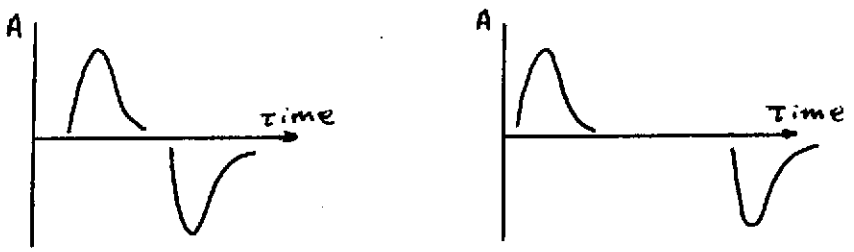

The time between the acceleration pulses in opposite directions will equal the total time during which the astronaut is moving through the vehicle. If the Containerless Processing Facility can provide an acceleration to the specimen as great as 10^{-3} g, the specimen can be moved rigidly with the total facility and undergo an acceleration history just like that shown in the sketches. For this reason provision of an acceleration capability of at least 10^{-3} g has been adopted in later sections of this report. We shall now argue that the provision of even lower accelerations to the specimen would normally be sufficient to prevent contact of the specimen with the positioning coils or other equipment in the facility, provided that an inch or so of free space is provided surrounding the specimen.

Eq. 4.7.1-1 results from the conservation of momentum for the center of mass of the total system M + m. If the displacement of the centers of mass of vehicle and of the astronaut from the combined center of mass are denoted as

$\vec{R}$ and $\vec{r}$ respectively, the definition of the combined center of mass can be written as

$$M\vec{R} + m\vec{r} = 0 \qquad (4.7.1\text{-}2)$$

In fact, Eq. 4.7.1-1 is derived by double time differentiation of Eq. 4.7.1-2. The latter equation shows direction that the maximum excursion $\vec{R}$ of the total vehicle and Containerless Facility relative to a freely falling coordinate system is given by

$$\vec{R} = -\frac{m}{M}\vec{r} \qquad (4.7.1\text{-}3)$$

where $\vec{r}$ is the maximum excursion of the astronaut. For reasonable astronaut excursions within a compartment, $\vec{r}$ will be limited to the order of 100 inches or so. Since the ratio m/M will be less than 10^{-2}, the positioning coil assembly, rigidly mounted to the facility and vehicle could never move by as much as one inch relative to the freely floating specimen in free fall during such a maneuver, even if no position control forces are applied to the specimen. For such large astronaut excursions, several seconds or more would be normally required. If it were desired to correct a resultant one inch position error within a time of, say, five seconds, the required acceleration furnished by the positioning system need only be about 1/5 cm sec^{-2} which is only $2 \cdot 10^{-4}$ g. Thus we see that a position control acceleration as high as 10^{-3}g, which would cause the specimen to partake of the facility accelerations as if it were rigidly attached, may be conservative.

4.7.2 ELECTROSTATIC FORCES

The largest electrostatic potential which the specimen may acquire will probably be due to bombardment by an electron beam if this heating method is employed. Assuming the specimen to be surrounded by conducting materials at a potential near ground such as not to cause additional electric fields within

the processing chamber, electrostatic forces will be exerted upon the specimen resulting from induced image charges in the surrounding conductors induced by the specimen's charge. To the extent that the surrounding conducting materials are symmetrical with respect to the specimen, no net force would result. However, if one assumes asymmetries in the disposition of this material and assumes, as an extreme case, that the charged specimen is located within a few centimeters, 5 centimeters for example, of a grounded conducting plane lying entirely on one side of the specimen then an image charge will be induced in the grounded conductors whose effective distance from the specimen is ten centimeters.

Consider now the magnitude of the charge on the specimen and the equal charge represented by the image. In Section 4.2.2 it was pointed out that the net electron current to the specimen must vanish at specimen potentials of no more than a few tens of volts relative to the surrounding space charge. If this surrounding space charge is limited to a few tens of volts potential by provision of suitable grounded conductors, then the potential of the specimen relative to the grounded plane will not exceed a few tens of volts. In electrostatic units, in which the capacitance of the conducting sphere is equal to its radius in centimeters, the electrostatic charge on a specimen of 1.0 cm radius will equal its potential in e.s.u. Since one e.s.u. of potential corresponds to 300 volts, if specimen potential is 30 volts, the consequent charge will thus be on the order of only 0.1 e.s.u. The electrostatic force between the specimen charge Q and the image charge Q' is given in dynes by

$$F = QQ'/R^2 \qquad (4.7.2\text{-}1)$$

where R is the separation between specimen and image. Assuming the values for these parameters previously discussed, the force would be $F = 0.1 \times 0.1/10^2$ or 10^{-4} dyne.

If, as another extreme case, a specimen radius of four centimeters is assumed, the product of charges QQ' would go up by a factor 16, but in this case the separation R would be greater in the same proportion assuming the entire facility is scaled up equally, leaving the force unchanged at 10^{-4} dyne. The electrostatic forces will be very low relative to one dyne. With the geometrical factors discussed here, it would require a specimen potential about 100 times greater than the 30 volts to produce an electrostatic force of one dyne. Potentials of three kilovolts could never be attained with the type of electron beam operation outlined in Section 4.2.2 above.

4.8 REFERENCES

4-1 Free Suspension Processing Systems for Space Manufacturing, General Electric Company, Contract NAS 8-26157, Final Report, June 15, 1971.

4-2 Smythe, W. R., Static and Dynamic Electricity, McGraw-Hill, New York, 1950.

4.3 Fromm, E. and Jehn, H., "Electromagnetic Forces and Power Absorption in Levitation Melting," Brit. J. Appl. Phys., 16, 653, 1965.

4-4 Wang, T. G., "Acoustic Positioning Chamber," to be presented at the Third Space Processing Symposium at the George C. Marshall Space Flight Center, 1974.

4-5 Whymark, R. R., "Acoustic Field Positioning for Containerless Processing," to be presented at the Third Space Processing Symposium at the George C. Marshall Space Flight Center, 1974.

4-6 Stephan, H. and Leybold, H., "Theory and Principles of Electron Beam Melting and Vapor Deposition Equipment and Practices," Electron Beam Metallurgical Processing Seminar, Universal Technology Corp., Dayton, Ohio, February 1971.

4-7 Dekker, A. J., "Secondary Electron Emission," Solid State Physics, 6, Academic Press, 1958.

4-8 Dobretsov, L. N. and Gomayukova, M. V., "Emission Electronics," Israel Program for Scientific Translations, Jerusalem, 1971.

4-9 Neumann, Leo and Huggins, Robert A., "Technique for the Zone Melting of Insulators," Rev. of Sci. Instr., 33, No. 4, April, 1962.

4-10 Steinherz, H. A., Handbook of High Vacuum Engineering, Reinhold Pub. Corp., 1963.

4-11 Machlin, I., Begley, R. J. and Weisert, E. D., Refractory Metal Alloys, Metallurgy and Technology, Plenum Press, N.Y., 1968.

4-12 Bunshah, R. F., Vacuum Metallurgy, Reinhold Pub. Corp., N.Y., 1958.

4-13 Happe, R. A., "Possibilities for Producing New Glasses in Space," Space Processing and Manufacturing, NASA Pub. ME-69-1, 1969.

4-14 Fast, J. D., Interaction of Metals and Gases, 1, Academic Press, New York and London, 1965.

4-15 Lamb, Horace, Hydrodynamics, Dover Pub., N.Y., 1945, Chapter XII.

4-16 Chandrasekhar, S., "The Stability of a Rotating Liquid Drop," Proceedings of the Royal Society, Series A, 286, p. 1, 1965.

SECTION 5

GENERAL FACILITY REQUIREMENTS AND TRADE-OFF STUDIES FOR OPTIMUM FACILITY

5.1 FORCE REQUIREMENTS AND CALCULATIONAL METHODS

5.1.1 INTRODUCTION

The purpose of this section is to outline other requirements for the electromagnetic Containerless Processing Facility in addition to those for heating, melting and rotation discussed in Section 4. Perhaps the most important additional requirement is the sensing and controlling of specimen position errors to ensure that the specimen does not contact surrounding objects. Typical motivations here are the avoidance of specimen contamination or achievement of significant undercooling by avoidance of nucleation induced by such contact. Numerous analyses of electromagnetic field configurations for terrestrial levitation can be found in the literature. (Ref. 5-1, 5-2, 5-3, 5-4) In zero-g, these fields must provide for three dimensional containment in the absence of any weight, for small forces for position correction and for damping of position oscillations. A study has been carried out and described in Section 5.2 below of a wide variety of field producing coil arrangements for these purposes.

5.1.2 POSITION CONTROL FORCES - COMPUTATION METHODS

The basic mechanism for the provision of a translational force upon an electrically isolated conducting object by means of an applied alternating electromagnetic field is the following. The applied alternating magnetic field induces circulating eddy currents in the specimen. Between these induced currents and the applied magnetic field there are Lorentz magnetic forces. In the case of a uniform applied field these forces will balance out to zero by symmetry. However, if the applied field is nonuniform, there will be a net translational force on the specimen. The most accurate way to solve the problem is to calculate the eddy current distribution within the specimen which satisfies the appropriate

boundary conditions, to compute the distributed electromagnetic forces $\vec{j} \times \vec{B}$ and then integrate over the specimen volume. This problem is tractable for certain simple geometries such as a spherical specimen and an applied field having axial symmetry. Some such calculations are reported in the following sections. For a general conceptual facility study as reported here, however, it is more appropriate to utilize a simpler theoretical approach which allows a rapid comparison amongst various coil and field configurations for screening purposes. Such an approach is allowable as long as the differences among the various configurations considered are greater than the errors incurred in use of the approximation. Thus in the sections which follow, the simple formulae derived by Smythe (Ref. 5-1) and Okress (Ref. 5-2) are utilized for the initial screening and elimination of many non-optimum coil types. Subsequent computations to evaluate the forces more accurately are used when studies or comparisons are made amongst the final candidate systems. We shall first review the simplest approach to the computation of specimen translational force and apply this to some of the simplest coil geometries.

5.1.3 APPROXIMATE FORMULA FOR TRANSLATIONAL FORCE ON SPECIMEN

The problem of a spherical conductor immersed in an alternating uniform magnetic field was solved by Smythe (Ref. 5-1). He considered the distribution of induced eddy currents within the spherical body which satisfy the boundary conditions both at infinity and on the spherical surface, and derived the induced magnetic dipole moment. Okress (Ref. 5-2) applied these formulae to the calculation of the net forces exerted upon the induced current system for problems of interest in terrestrial levitation experiments. This work used the approximation that the applied field is sufficiently uniform that, before introduction of the spherical specimen, the variation in applied field over the volume to be occupied by the specimen is small compared to its average value within the specimen. The resulting formula for the force acting on the specimen is

$$F = \frac{-10^7}{4} a^3 \, G(x) \, \text{grad} \, B^2 \qquad \text{(MKS units)} \qquad (5.1.3\text{-}1)$$

where a is the specimen radius, B is the value of the applied flux density in webers m^{-2} before introduction of the specimen and G(x) is a function of a parameter x, defined as the ratio of spherical specimen radius a to electromagnetic skin depth within the specimen. The skin depth is a function of the electrical resistivity of the specimen and the frequency of the applied field. For the applications discussed in this report the magnetic permeability of the specimen is assumed to be approximately unity. Graphs of skin depth as a function of resistivity and frequency are given in Section 4.1.

Since meter-kilogram-seconds (MKS) and (CGS)-gauss units are used without prejudice in this report, we give here the equivalent force formula in the latter units.

$$F = -\frac{a^3}{4} G(x) \text{ grad } B^2 \qquad \text{(CGS)} \qquad (5.1.3\text{-}2)$$

Here a is measured in centimeters, B in gauss (10^4 gauss = 1 weber m^{-2}) and the force in dynes. The reason for the occasional use of the latter units is that many existing magnetic field programs were already available at the beginning of this study which utilized gauss units. In addition, the sizes of specimens considered are normally such that specimen dimensions are on the order of centimeters rather than meters which makes the CGS-gauss units rather convenient. A plot of the function G(x) is shown as Figure 5-1. For large x (skin depth short as compared to specimen radius) the function G(x) approaches unity. This is the normal mode of operation for the facility discussed at the end of this report. For decreasing x the forces achievable with reasonable power levels drop precipitiously.

In CGS-gauss units the magnetic flux density B and the magnetic intensity H become identical for a medium such as air for which the relative magnetic permeability is unity. Thus formula (5.1.3-2) above in CGS-gauss units can equally well be written

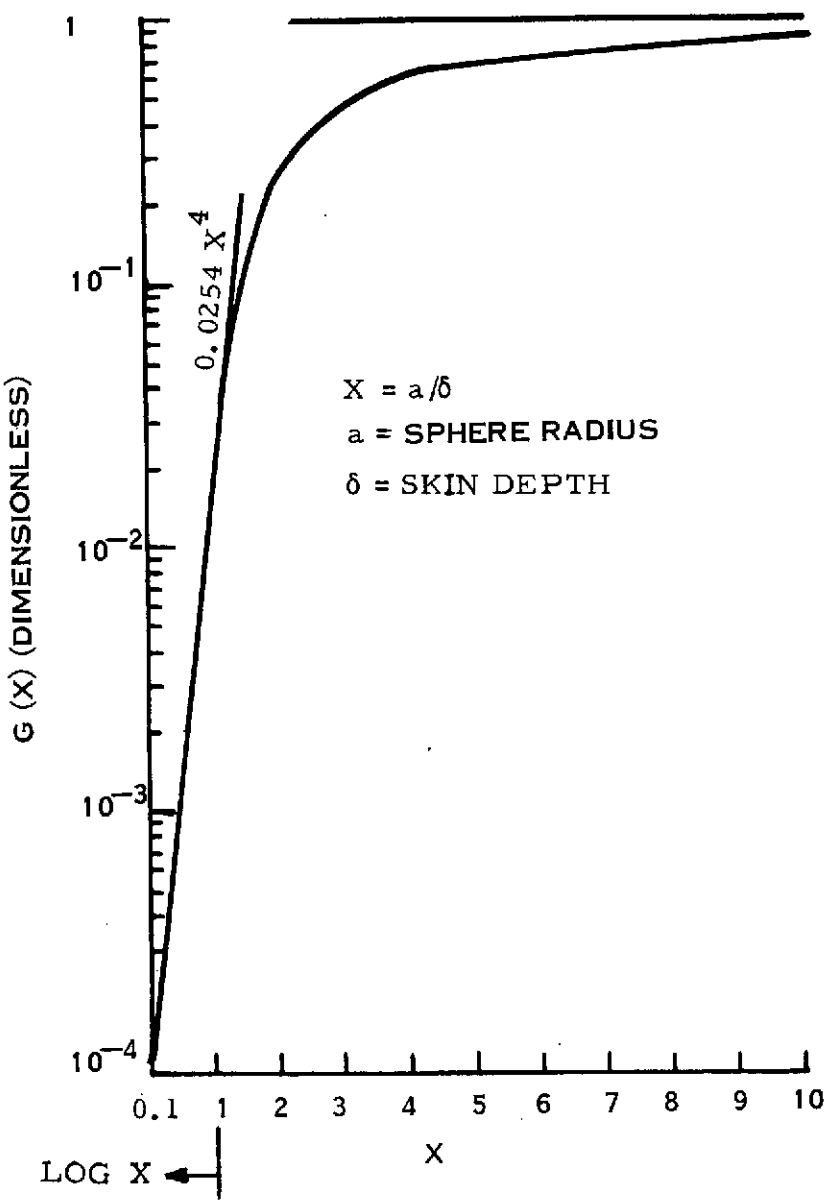

Figure 5-1. Body Force Function

$$F = -\frac{a^3}{4} G(x) \text{ grad } H^2 \qquad \text{(gauss-CGS units)} \qquad (5.1.3\text{-}3)$$

where H is the applied field intensity measured in oersteds. Thus B and H can be used interchangeably whenever gauss units are used. When using the MKS formula the constant of proportionality in the force formula will be different according to whether the force is considered proportional to grad B^2 or grad H^2.

The equation 5.1.3-1 involves an inconsistency in that the dipole moment is calculated on the basis of a uniform applied field which later is assumed to have a gradient in order that it be able to exert a force on the specimen. The error involved in this approximation is small provided the specimen does not approach too closely to the field producing windings or if magnetic fields having a cusp-like node within the specimen volume are avoided. As discussed below, however, one of the coil configurations showing the most favorable overall characteristics for the Electromagnetic Containerless Facility is just such a configuration. More exact computations were carried out for this case. The approximations were also tested for other cases of interest to determine the errors incurred by use of the simple formula. Two types of more exact computations were utilized. The first involved a computation of the actual Lorentz forces acting on each of 20 discs into which the spherical specimen was divided. The large x (small skin depth) regime was considered and the 20 self-consistent loop currents in each disc were calculated which satisfied the boundary condition that the magnetic field just exterior to the spherical surface would be parallel to that surface. Individual forces on each eddy current loop were then calculated and summed. Results of these calculations are given in following sections where appropriate. A second method was to use the simple formula 5.1.3-2, but to compute grad B^2 on the basis of the applied field B^2 averaged over the specimen volume. This approximation, for the circular coil, yielded forces which agreed better with the more exact 20 segment calculations and with experiment than those computed from the simple formula with B evaluated at the specimen center.

In the cusp coil, for which the simple formula would be expected to break down badly near the cusp region of the field, the use of the volume average B^2 values gave reasonably good agreement with the 20 segment method. Agreement with experiment was less good, this being attributed to dimensional uncertainties and approximations used to represent the experimental coils that were used in the laboratory.

5.2 SELECTION OF MAGNETIC FIELD CONFIGURATION

With each coil type, studies were done where appropriate to find that set of coil parameters representing an optimum. Comparisons were then made among these optima for various coil types based on several criteria applying to the achievable translational forces for a given expenditure of electrical power. The coil types were also compared on the basis of efficiency for electromagnetic induction heating since, as discussed in Section 4.3.1 above, this represents probably the most efficient heating method to be considered in those cases where electron beam heating is inappropriate. Induction heating will represent, for initial Space Lab experiments, a heating method easier to implement than radiant heating or solar heating through the use of large sun-oriented flux-collecting mirrors. The latter approach will almost certainly be considered for large manufacturing facilities but will require constraints to be placed upon the orientation and possibly orbit parameters of the space facility.

As the study proceeded, it became clear that some of the coil configurations thought to be distinct candidates could alternately be considered as variants upon the same basic topological configuration. For example, the Alice coil can be considered as the simplest Joffe bar configuration in which account is taken of two single end loops serving as mirrors for the quadruple bars (See Figure 5-2). In fact, this realization historically led to the evolution of the Alice system from the original Joffe configuration. Likewise, the member of the baseball family in which the coil loops lie in orthogonal planes closely resembles the Alice configuration and its properties are not greatly changed by the rounding of the

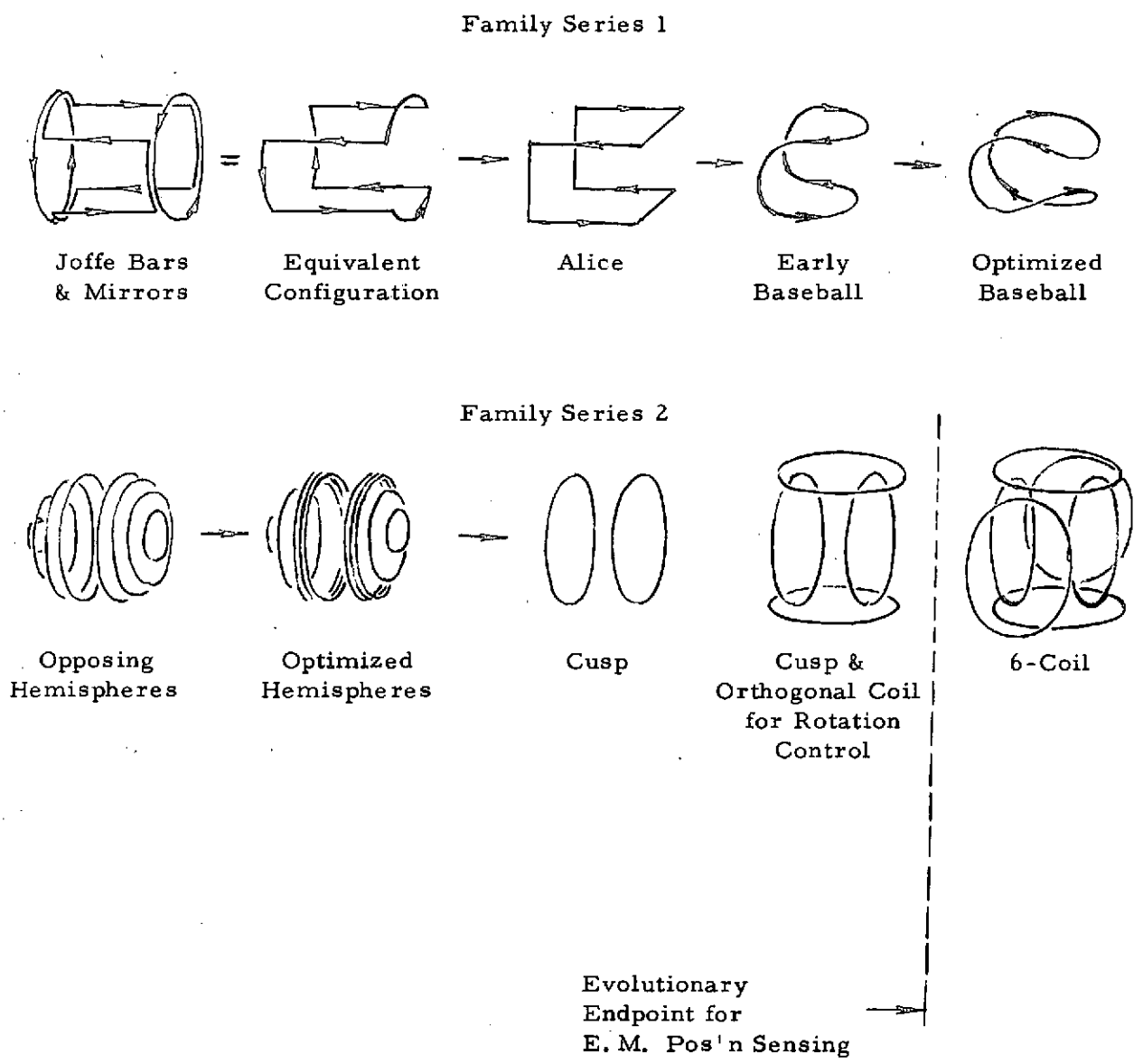

Figure 5-2. Family Relationships Amongst Various Coil Types

corners of the Alice cube. Detailed studies carried out on optimizing coil plane angles in the baseball family thus represent what can be considered the final evolutionary stage in a whole series which included several other coil types.

Similar detailed studies of the opposing hemisphere coil configuration showed an optimum consisting of three contiguous turns near the equator of each hemisphere with the remaining turns greatly reduced in influence. It was later found that operating the coil pair in phase opposition (the so-called cusp configuration) gave, when optimized, symmetrical force fields, reasonable RF heating efficiency and permitted elimination of the coil turns of smaller diameter on the hemispherical surface. This simplification of coil geometry provides the great advantage of greater accessibility to the specimen position for injection or ejection into, or out of, the coil.

A third example of the "dequantization" of formerly discrete, qualitatively different systems through discovery of intermediate cases resembling a continuum is related to the cusp and 6-coil configurations. The cusp, when it is considered in a system which can provide rotation control, must be used in conjunction with a second orthogonal system. If this second coil system is chosen to be a second pair of opposing coils, the resulting configuration resembles very closely the original 4-coil mock-up of the 6-coil system which was used in this laboratory to demonstrate position control and damping in a horizontal plane for a specimen suspended on a long pendulum. In a sense, it may be said that it has been learned how to achieve both three axis position and rotation control about a single axis with only four coils of the 6-coil system.

Although there are probably other equally valid alternate ways to consider the comparisons among coil types, in the present study the sense of an evolutionary development proceeding on detailed numerical studies of each coil type has been very strong. The conclusions of the present study as discussed in the

following sections indicate that the baseball and cusp systems appear optimum for consideration in the earliest Space Laboratory Containerless Processing Facility. This conclusion is based upon considering a number of engineering factors discussed in detail below. The 6-coil system might be considered for pilot plant or manufacturing facilities in the event that spin control about all three axes is required for certain special processes or if electromagnetic specimen translation into or out of the facility in various directions is required. It suffers, however, in terms of overall system complexity and requires, at this stage of technology, electro-optical position sensing because the provision of electromagnetic position sensing is difficult in such a complex coil configuration.

5.2.1 MAGNETIC FLUX DENSITY FOR CIRCULAR COIL

Because of its importance as an element in several coil configurations, special attention is first given to the simple circular coil. In arrangements in which several separate circular windings (e.g., cube, tetrahedron, opposing hemispheres) are operated at discrete frequencies, it may be shown that the time averages of the squared field intensity, $\overline{B^2}$, add linearly for the combination of the separate coils. This is also true for grad B^2. Thus the calculations shown in this section will be used later to construct force fields for some of these other more complicated coil configurations which are composed of circular coils.

Smythe (Ref. 5-1, p. 270) gives the flux density anywhere for a circular coil in terms of an axial component, B_z, and a radial component, B_r, expressed as functions of complete elliptic integrals.

$$B_z = \frac{\mu I}{2\pi} \cdot \frac{1}{\left[(R+r)^2+z^2\right]^{1/2}} \left[K + \frac{R^2-r^2-z^2}{(a-r)^2+z^2} E\right] \qquad (5.2.1\text{-}1)$$

$$B_r = \frac{\mu I}{2\pi} \cdot \frac{z}{r\left[(R+r)^2+z^2\right]^{1/2}} \left[-K + \frac{R^2+r^2+z^2}{(R-r)^2+z^2} E\right] \qquad (5.2.1\text{-}2)$$

B_z and B_r are in webers/meter^2, K & E are the dimensionless complete elliptic integrals as tabulated by Peirce (Ref. 5-5, p. 121), μ is the permeability of free space, $4\pi \times 10^{-7}$ henry/meter, I is the current in amperes, R, z and r are the radius of the coil, axial distance from the coil, radial distance from the axis, respectively, all in meters. (The factor $\mu I/2\pi$ is equal to 2×10^{-7} weber/meter for I = 1 ampere, and 1 weber/meter^2 is equal to 10^4 gauss.)

The results of the use of these equations are given in Figures 5-3 and 5-4. Figure 5-3 gives grad$\left(\frac{B}{NI}\right)^2$ as well as the direction of grad$\left(\frac{B}{NI}\right)^2$; Figure 5-4 gives lines of equal $\left(\frac{B}{NI}\right)^2$ as contour lines on an r vs. z grid.

5.2.2 FORCE MEASUREMENTS AND CALCULATIONS FOR A 3-TURN CIRCULAR COIL

In order to test the validity of the several computational procedures for total body force, these were applied to circular geometry force measurements carried out in the laboratory. The coil consisted of three turns of one-quarter inch diameter copper tubing 5.5 cm in diameter. A solid aluminum sphere 2.54 cm diameter was used as a test body. The coil was mounted with its axis of symmetry in the vertical direction and mounted upon a positioning device which permitted the coil to be raised or lowered. The solid aluminum sphere, mounted upon a non-conducting, counterbalanced arm which hung from a balance, as shown in Figure 5-5, was positioned on the axis of the three turn coil. The distance between the coil and sphere was measured with the aid of a telescope 170 cm from the sphere. The circuit of Figure 5-6 was used to cause an alternating current (frequency $\simeq$ 100 KHz) of 50.5 amp rms to flow in the coil and the balance was used to measure the force exerted upon the sphere. The accuracy of each individual force measurement for this experiment is estimated

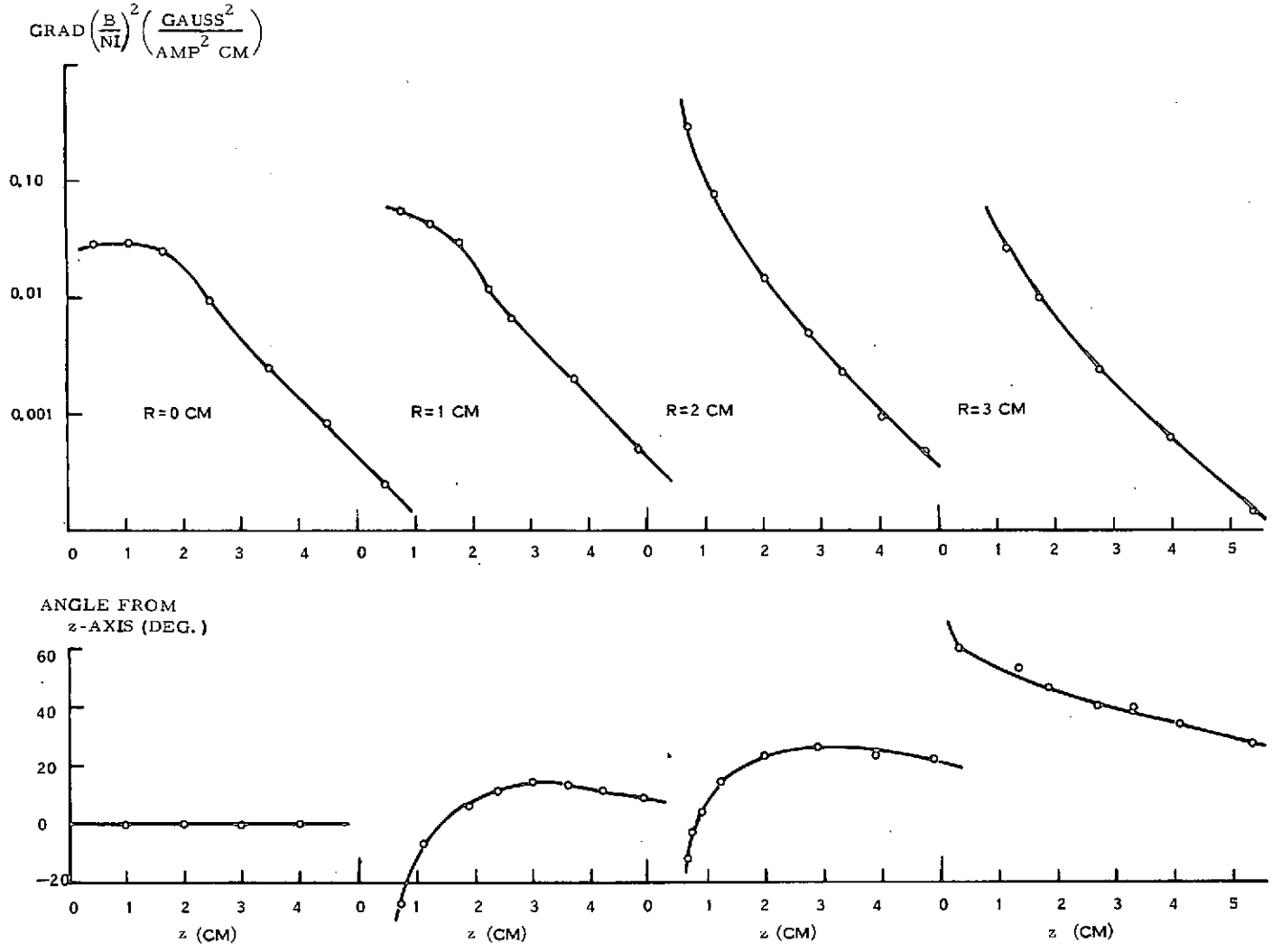

Figure 5-3. Magnitude and Direction of Gradient of Flux Density Squared for Circular Coil

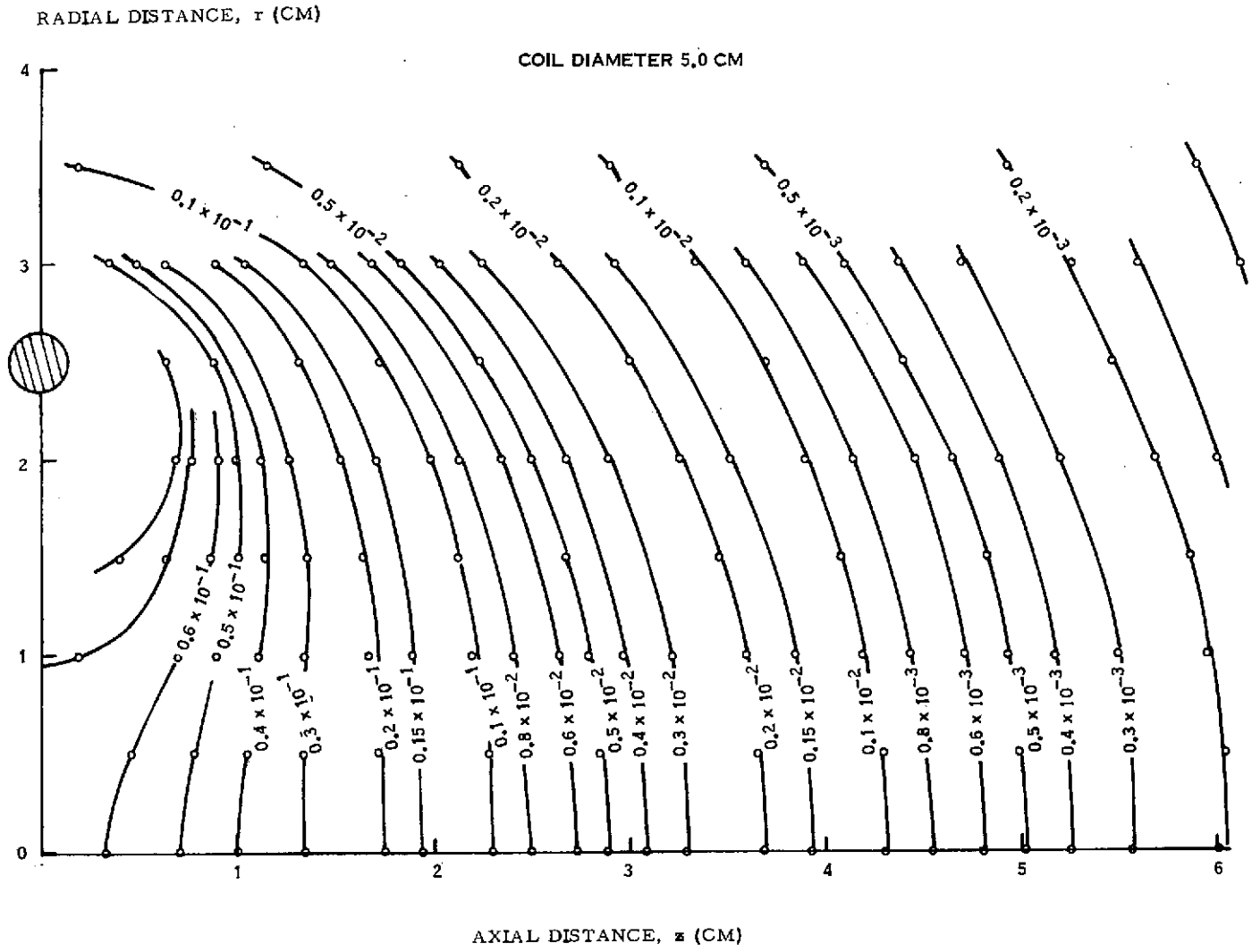

Figure 5-4. $\left(\frac{B}{NI}\right)^2$ for Circular Coil
(Contours are labeled in gauss^2/amp^2)

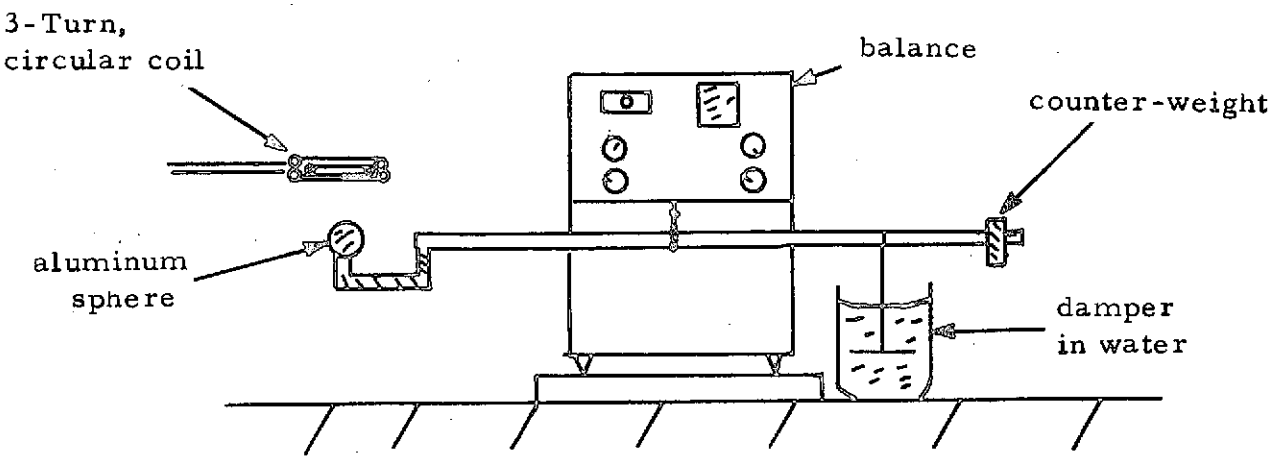

Figure 5-5. Apparatus for Force Measurement

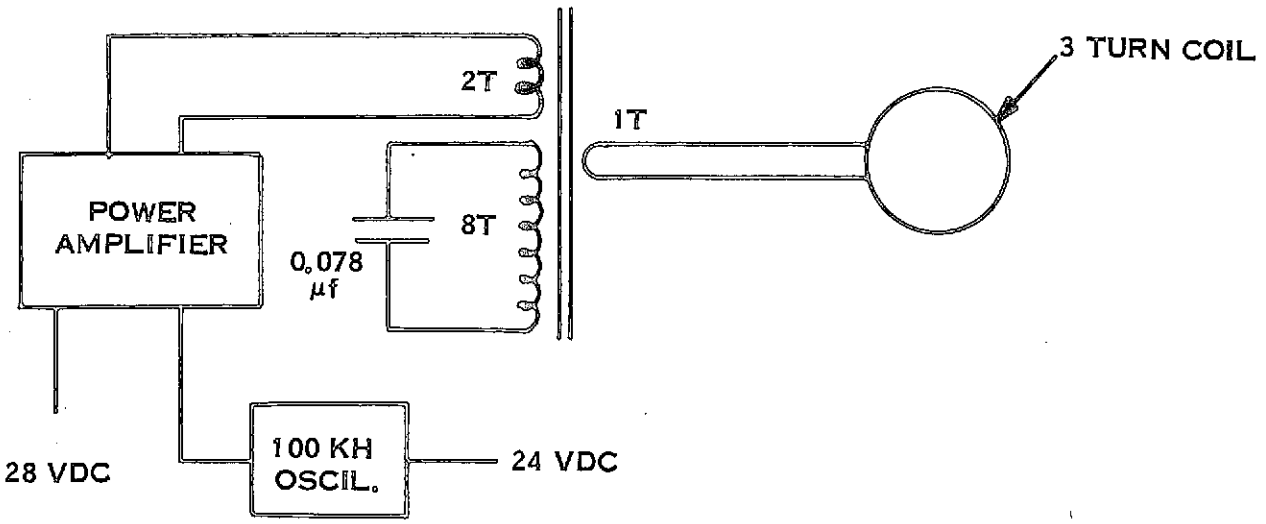

Figure 5-6. Circuit for Excitation of Three-Turn Coil

to be ± 0.001 gram or ± 1 dyne. The forces measured, plotted in Figure 5-7, ranged from 13 to 239 dynes.

The computer program which sums the individual forces on each of 20 planar discs into which the sphere was conceptually divided had previously yielded results for a 5.0 cm diameter coil carrying a current of 100 amperes exerting a force on an aluminum sphere of 2.5 cm diameter. These results were multiplied by $3^2\left(\frac{50.5}{100}\right)^2\left(\frac{5.0}{5.5}\right)^3 = 1.7$, to account for the actual use of a 3 turn coil of 5.5 cm diameter carrying 50.5 amp and are plotted in Figure 5-7 with the distance from the coil = 1.1 x (distance in calculation) to account for use of a 5.5 cm diameter coil. We note that there is excellent agreement between the measured forces and those calculated on the basis of the 20 disc eddy current ring model over most of the range but that there is a noticeable discrepancy as the sphere approaches close to the coil plane. These differences are attributed to dimensional uncertainties arising from the representation of the current flowing in the three windings of the coil by a single filamentary winding in the computational model. (See Section 5.2.9.1 for discussion of the filamentary approximation.) It should be noted, however, that the region of good agreement between the theory and measurements is just that region which will be considered as the confinement region for specimens in practical coil systems; close approach of the specimen to the coils would be avoided in most practical facility arrangements.

Since it is expected from the simple force model that the force will be proportional to a^3 G(x) grad B^2, it is of interest to compute the ratio $F/a^3 G(x)$ grad B^2 from the measured values of F and to compare to the ratio 0.25 predicted by the simple force model. The values of this ratio using the measured force values given in Figure 5-7 and the conveniently available calculated values of B^2 are shown as the hexagonal points in Figure 5-8. Here the values of B^2 are taken corresponding to the central position of the spherical specimen volume. The ratio approaches a constant of about 0.28 using this procedure.

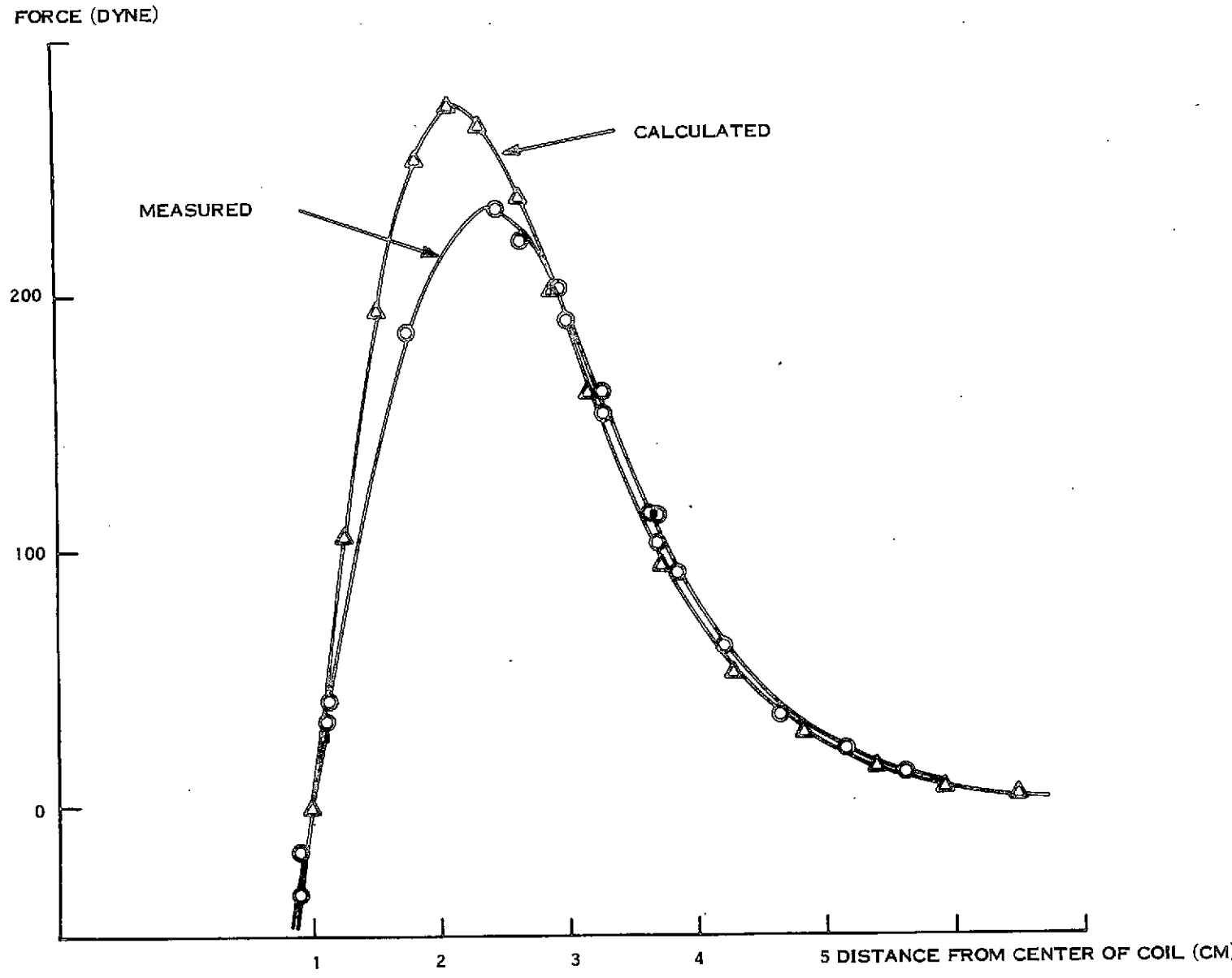

Figure 5-7. Force Exerted Upon a 2.54 cm Diameter Solid Aluminum Sphere by a 5.5 cm Diameter 3-Turn Circular Coil Carry 50.5 amp (rms), f = 100 KHz

The procedure used for most of the coil comparisons carried out during the study was next tested. This consists of averaging the values B^2 over the spherical specimen volume before calculating grad B^2. This procedure yields the points shown as triangles in Figure 5-8. We see that the ratio is quite accurately 0.25 if we avoid positions too close to the coil winding. It may be concluded that the use of the simple formula $F = 0.25\ a^3 G(x)$ grad B^2, where B^2 is evaluated as an average over specimen volume, is to be preferred over the use of the simple formula without averaging. In fact, for this particular case, the averaging procedure yields results equally as good as the 20 disc model.

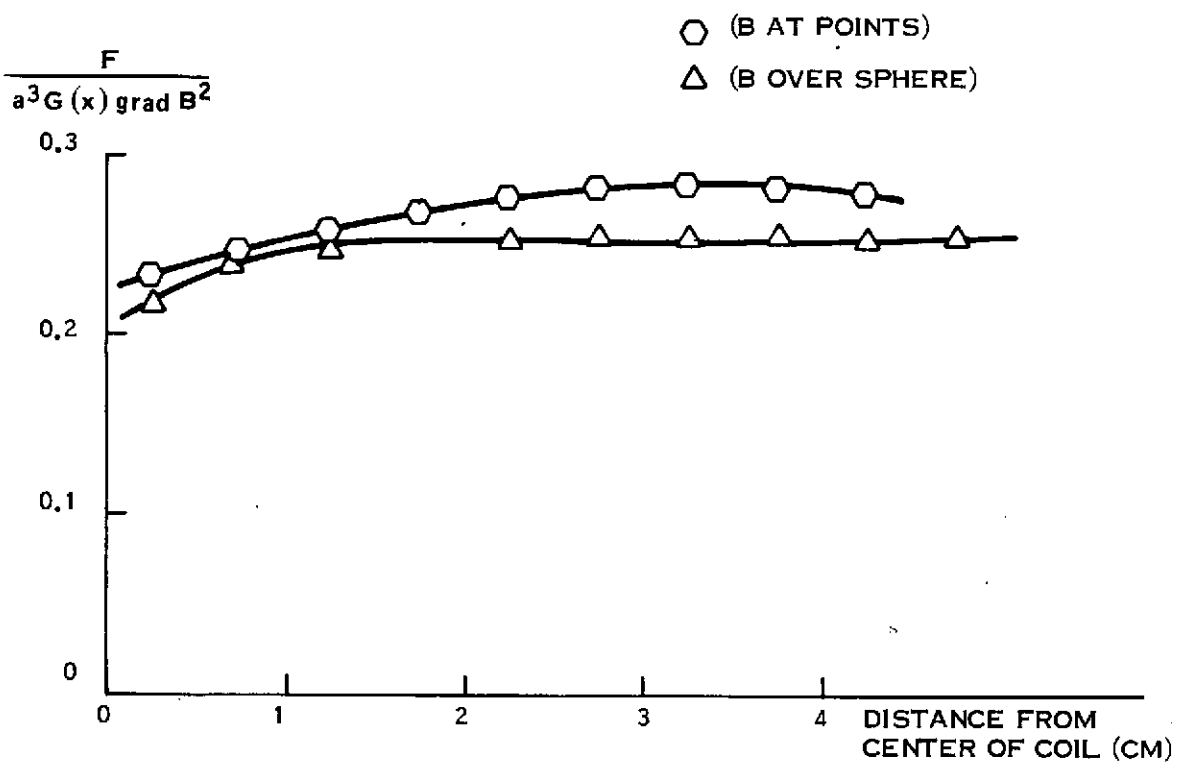

Figure 5-8. $F/a^3 G(x)$ grad B^2 (dimensionless) vs. Distance

An attempt was made to evaluate B^2 and its gradient by use of a search coil whose plane was parallel to the axis of the field producing coil. The search coil effectively averaged the field over the area enclosed by its winding which was

2.54 cm in diameter. This average can be considered an average over the equator plane of the spherical specimen which was used in the test. It was found that these measured averages gave predicted forces low by almost a factor 2 for specimen positions close to the coil and high by approximately 25 percent far from the coil when these planar average fields were introduced into the simple force formula. From this it is concluded that the type of field averaging carried out is important, a volume average apparently being appropriate, as would be expected from consideration of the energy density $B^2/8\pi$ in the magnetic field.

5.2.3 FORCE CALCULATIONS FOR CUBE AND TETRAHEDRON ARRANGEMENTS OF CIRCULAR COILS

If it is assumed that there are no large effects due to mutual inductances among the several coils in an array of circular coils, the data given in Section 5.2.1 can be used to calculate the $\text{grad}\left(\frac{B}{NI}\right)^2$ at any location within such an array. This has been done for certain directions for four such systems; two are the cube and tetrahedron systems studied previously in this laboratory in which the radius of the spherical volume enclosed by the coils is equal to twice the radius of each coil; the other two are the cube and tetrahedron systems in which the radius of the spherical volume enclosed by the coils is equal to one-half the radius of each coil. The latter arrangement will be referred to as an "overlap" configuration due to the fact that windings of the coils must cross windings of other coils in the configuration.

The reason for the sharp division in values of the parameter defined as the ratio,

$$\frac{\text{spherical volume radius}}{\text{coil radius}}$$

into ranges near two or one-half is the desire to avoid values of this parameter near unity. A coil radius nearly equal to the radius of the sphere on which the coils are circumscribed would lead to very large mutual inductances between coil pairs. Laboratory studies had previously indicated engineering complications

in operation of such a highly inductively coupled system. Experiments had indicated that the mutual inductance effects were tolerable when the coil radius did not greatly exceed 1/2 the radius of the sphere to which the coil planes are tangent. Since it is known that these mutual inductances would also be small if the coils are large enough so as to cross nearly at right angles, this latter configuration, known as the "overlap" configuration was also studied. As will be seen from the data below, however, the overlap configurations must be rejected on grounds of unsuitability of the force fields which they produce.

The component of the total force directed inward along three axes of symmetry was calculated for each of these systems by calculating the angle such an axis forms with the z-axis in Figure 5-3, drawing the axis on that figure and finding both $\text{grad}\left(\frac{B}{NI}\right)^2$ and its direction at several points along that axis. These three axes are

a. Axis of a single circular coil

b. Axis of symmetry between two adjacent coils (angle for cube is 45°; for tetrahedron 54.8°)

c. Axis of symmetry among three adjacent coils (angle for cube is 54.7°; for tetrahedron 70.8°).

These data are plotted for an enclosed spherical volume of diameter 5.0 cm in Figure 5-9 for the cubical coil arrangement with coil radius equal to one-half of the enclosed sphere radius. Because of the existence of gradients within the specimen volume, these calculated values of force for a conducting sphere of any appreciable size (such as a 1 cm diameter sphere in a 5 cm diameter volume) are expected to be somewhat smaller than the actual forces.

Figure 5-10 shows corresponding results for the "overlap" cubical arrangement for which the coil radius is twice the sphere radius. The corresponding data for the "normal" and "overlap" tetrahedronal systems are shown in Figures 5-11 and 5-12. Inspection of Figure 5-11 indicates that the forces available on a

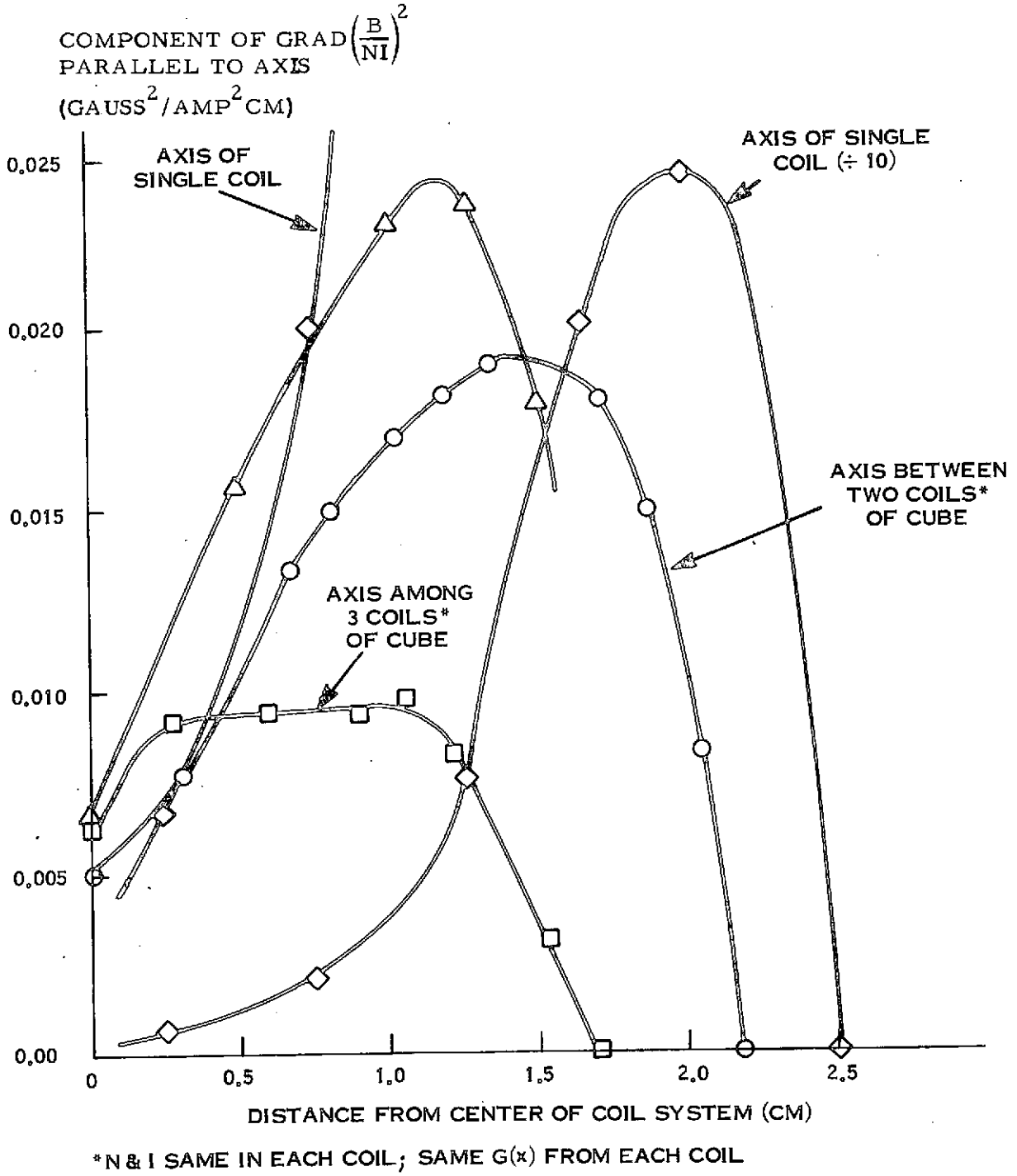

Figure 5-9. Calculated Force Along Axes of Symmetry for Cube with Coils of Radius 1.25 cm, a Distance 2.5 cm from the Center of the Coil System

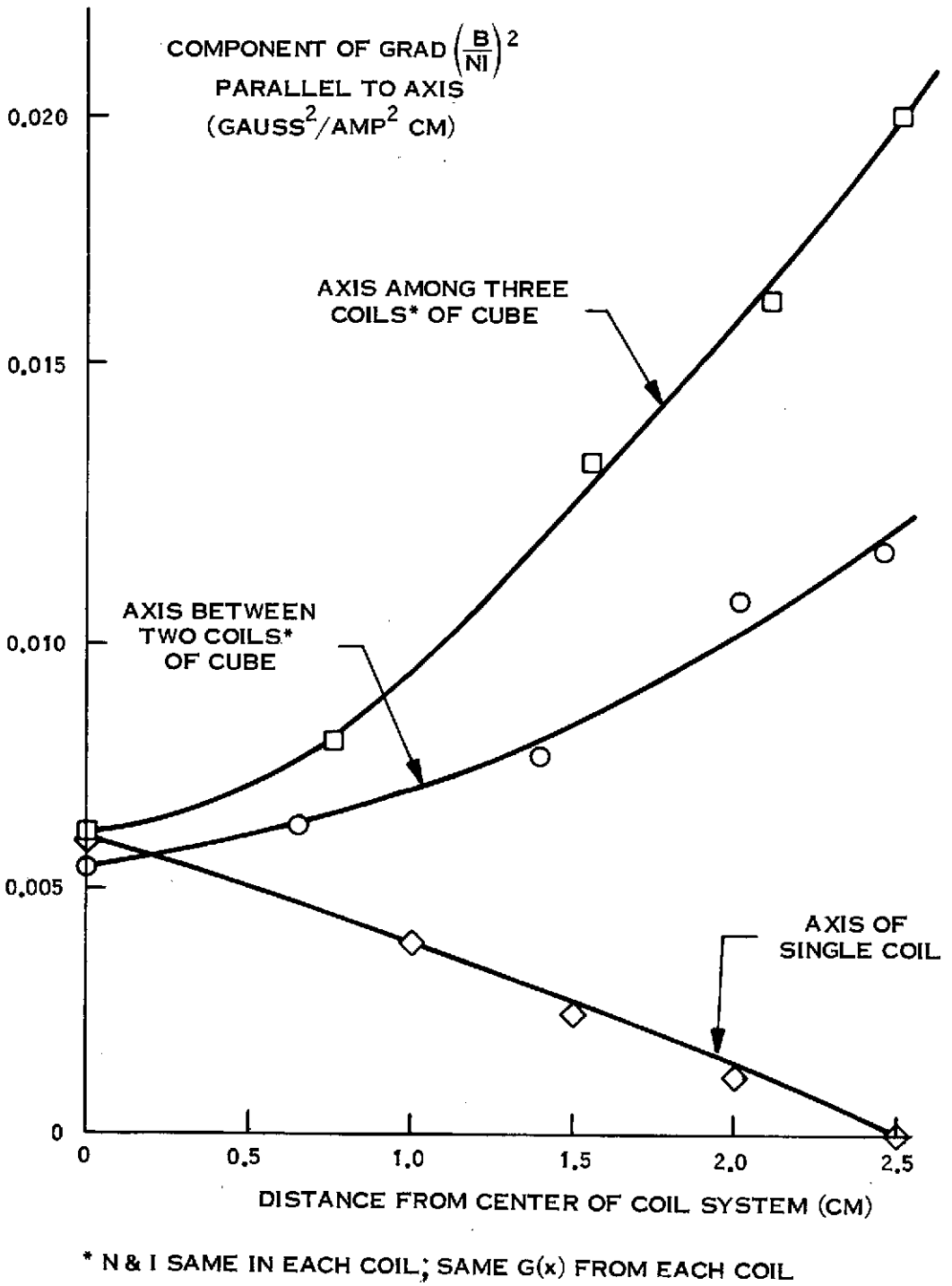

Figure 5-10. Calculated Force Along Axes of Symmetry for Cube with Coils of Radius 5.0 cm, a Distance 2.5 cm from the Center of the Coil System

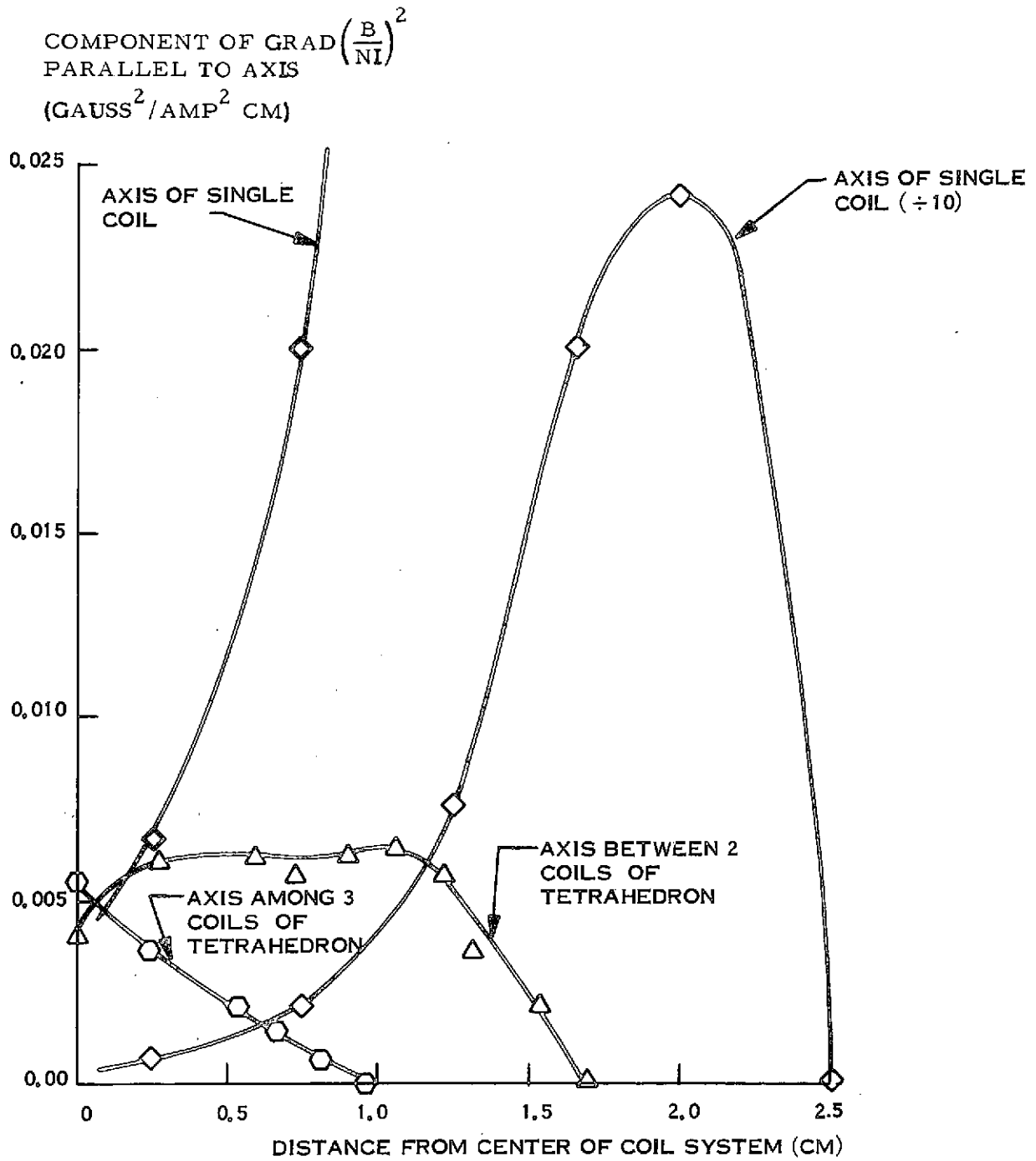

Figure 5-11. Calculated Force Along Axes of Symmetry for Tetrahedron with Coils of Radius 2.5 cm, a Distance 2.5 cm from the Center of the Coil System

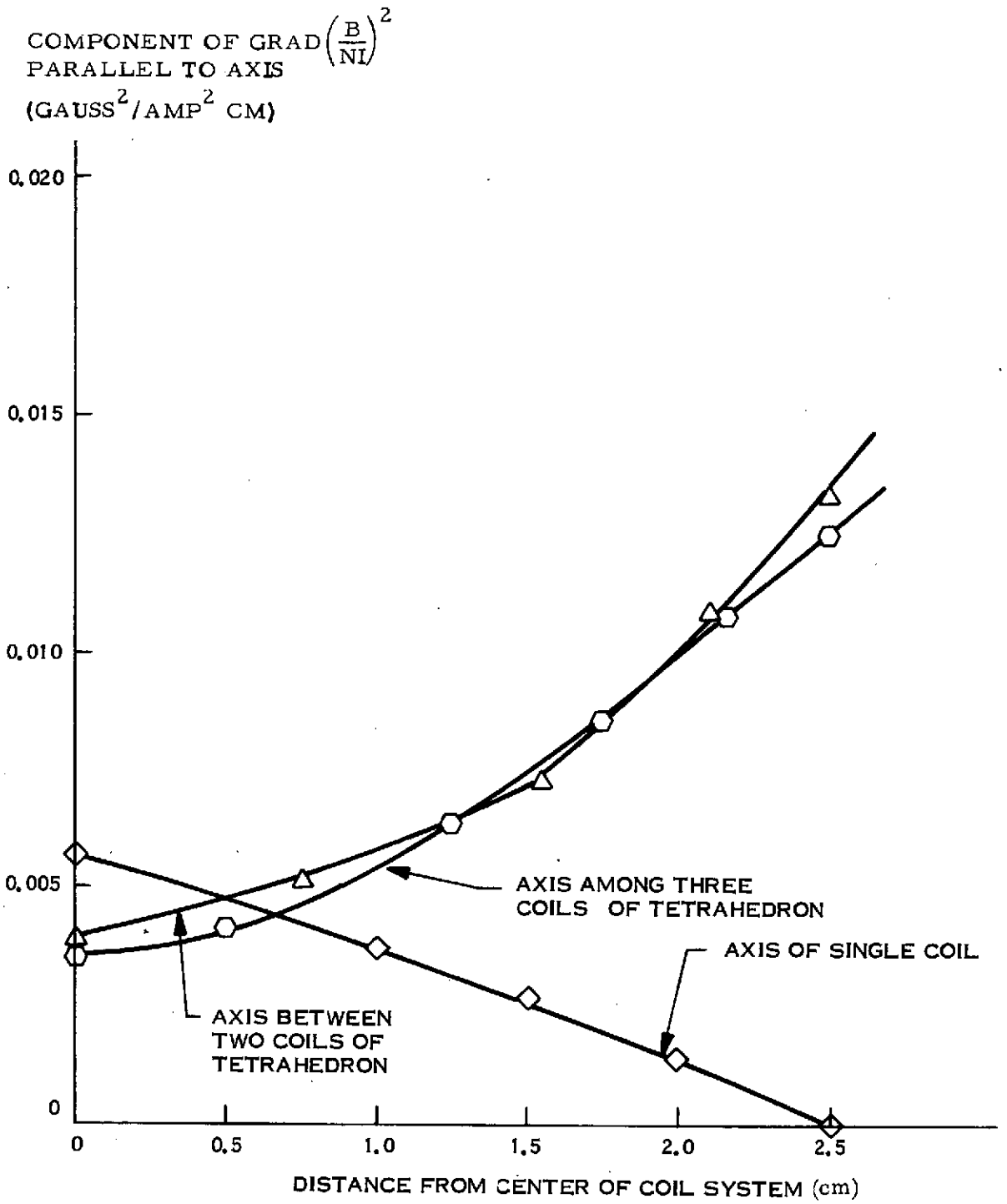

Figure 5-12. Calculated Force Along Axes of Symmetry for Tetrahedron with Coils of Radius 5.0 cm, a Distance 2.5 cm from the Center of the Coil System

traverse towards the vertex of a "normal" tetrahedron are so small relative to the corresponding forces in a cubical arrangement as to make the tetrahedron compare very unfavorably. The forces available from both "overlap" arrangements (Figures 5-10 and 5-12) are low as compared to the "normal" arrangements in the central region of the facility. The reason for the very low forces when moving towards a vertex of the normal tetrahedron is the very unfavorable angles between the field gradients due to individual coils. These acquire large angles with respect to one another near the vertex so that total gradient of B^2 becomes greatly reduced. The forces available with the "normal" cubical arrangement show this to be the best of the force arrangements studied here. We note, however, that the forces available when moving towards the vertex (Figure 5-9, square data points) are considerably smaller than for the other directions. Part of this is due to the use of the simple formula based on field values at the center of the specimen volume. For this reason additional calculations were carried out for which grad B^2 was based on a specimen volume average. These data are shown in Figure 5-9 as the triangular points.

In the summary of available forces and heating efficiencies for the various coil types considered in Section 5.2.10 below, the differences amongst coil types are generally so great that errors incurred by the use of the simplest computational procedure are unimportant. More exact calculations were carried out for the few coil systems which survived the initial screening given in Section 5.2.10 below.

5.2.4 FIELD AND FORCE COMPUTATIONS FOR OPPOSING HEMISPHERICAL COILS

The earliest work to develop simplified position control servo damping for specimen oscillations by means of electromagnetic position sensing was carried out in this laboratory in late 1972 utilizing a single hemispherical coil with vertical axis. This type of coil, or variations thereof, had previously been studied for terrestrial levitation work in which the axial field gradient is made

large compared to the radial gradient in order to maximize levitation forces. This type of coil is known to have relatively high efficiency for RF induction heating which can be increased when utilized with the position stabilizing servo which allows much tighter coupling to the specimen through minimization of coil size.

In this section we give results of computations carried out to adapt an opposing pair of such coils to the zero gravity environment. The second opposing coil substitutes for the role of gravity in the simplest terrestrial arrangement in that it returns a specimen to the first coil as the specimen drifts away from the first coil and vice versa. A number of variations of coil spacings and windings were analyzed to find that configuration giving nearly equal square field gradients (grad B^2) in the three orthogonal directions. In Figure 5-13 the results of calculation of $(H/I)^2$ ($=(B/I)^2$ in gauss units) vs. distance from the center of such a pair of coils is shown. It was assumed in this calculation that each coil of each pair is as described in the sketch of a single coil above the graph and that each coil of each pair has the same amount of current flowing through it but at different frequencies, so the force fields due to the two coils in each pair may be considered to be independent of one another. This situation is one which would be found in a cup coil pair when the pair is inductively heating a specimen, while also containing the specimen assuming no benefit of any position sensing system and control loop. The force at a point may be obtained by taking the slope of the plotted curves. The cup coil pair labelled "D" was the system chosen for use in the preliminary coil comparison based upon point values of H.

With the two coils operated at different frequencies, the total time averaged B^2 is equal to the sum of the separate time averaged B^2's furnished by the individual coils as mentioned previously. This follows because of the zero average for the cross term $\vec{B}_1 \cdot \vec{B}_2$ due to the incommensurability of driving frequencies. Operation of the two coils at the same frequency in an out of phase arrangement can also be considered. In this mode the turns near the polar

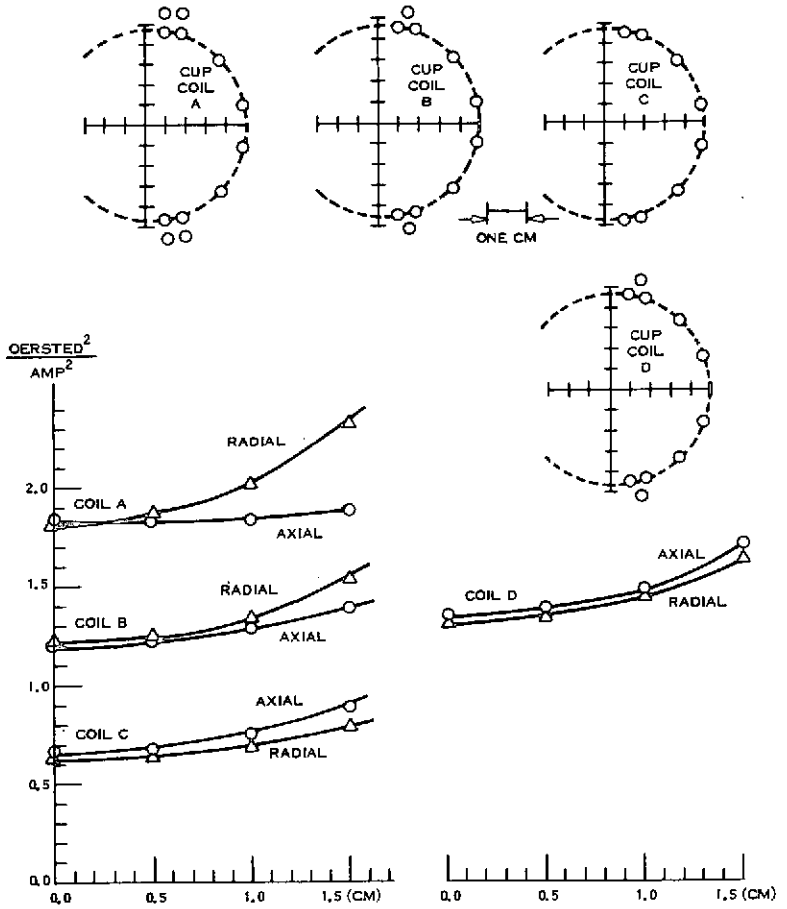

Figure 5-13. $\left(\frac{B}{I}\right)^2 = \frac{H^2}{I^2}$ vs. Distance from Center of Cup Coil Pair for Several Different Cup Coils

regions are relatively ineffective. This configuration, with elimination of turns not in the equatorial region, is discussed in detail as the "cusp" coil in a later section.

The slope of each curve given in Figure 5-13 is proportional to the force exerted upon the specimen. It may be seen that cup coil A has strong radial forces but virtually no axial force and that, after the number of equatorial turns has been reduced, cup coil C has somewhat stronger axial forces than radial forces. Cup coil D is the best of the four configurations shown because it has very nearly equal axial and radial forces, and, in addition, the increased size of the smallest turn enhances the accessibility to the coil's interior.

5.2.5 MAGNETIC FLUX DENSITY CALCULATION FOR SEVERAL BASEBALL COILS

The term "baseball coil" in this section is used to describe a coil wound on the surface of a sphere, much like the seams of a baseball, in such a manner that the coil results in four arcs or segments of a plane circle, each arc joined to two others at its ends. A sketch of such a coil is given in Figure 5-14. Other configurations are possible where the winding does not consist of such planar segments. However, it is found that by considering the coil family consisting of four such contiguous planar sections where only the angles of the planes with respect to one another is varied over a large range, configurations can be found which give nearly symmetrical field gradients in the central region.

The baseball coil may be considered a logical evolutionary development from the Joffe bar quadrupole arrangement discussed in the introduction to Section 5.0 when account is taken of the end loops formed by the interconnections among the four bars. Although some computational studies were available by courtesy of Dr. Henning of the Livermore Laboratory, a special computation program was written for the optimization studies given in this section. This program approximates the baseball winding as a series of straight segments and computes the field B and B^2 for a number of points within the region enclosed by the winding.

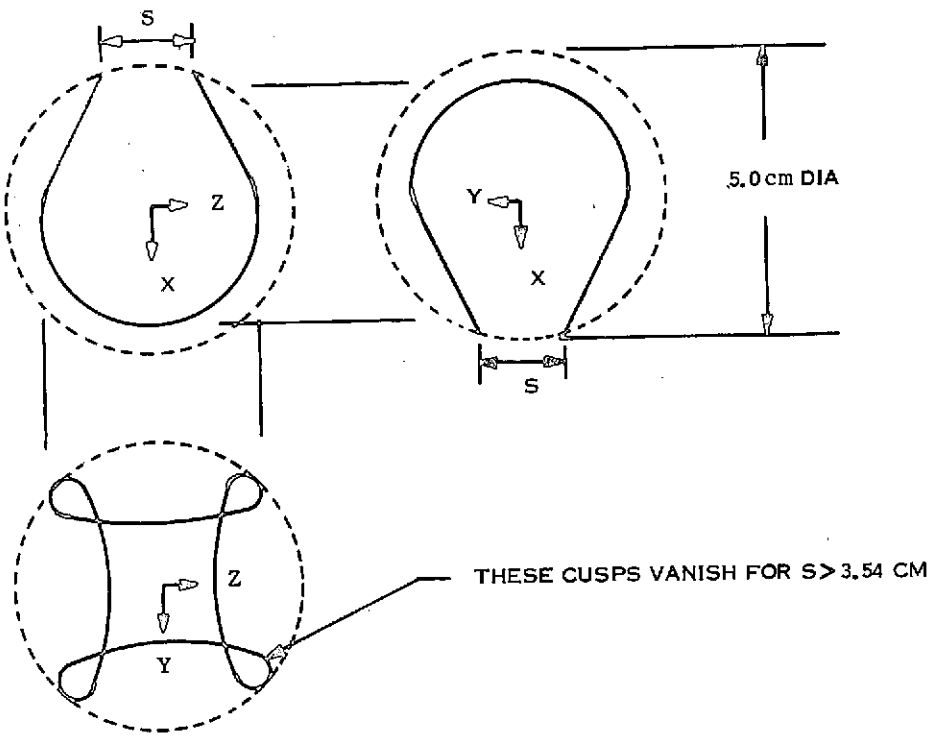

Figure 5-14. Baseball Coil Geometry

In Figure 5-15, the several baseball coils are identified by the parameter "s" which is the closest spacing between two portions of the coil in the x-y or x-z planes, defined in that figure. The parameter s is given in increments of 0.50 cm, except in two cases. Instead of 3.50, a value of 3.54 was selected to give a coil in which the plane arcs on opposite sides of the x-axis are parallel to one another, i.e. the coil is then somewhat like an "Alice" coil, and a value of 2.15 cm is given because this is the value of s for the coil used in force measurements in the laboratory.

Because the calculation of flux density was performed on the axes of the coil, calculation of $\text{grad}\left(\frac{B}{NI}\right)^2$ results in the x, y and z components of $\text{grad}\left(\frac{B}{NI}\right)^2$ on the x, y and z-axes, respectively. However the x component, on the x-axis is equal to the total $\text{grad}\left(\frac{B}{NI}\right)^2$. Elsewhere, the direction of $\text{grad}\left(\frac{B}{NI}\right)^2$ is generally not parallel to the axes. Figure 5-15 shows values obtained along the

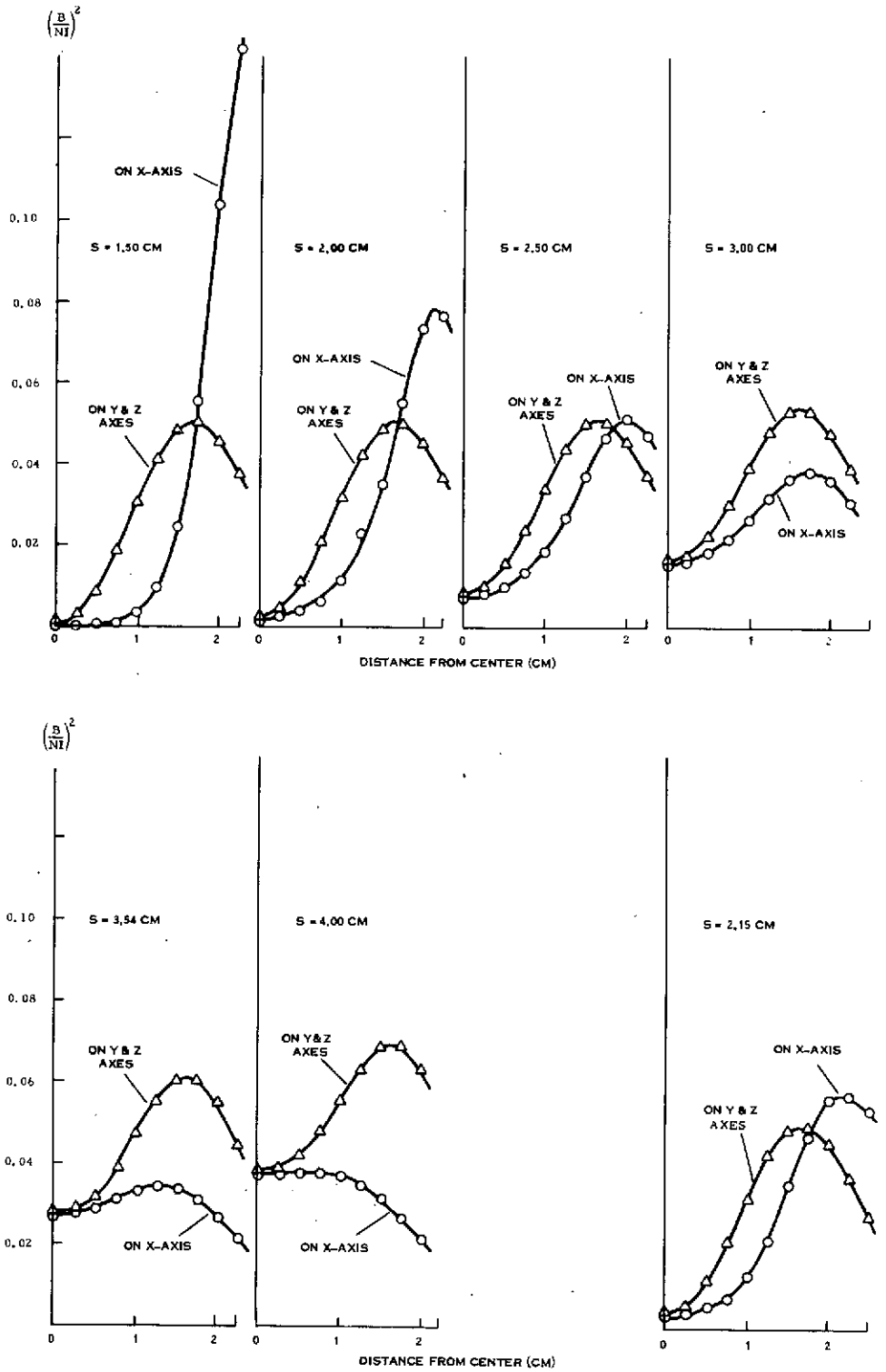

Figure 5-15. Total Flux Density Squared on Each Axis for Baseball Coil of 5.0 cm Diameter

x-axis. We note that s = 2.5 represents an optimum with respect to yielding approximate symmetry to the height of the "potential barrier," B^2, in orthogonal directions.

5.2.6 BASEBALL COIL FORCE CALCULATIONS AND MEASUREMENTS

Simple body force calculation based on values of grad B^2 at points corresponding to the center of a 2.5 cm diameter aluminum sphere were carried out for a filamentary baseball coil winding of 150 rms ampere turns on a 5 cm diameter sphere. These are shown as the calculated data in Figure 5-16. Force measurements were carried out in the laboratory for a baseball coil of equal average dimensions carrying 75 amperes in two turns separated by 1 cm. These measurements are also shown in Figure 5-17. The calculated and measured forces agree on the average although the slopes are different by an appreciable amount. These differences are attributed partly to the use of point values of grad B^2 and also due to the approximation of the two turn coil in the calculations by a single filamentary turn. Calculations for the cusp coil to be shown in the next section indicate that taking account of both these factors generally gives much better agreement with experiment as was already noted for the simple circular turn coils.

5.2.7 OPTIMIZATION OF CUSP COIL

A number of computations were carried out for flux densities and gradients of B^2 (or equivalently H^2) for cusp coils over a range of ratios of coil diameter to coil plane separation. The sketch shows the coil configuration and nomenclature for the separation s of the two coil planes. Figure 5-18 shows the values of grad B^2 obtained at the points corresponding to the center of a specimen as it moves axially or radially away from the central position. Figure 5-19 shows corresponding results when the squared field is averaged over the specimen volume to

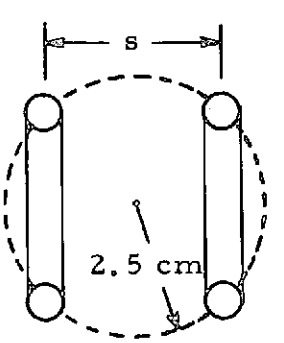

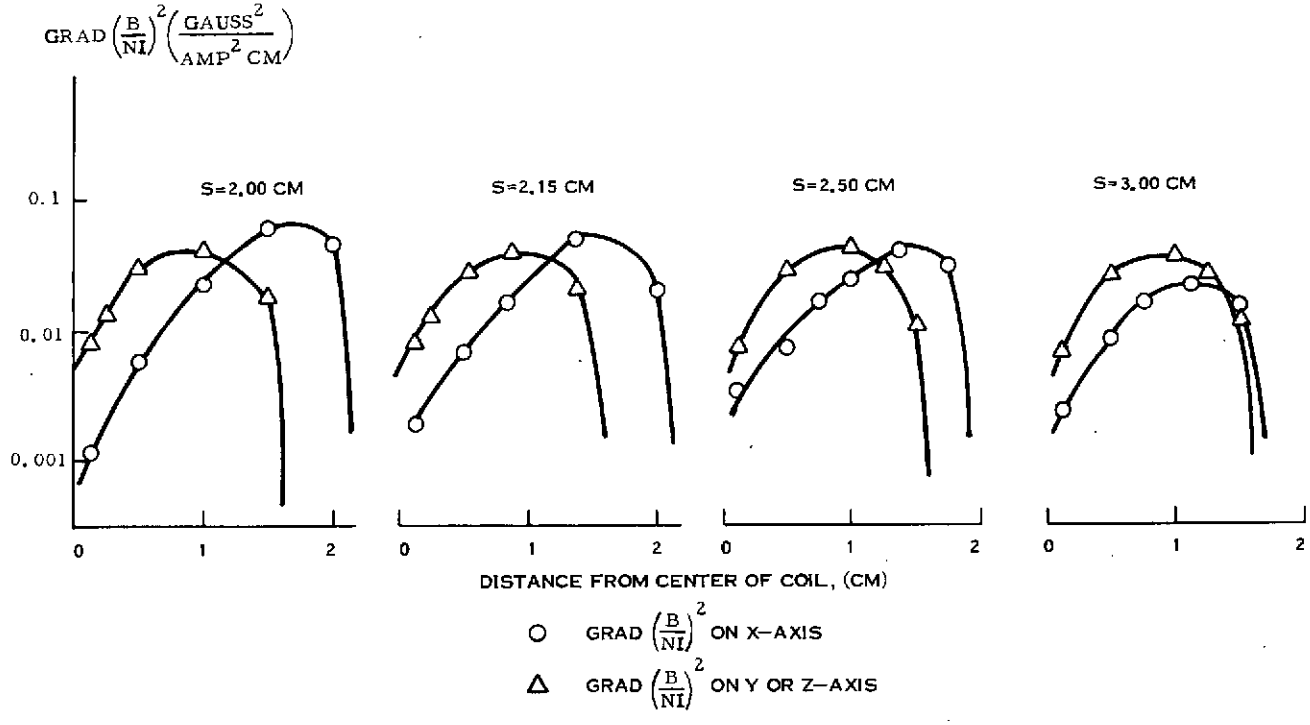

Figure 5-16. Gradient of Total Flux Density Squared, for Baseball Coil, Diameter = 5.0 cm, on Each Axis

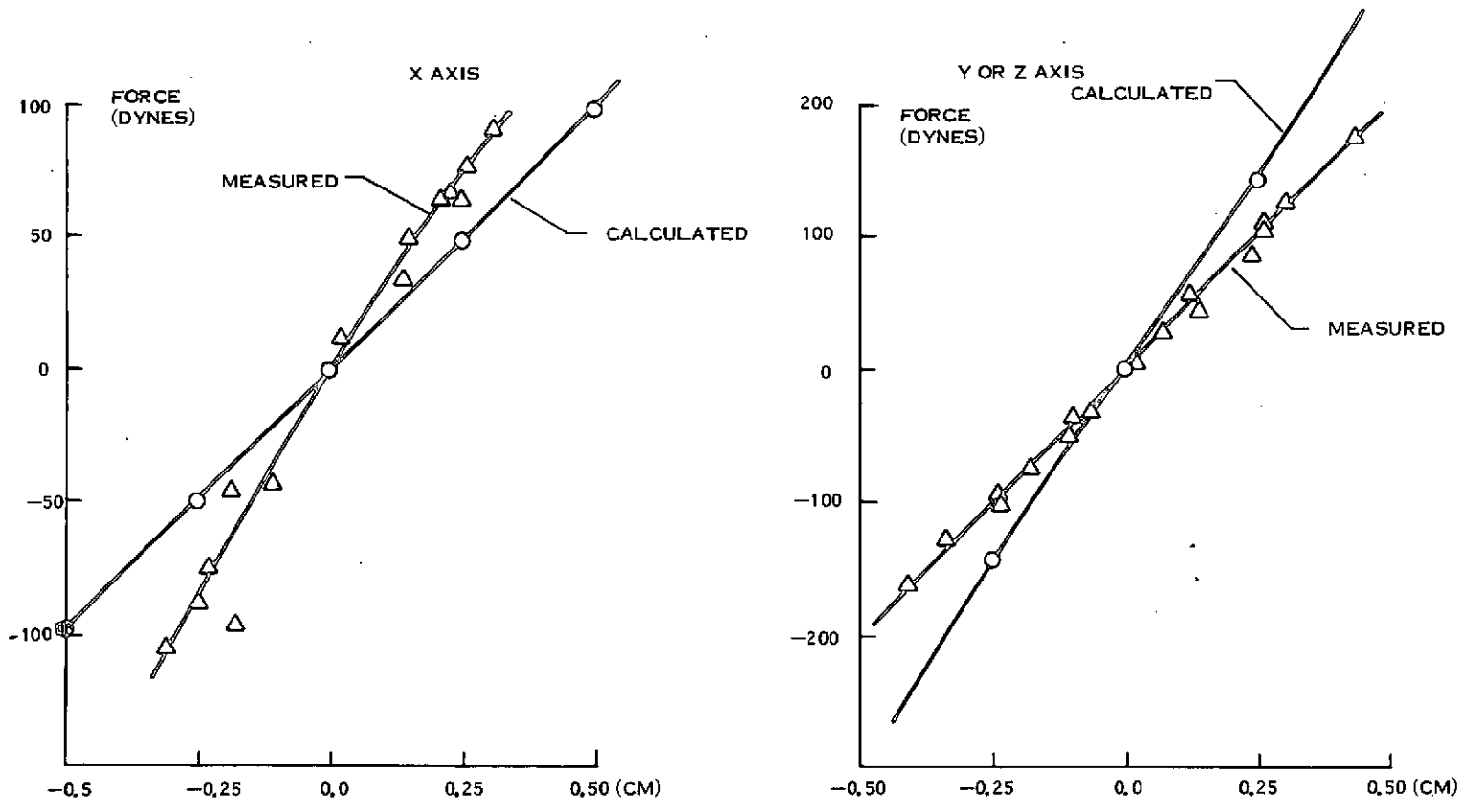

Figure 5-17. Measured & Calculated Forces in a Two Turn, 5.0 cm dia. Baseball Coil, with a 2.5 cm. dia. Aluminum Sphere (I = 75 amp rms)

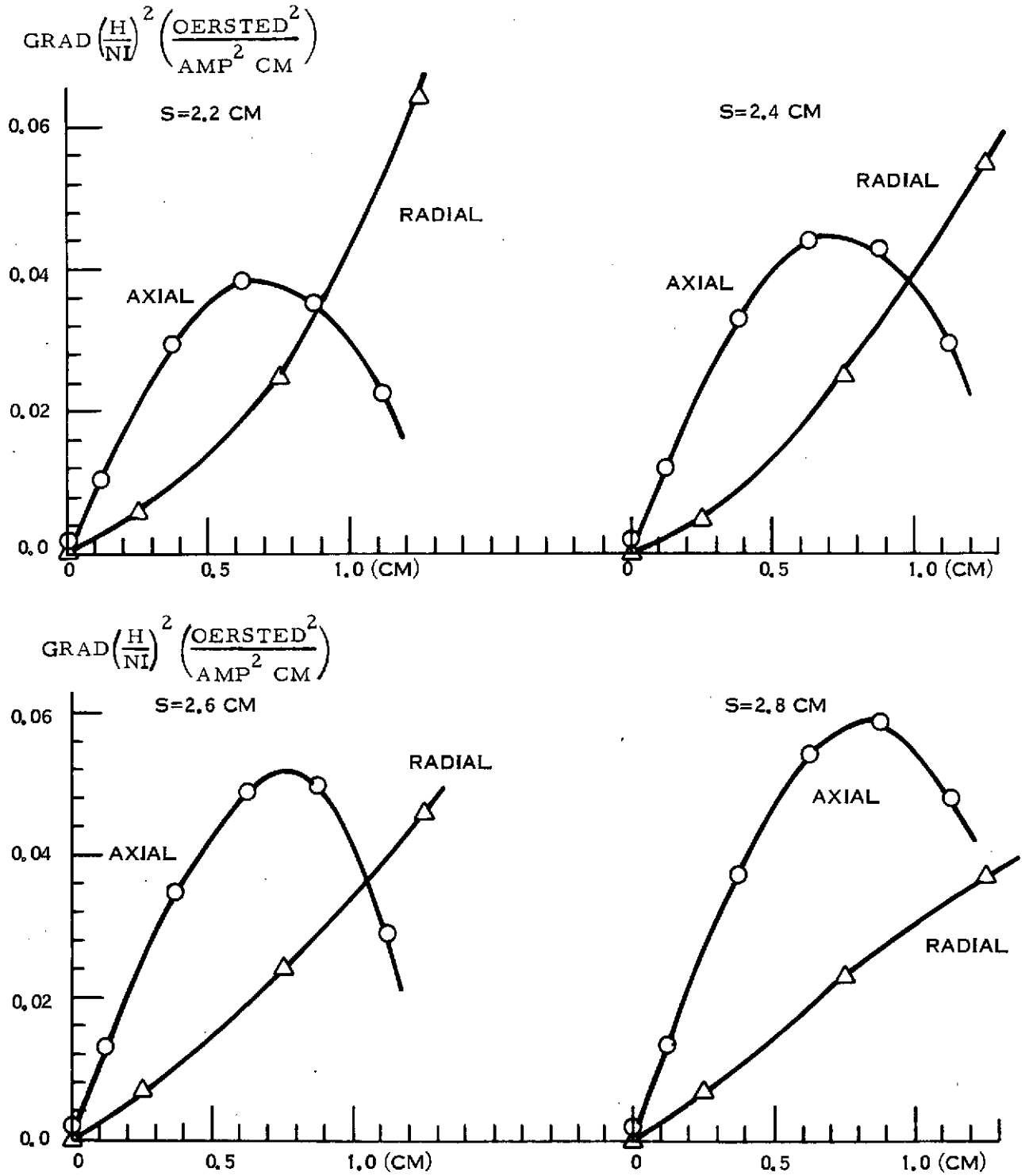

Figure 5-18. Radial and Axial grad $(H/I)^2$, for Cusp Coil Based on Values of H at Points, vs. Distance from Center of Coil for Several Different Coil Spacings

(Coils are wound on a 5.0 cm dia. sphere.)

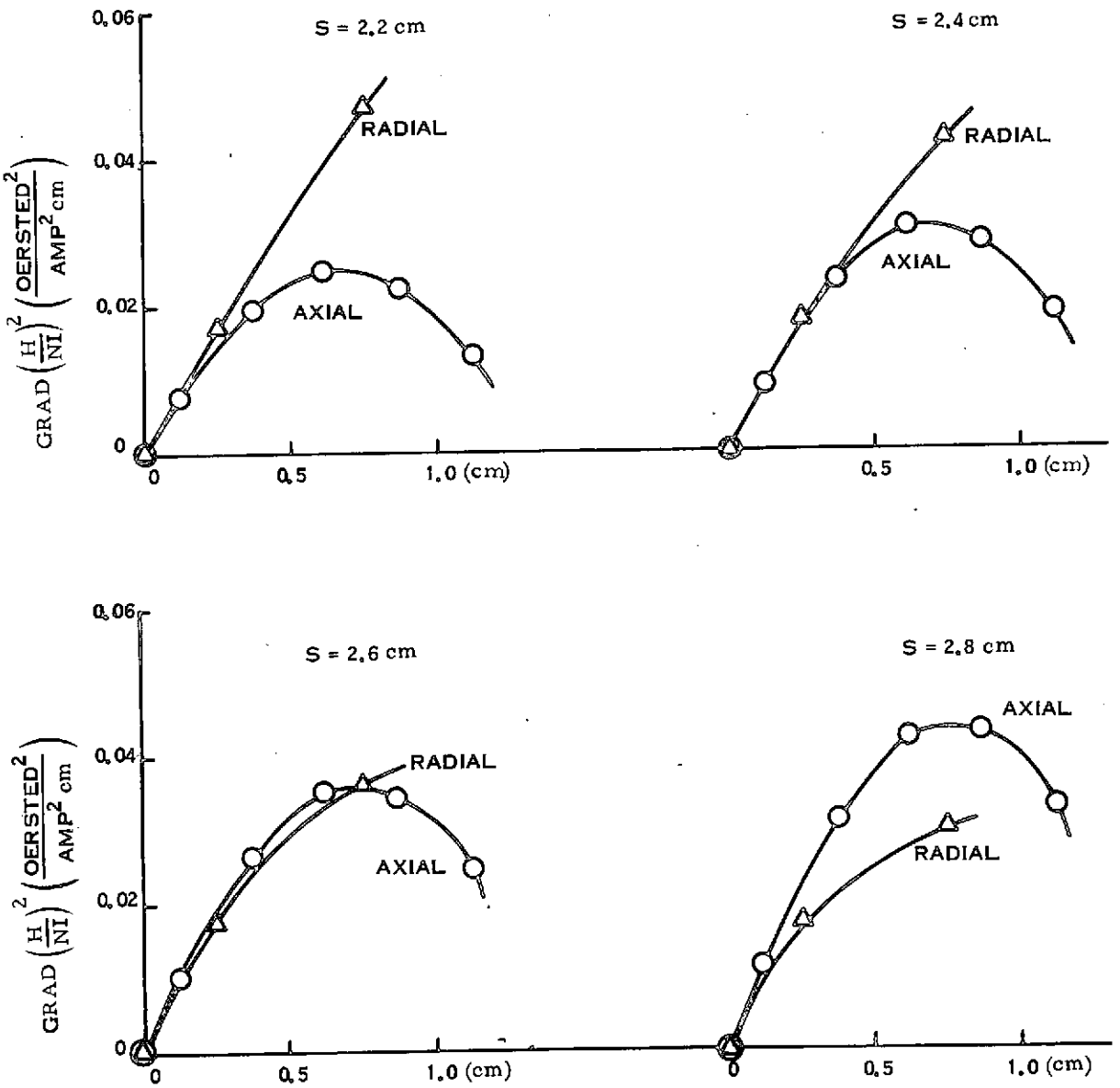

Figure 5-19. Radial and Axial grad $(H/I)^2$ (Vol. Aver.) for Cusp Coil vs. Distance from Center of Coil for Several Different Coil Spacings (Coils wound on 5 cm dia. sphere)

compute grad B^2. It is seen that a coil separation of 2.6 cm gives approximate symmetry in the radial and axial forces for small specimens for displacements as great as 0.75 cm from the center.

5.2.8 FORCES FROM CUSP COIL

Calculations were carried out using the computer program which yields forces on each of 20 sections of the spherical specimen. These data are shown as the solid lines in Figure 5-20 for coils of diameter 2.54 cm with separation distance 3.54 cm and for three different sphere volumes, namely 1.0 cm, 2.0 cm and 3.0 cm. This figure illustrates the approximate proportionality of force to specimen volume. Shown also for the 2.0 cm specimen diameter as the dashed lines are the forces calculated utilizing the grad B^2 formula with B^2 values estimated at the center of the sphere and for the sphere volume average respectively.

Some forces were measured in the laboratory in order to confirm the magnitude of the computed forces, since in the case of cusp coil near the central position where the field vanishes, the difference obtained in computations with or without field averaging over specimen volume should be especially important. The coil configuration for the laboratory test set-up is shown in the sketch on Figure 5-21. The two turn cusp coil had a 2.0 cm mean radius with a 2.7 cm spacing between coils. The calculations took actual account of the two separate but closely spaced windings on each coil and also computed grad B^2 averaged over the spherical specimen volume at each point. Since a computer program was available which averaged B^2 values over a 2.0 cm diameter sphere whereas the experiment utilized a 2.5 cm diameter aluminum sphere, scaling of the theoretical computation were made before plotting as the solid curves in Figure 5-21. Scaling will be discussed in Section 6. Also shown as the dashed line are the axial forces measured with the balance arrangement described previously.

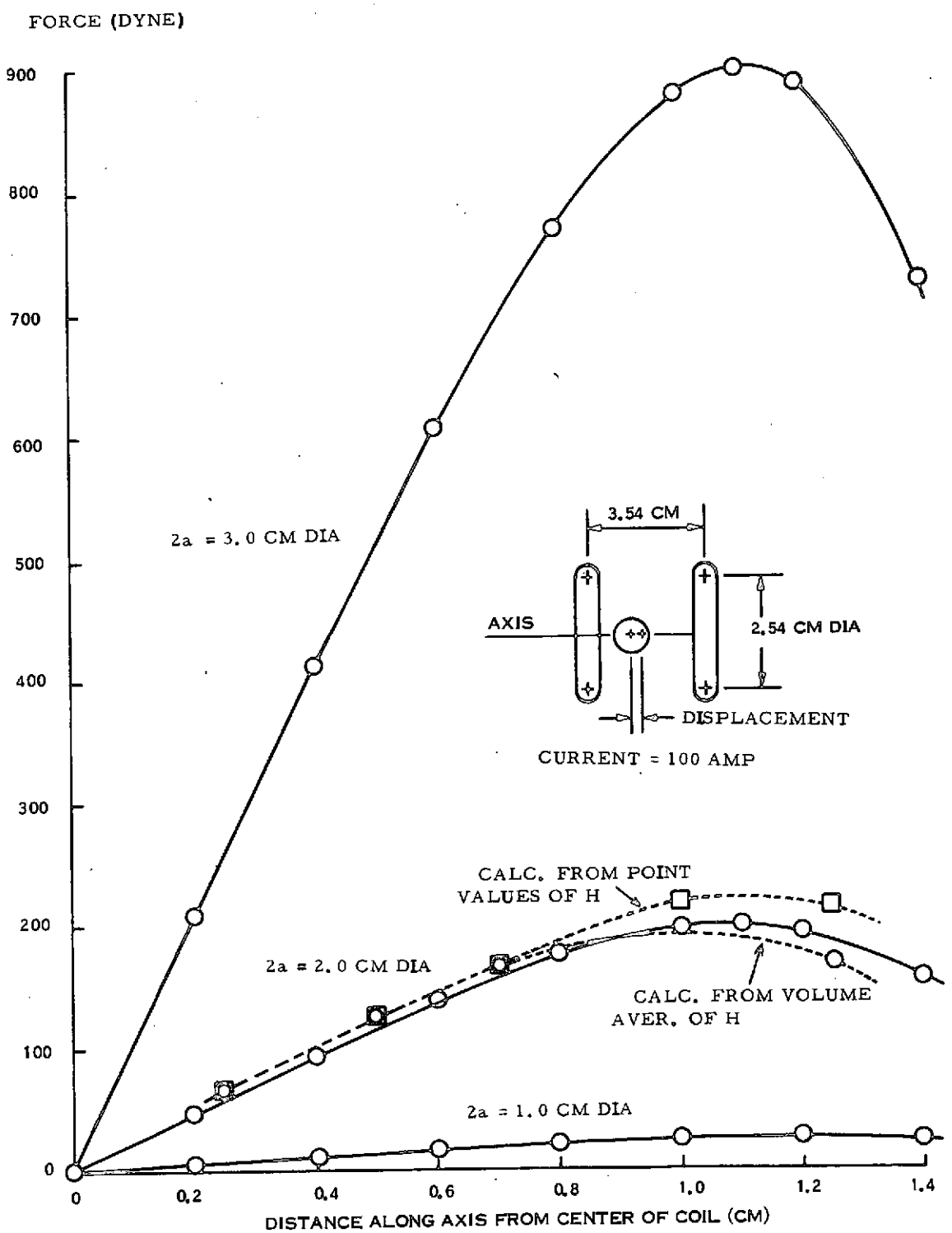

Figure 5-20. Force Exerted by Cusp Coil Upon Sphere of dia. D vs. Distance from Center of Coil I = 100 amp. rms

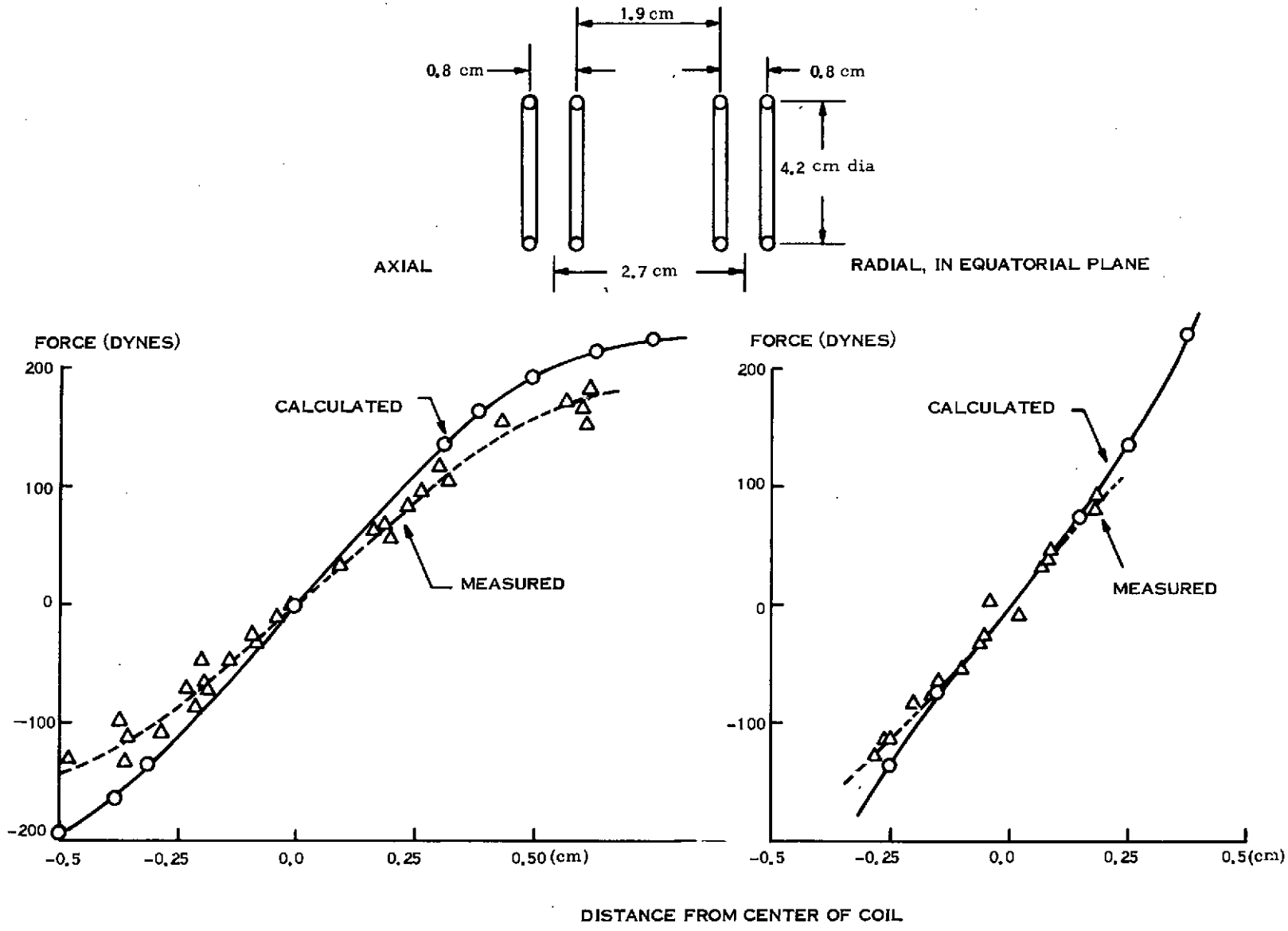

Figure 5-21. Measured & Calculated Forces in a Two Turn Cusp Coil, 2.1 cm Radius, 2.7 cm "Spacing" with a 2.5 cm dia. Aluminum Sphere. (I = 67 amp, rms)

5.2.9 COMPARISON OF SEVERAL COIL TYPES, WHEN USED WITH SMALL SPECIMENS

5.2.9.1 Introduction

This section makes a comparison, based on several simple engineering criteria, to evaluate performance in a free suspension processing system of several of the coil types discussed above. The "cube overlap," tetrahedron and tetrahedron overlap arrangements were eliminated from further consideration on the basis of inferior performance as already noted as compared to the 6-coil "normal" cubical system. This comparison is made upon the basis of B^2 and grad B^2 comparisons where B^2 is evaluated at points corresponding to the center of the specimen. This comparison will be valid for specimens whose size is small compared to the coil dimensions. As already noted, this simple approach becomes less accurate as the specimen dimensions become very large (diameters on the order of one-half the coil dimensions) and will be particularly important for the cusp coil where B^2 evaluated at the central point will vanish but its average over a specimen of appreciable size will not. Additional computations have been carried out for all coil systems to evaluate the effects of flux averaging over the specimen volume. These effects are as large as a factor of 2 for certain systems, e.g. the 6-coil cubical system when considering a traverse towards a cube vertex during which the specimen's surface gets close to the coil windings. (See Figure 5-9.) For all other cases, with the exception of the cusp coil, the effects are much smaller. Within this approximation the following comparison is considered to be valid and rigorously so when smaller specimens are considered. The cusp coil is an exception and needs separate treatment with respect to heating (B^2) considerations.

Other approximations implicit in the comparison, to be made in this section as well as later, should be mentioned at this point. The first relates to redistribution of current in the conductors due to skin depth effects in multiple turns in close proximity one to another. In the simple comparisons shown in the following tables, a filamentary coil winding is assumed (except for the hemispherical

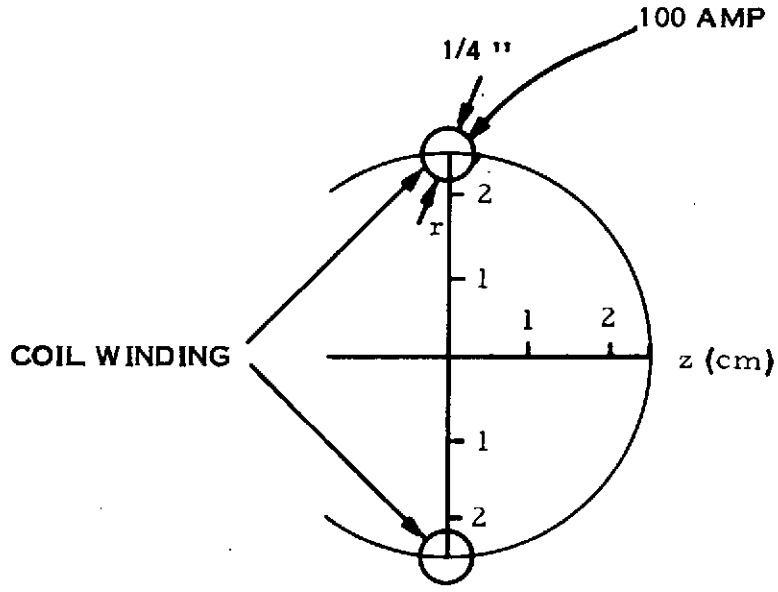

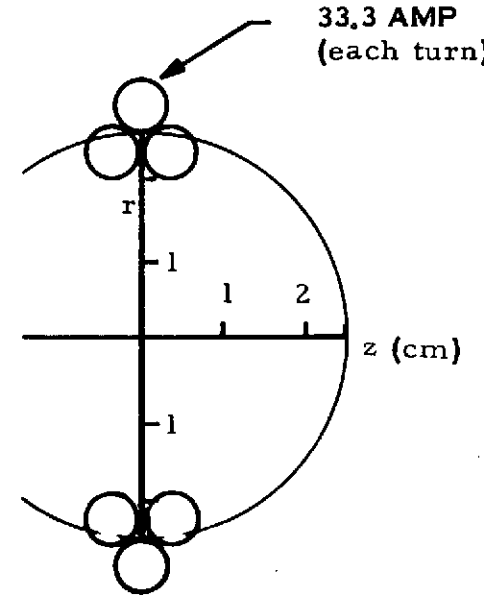

AVERAGES: TOTAL H, SQUARED OVER VOL OF 2 CM DIA SPHERE

	R = 0.0	0.5	1.0
Z = 0.5	633.	660.	839.
Z = 0.5	563.	595.	733.
Z = 1.0	421.	422.	501.
Z = 1.5	269.	232.	292.

AVERAGES: TOTAL H, SQUARED OVER VOL OF 2 CM DIA SPHERE

	R = 0.0	0.5	1.0
Z = 0.0	599.	619.	732.
Z = 0.5	549.	569.	677.
Z = 1.0	424.	444.	528.
Z = 1.5	280.	294.	320.

Figure 5-22. Effect of Approximating 3 Turn Circular Winding as Single Filamentary Turn

or cup coil winding), whereas engineering studies have shown that optimum efficiency of coupling to power amplifiers and tank circuits generally requires two or more turns. Computations were carried out for the skin depth and proximity effects by means of a computer program available in the General Electric Researc and Development Center. This program takes account of the nonuniformity of distribution of the current around the surface of each of several turns (i.e., the "proximity-effect," which is significant on account of the proximity of the adjacent turns). From this work effective resistance values of these multiple turn coils were computed and were utilized in the engineering calculations given in Section 6.

The order of magnitude of the errors incurred by assuming the location of the currents in each of two or three separate windings to be concentrated in a single filamentary current located at the mean position of the winding was also examined. This computation was carried out for the case of a circular winding where three 1/4 inch diameter turns were approximated by a single filamentary winding located in the mean position of the three windings. (See Figure 5-22.) Table 5-1 gives the volume average H^2 over a 2 cm diameter sphere located at various axial positions, z, measured in cm from the coil center. It is to be noted that little difference is encountered from the filamentary approximation until the sphere coordinates move to regions in which the spherical surface is approach ing the winding.

5.2.9.2 Coil Types and Assumptions

The coil comparisons are all made corresponding to a configuration for which the coils are wound upon a 5 cm diameter volume within which the specimen is free to move. Section 6 discusses the scaling laws for B^2 and grad B^2 which shows that the comparisons given below will be valid when comparing any two systems of the same dimensions.

The types of coils considered in this section are

6-coil cube
Baseball
Cup coil pair
Cusp coil

The same relatively small spherical specimen is assumed to be present in each coil. The assumptions in the comparisons are illustrated by Table 5-1:

Table 5-1

Assumptions Made in Comparison of Coil Systems

a. Nominal 5.0 cm diameter containment volume.

b. No interaction among coils (one exception which will be noted, for cup coil pair).

c. Each system operates upon a relatively small specimen with the same x value (ratio of radius to skin depth).

d. Single filamentary winding (except for the cup coil pair, which, by its nature, is a multiple winding).

5.2.9.3 Coil Descriptions

A brief summary description of each coil is given in Table 5-2 and a simple sketch of each type, of the dimensions assumed in this comparison, is given in Figures 5-23 through 5-26. The configurations given here have been optimized based upon computations described in previous sections.

5.2.9.4 Resistance of Coils

Numbers illustrating the relative resistance of each coil type are developed in Table 5-3 in which it is assumed that the skin depth in the copper tubing of which the coils are made is considerably smaller than the radius of the tubing. Hence the relative power dissipation P is proportional to the total length of tubing through which current passes and inversely proportional to the diameter of the tubing. In magnetic field and winding length calculations the current is assumed to lie on a filament on the tubing's axis. Computations given in Section 6 take account of skin depth and proximity effect for the multiple turn coils finally selected.

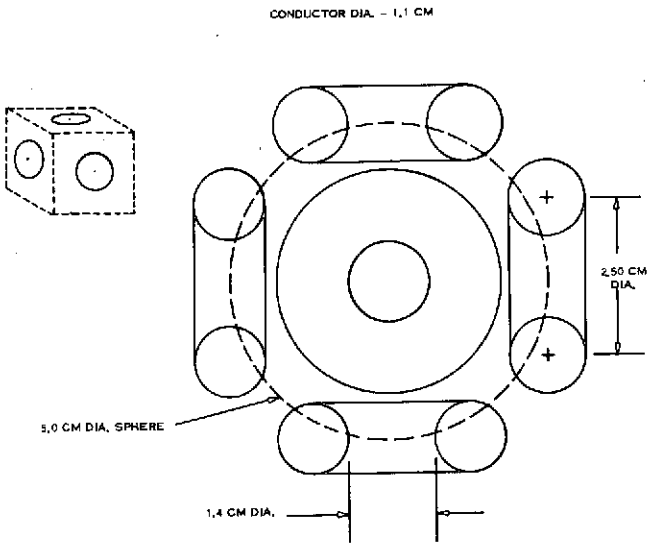

Figure 5-23. Cube

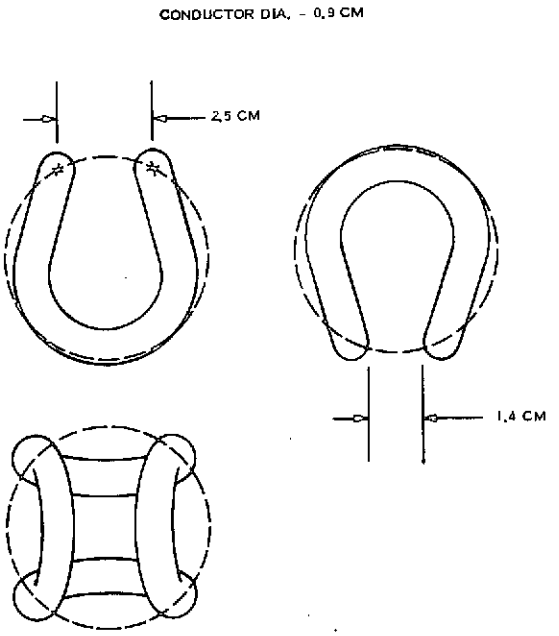

Figure 5-24. Baseball

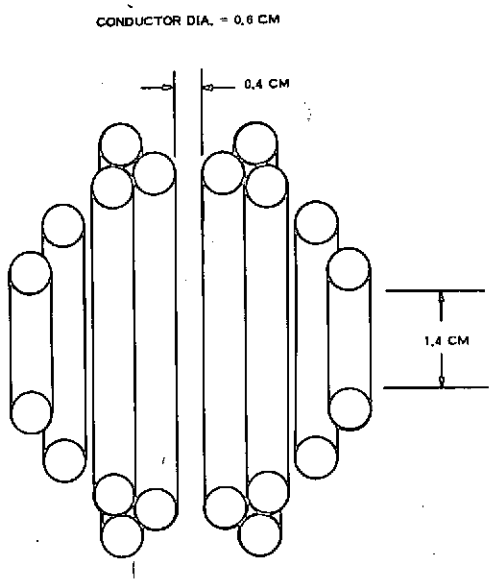

Figure 5-25. Cup Coil Pair

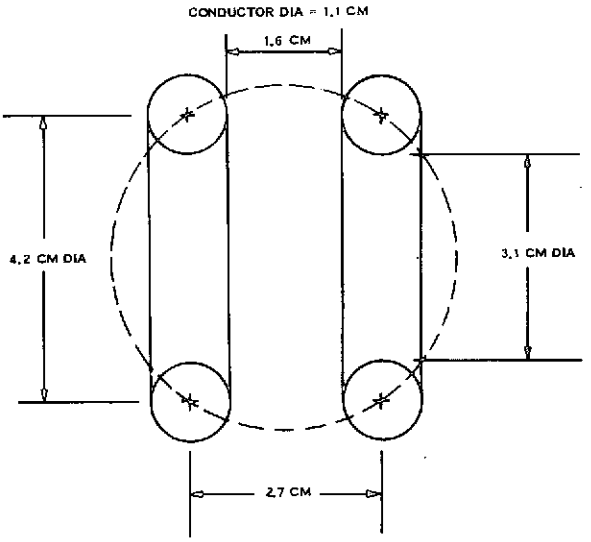

Figure 5-26. Cusp Coil

Table 5-2

Description of Coil Types

Cube

Six coils tangent to 5.0 cm dia. sphere.
Each coil has 2.5 cm diameter.
Each coil operated independently, each at a different frequency.

Baseball

One coil wound on 5.0 cm dia. sphere.
Closest spacing between different points on the coil axis is 2.5 cm.

Cup Coil Pair

Two coils wound on 5.0 cm dia. sphere.
On each, three turns 0.7 cm, one at 1.8 cm and one at 2.4 cm from equatorial plane. Coils operated at different frequencies.

Cusp Coil

Two turns wound on 5.0 cm dia. sphere, 2.7 cm spacing between their centers.
The two turns are connected in series such that their magnetic fields are in opposition at the center of the coil.

Table 5-3

Relative Resistances of Coils

Coil Type	No. of Coils Excited, n	Length of Coil, ℓ	Dia. of Tubing*, d	Relative Power, P**
Cube	1	7.9 cm	1.1 cm	7.2
	3	23.7		21.6
	6	47.4		42.2
Baseball		24.9	0.9	27.7
Cup Coil Pair	1	92	0.6	153
	2	184		306
Cusp Coil		26.4	1.1	24.0

*Maximum size consistent with the volume which is available.
**Per unit current

5.2.9.5 Containment Ability per Unit Power

The value of H^2/I^2 at the center of each coil and its maximum value on the surface at which the force exerted upon the spherical specimen is zero are given in Table 5-4 as well as the difference $\Delta(H/I)^2$ between these two values. This difference is proportional to the depth of the potential well (from the fact that force is proportional to grad H^2) which contains the specimen and, in the case of coil types containing more than 1 single-frequency coil, e.g. cube and cup coil pair, this assumes suitable position sensing and switching of power to the proper coil(s). The last column in Table 5-4 gives the ratio of the differences to the corresponding figures from Table 5-3 to yield numbers proportional to the depth of the potential well per unit power dissipated in the coil. Note that no dimensions are given here since the absolute resistivity of the coil has been omitted for simplicity.

Table 5-4

Ability to Contain a Specimen

Coil Type	No. of Coils Excited, n	H^2/I^2 at Center	$(H^2/I^2)_{min}$ on F=0 Surface	$\Delta\left(\frac{H}{I}\right)^2$	$\Delta\left(\frac{H}{I}\right)^2 \Big/ \left(\frac{P}{I^2}\right)$
Cube	3	0.006	0.018	0.012	5×10^{-4}
Baseball		0.008	0.051	0.043	16×10^{-4}
Cup Coil Pair	2	1.3	1.9	0.6	20×10^{-4}
Cusp Coil		0.0	0.050	0.05	21×10^{-4}

5.2.9.6 Induction Heating Efficiency

Values of H^2/I^2 are given in Table 5-5 which are then divided by the corresponding resistance factors of Table 5-3 to indicate heating ability per unit of power dissipated in the coil. It should be noted that it is inappropriate to evaluate H^2/I^2 at the center of a cusp coil for very small specimens which would yield zero heating

efficiency. As shown in following sections, computations and measurements indicate that the magnetic field intensity rises so rapidly at positions near the central field null as to give very appreciable heating efficiencies for this coil system.

Table 5-5

Ability to Heat

Coil Type	No. of Coils Excited, n	H^2/I^2 at Center	$(H/I)^2/\left(\frac{P}{I^2}\right)$
Cube	6	0.012	2.8×10^{-4}
Baseball		0.008	2.9×10^{-4}
Cup Coil Pair	2	1.3	43×10^{-4}
Cusp Coil		--	--

5.2.9.7 Positioning Ability per Unit Power

The maximum force per unit power dissipated in the coil is evaluated in Table 5-6 by starting with the maximum average gradient in H^2/I^2, between the center of the coil and a distance 0.5 cm from the center, and then again dividing by the corresponding relative resistance.

Table 5-6

Ability to Resist an External Force Along Strongest Axis

Coil Type	No. of Coils Excited, n	Maximum Gradient Near Center	Max. Grad/$\left(\frac{P}{I^2}\right)$
Cube	1	0.012	17×10^{-4}
Baseball		0.03	11×10^{-4}
Cup Coil Pair	1	0.59	38×10^{-4}
Cusp Coil		0.04	17×10^{-4}

5.2.9.8 Other Considerations

Other bases upon which coils may be compared are given in Table 5-7. It should be noted that no conclusions can be made for the adaptability of the cusp coil to electromagnetic position sensing on the basis of evaluation of B^2 at a point since, as already noted, this vanishes near the center of the cusp facility. As will be shown later, computations and measurements of power absorbed for a finite size specimen show that the cusp is also adaptable to electromagnetic position sensing.

Table 5-7

Additional Considerations in Comparison of Coil Systems

Coil Type	Regions of Access to Containment Volume in Terms of Circular Areas		Compatible Position Sensing Techniques	
	Number	Diameter (cm)	Electromagnetic	Optical
Cube	6 8	1.4 1.6	No	Yes
Baseball	2 4	1.4 2.7	Yes	Yes
Cup coil pair	2 1	1.4 0.4 wide band	Yes	No
Cusp Coil	2 1	3.1 1.6 wide band	---	Yes

If the value zero for the heating efficiency of the cusp coil be excepted as an anomaly to be treated later, all of the systems considered receive appreciable scores in all areas. The cup coil pair receives the highest score when all columns are considered. When account is taken of the anomalous situation of the cusp coil as regards this simple comparison it appears that all of the above four systems are capable of adequate performance.

5.2.9.9 Preliminary Conclusions

In conclusion it may be said that the studies of magnetic field configurations given in this section have served to optimize each coil configuration type but do not serve to make the final recommended choice, other than the rejection of a few coil types. The final choice rests upon overall engineering considerations, including accessibility, efficiency for RF heating, suitability for use with simple electromagnetic position sensing which is closely related to induction heating efficiency, and suitability for use in conjunction with electron beam heating which requires more detailed considerations.

In the facility capability studies given in a later section it is seen that the primary limit to the capabilities of the Containerless Processing Facility will be the total power availability. The main power requirement is for furnishing surface radiation loss for the highest melting specimens such as tungsten. The power requirements for positioning are generally much less limiting. Since electron beam heating is to be considered for many specimens for which it can yield a higher efficiency than can RF induction heating, the ability of the facility to maintain the specimen accurately in the focus of an electron beam when subject to forces due to electron or ion bombardment and differential outgassing is important and will be discussed in the next section. For RF heating efficiency, it is necessary to consider specimen volume field averaging and to place great reliance on laboratory measurements because of the importance of this parameter. This will also be treated below.

5.3 OVERALL FACILITY ENGINEERING CONSIDERATIONS

5.3.1 INTRODUCTION

The optimization of the various coil and field configurations with each coil type and the elimination of a few of the candidate types was made possible by the field and field gradient considerations in the preceding sections. Amongst the remaining candidates, namely the 6-coil, baseball, opposing hemisphere

(or cup pair) and cusp configurations, some overall considerations of facility engineering and complexity may be applied. We may consider the finalists in more detail with regard to the following engineering criteria.

a. Mechanical accessibility for specimen introduction and removal including accessibility for observation of the process.

b. Compatibility with the simplest electromagnetic position sensing for damping of position oscillations.

c. "Stiffness" of control near the central position or the ability to maintain the specimen in the focus of an electron beam when subject to the attendant thrusts.

d. Engineering complexity due to cross coupling of multi-coil systems. This is especially important because of the requirement (to be shown later) for operation over a wide frequency range.

e. Relative efficiency for RF induction heating for those processes in which this is the simplest means of heating or for which electron beam heating is not applicable because of unfavorable values of the secondary electron emission coefficient.

5.3.2 SPECIMEN ACCESSIBILITY WITHIN COIL CONFIGURATION

Examination of Figure 5-25 shows that the opposed cup coils give poor accessibility when large specimens are considered for introduction or removal of the specimen, unless the coils were mechanically movable with respect to one another. Because of the requirement for this possible complication as well as poor visibility of the specimen for instrumentation, the cup coil pair obtains a low score in this area for the Containerless Processing Facility.

Examination of Figure 5-23 shows that the cubical coil arrangement also gives relatively poor accessibility for specimen introduction or ejection when

large specimens are considered. These conclusions regarding specimen access to and from the control position were summarized in Table 5-7. It might at first be concluded that this accessibility disadvantage might be overcome by scaling up the size of the coil facility without a consequent scaling up of specimen size. However, this would cause a large reduction in RF heating efficiency and the achievable force per unit power so that it is necessary to consider the comparison between coils on the basis of equal relative scaling of specimen and coil dimensions. As discussed in following sections, power for heating and melting will be a principal limitation in the electromagnetic Containerless Processing Facility. Hence the low score on specimen accessibility for the cubical and hemispherical coil configurations stands as a serious engineering drawback.

5.3.3 COMPATIBILITY WITH ELECTROMAGNETIC POSITION SENSING

Development work in this laboratory has shown that by sizing the six circular coils to a diameter of about one-half that of the sphere inscribed within the 6-coil configuration, the mutual inductance problem is tractable and the system can be made to operate for a given choice of frequencies of drive. Even so, as noted in Table 5-7, the 6-coil system is not adaptable to electromagnetic position sensing because of mutual inductances amongst the various coils. The necessity for operation of several coils at different frequencies also poses an equipment complication not present in the simpler coil configurations. Also, maintenance of adequate frequency separation over the wide band of frequencies recommended for a facility introduces the requirement for several multi-frequency band switching power amplifiers.

Although work has been done to develop an electro-optical position sensing system for use with this coil arrangement, this system is much more complex than the corresponding electromagnetic position sensing scheme developed later in this laboratory. The latter is expected to be much less subject to influence of metallic vapor deposits, etc. than would electro-optical sensors even when such sensors are protected by mirror optics and baffles. The recent development

of this servo control system which can damp specimen oscillations by detection of changes in RF loading upon the coil system can be regarded as a development which has superseded the earliest development of three dimensional position control and damping. This servo system is adaptable to the other final system candidates, e.g. baseball, cusp and, with some difficulty, the opposing hemispheres.

5.3.4 ELECTROMAGNETIC POSITION SENSING WITH OPPOSED HEMISPHERICAL COILS

The initial laboratory tests of the simplified electromagnetic position sensing servo were carried out with a specimen levitated in a single cup coil. Because of asymmetries introduced by the operation of two tightly coupled coils at different frequencies, additional laboratory tests were carried out of the electromagnetic position sensing signals obtained with two opposed coils excited.

The "optimum" configuration utilized here is that derived in Section 5.2.4 which equalizes the radial and axial B^2 gradients with both coils equally excited. The sensitivity for electromagnetic position sensing using a 2 centimeter diameter aluminum ball was measured in the laboratory with the following results.

5.3.4.1 Q Measurement - No Specimen

Initial Q measurements for the separate coils are shown as the first column in Table 5-8.

Table 5-8

Measurements of Q for Cup Coils

	Single Coil	Two Coils
Coil 1, 80 KHz	28	27
Coil 2, 120 KHz	29	22

With both coils in place the system demonstrated the expected shift in resonance positions by a small amount and the Q was remeasured at each of the shifted resonances. These values are shown in the second column. The large reduction in the Q corresponding to the shifted 120 KHz resonance should be noted. This shows a large and unsymmetrical absorption by the low frequency coil when the high frequency coil is excited.

5.3.4.2 Position Sensing Measurement

These measurements were made by using a constant current drive and noting the change in terminal voltage at resonance. The ball was moved in 1/2 cm steps. The position sensing signal, which is the change in terminal voltage at resonance as the specimen is displaced radially, is shown for the single 80 KHz coil in the absence of the 120 KHz coil in Figure 5-27. This available error signal (15%) is considerably larger for this "optimized" hemispherical arrangement as compared to the early laboratory studies referred to previously in which the axial (vertical) B^2 gradient was necessarily made much greater than the radial gradient for terrestrial levitation purposes.

With the second coil in place, the position sensing signals were again measured as changes in terminal voltages as each coil was separately driven at its displaced resonant frequency with the other coil connected to its amplifier but with no excitation. These results are shown in Figure 5-28. It is seen that the position sensing signal is on ly approximately 1/2% of the total terminal voltage. Previous laboratory work with this type of position damping control servo has shown that position signals of the order of several percent of the full terminal voltage are desirable for reliable operation. The present result thus indicates that further development would be required for reliable operation of a servo operating on the relatively small position signal of only 1/2%. This is considered to be an unfavorable result for the opposed hemisphere arrangement.

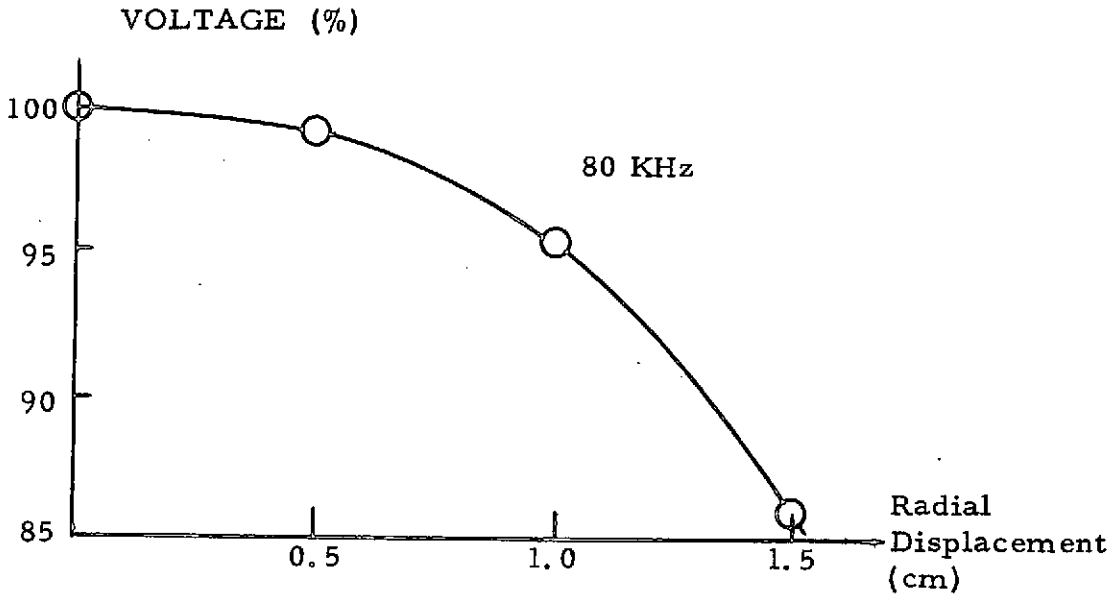

Figure 5-27. Terminal Voltage vs. Position of Aluminum Sphere (2.0 cm dia) for an Isolated Coil

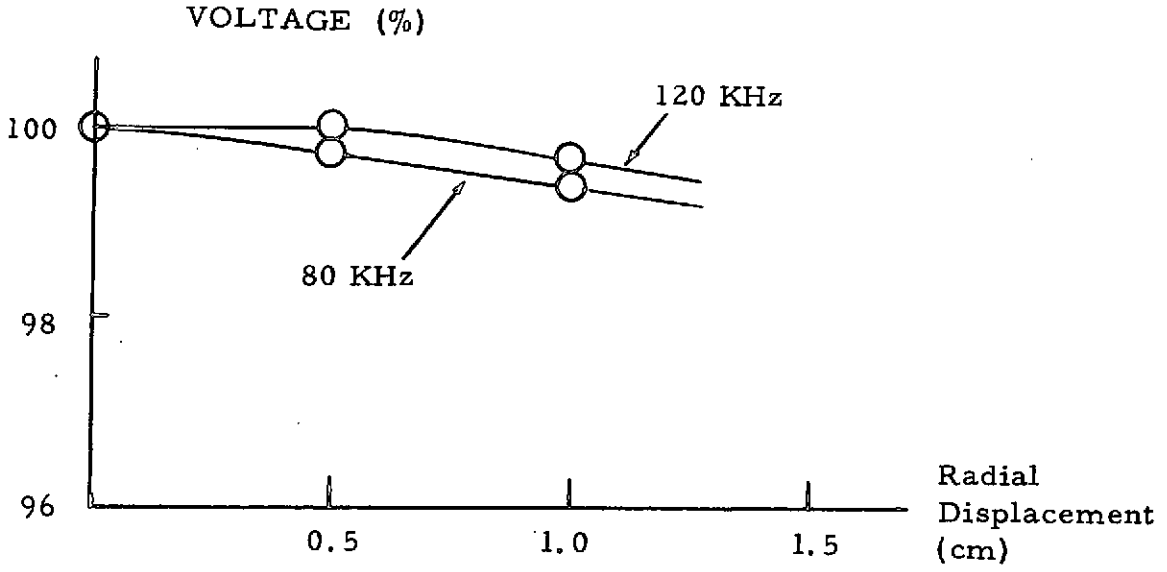

Figure 5-28. Terminal Voltage vs. Position of Aluminum Sphere (2.0 cm dia) for One Coil in the Presence of Another

Additional tests were carried out in which the coil spacing was increased from 0.7 cm to 1 cm and the number of equatorial turns was reduced from three to two. These steps were taken to reduce the mutual coupling of the coils which was held responsible for the large reduction in position sensing sensitivity as compared to the behavior of a single coil. It was found that although large enhancements could be made in the position sensing sensitivity for one of the coils, simultaneous improvement for both coils did not appear to be possible. Furthermore, these coil changes represent a departure from the optimum grad B^2 (force field) configurations derived in Section 5.2.4 above.

5.3.5 "STIFFNESS" OF CONTROL NEAR CENTRAL POSITION

Since, for some high resistivity specimens, electron beam heating and melting may be more efficient, as regards total required power, than eddy current heating, the suitability of the position control system to maintain the specimen accurately at the focal point of an electron beam will be important. For this reason the following computations were made of the distance through which a 2.0 cm diameter sphere with large x-parameter (ratio of radius to skin depth) will be pushed by a constant external force, such as might be caused by an electron beam, while suspended in a coil system in a weightless environment. Three different coil systems were assumed. Because of the low sensitivity of electromagnetic position sensing just derived for the opposing hemispherical coils, it was known that the "stiffness" of this system would be low and hence was not evaluated. The results are given in Tables 5-9, 5-10 and 5-11, and an explanation of the calculations which led to these results is given below.

5.3.6 BASEBALL COIL

5.0 cm diameter
2 turns
Conductor diameter = 0.25 inch = 0.64 cm
Total length = 50 cm
Frequency = 100 KHz
Resistance = 0.0011 ohm

In Section 5.2.6 data were given for a 5.0 cm diameter baseball coil exerting force upon a 1.0 cm dia. solid aluminum sphere. The data in Figure 2 of that section, for measurements along the X-axis, provide the basis for the calculations for the baseball coil given here. Earlier data were obtained assuming 102 amperes flowing in a single turn coil. An equivalent ampere turn strength for the two-turn coil described above requires dissipation of $(51)^2(0.0011)$ or 2.6 watts in the two-turn coil. Assuming power conversion circuitry in the free suspension facility to be 50% efficient, the total power to the facility would be 5.2 watts. (From data given below it is known that the fraction of total power absorbed by a 2.0 cm dia. sphere is of the order of only 6% for a specimen of such low resistivity. This was ignored in this calculation.) These 5.2 watts are sufficient to generate the forces measured on the 1.0 cm dia. aluminum sphere and to generate about 8 times such force on a 2.0 cm dia. sphere, as considered here. By assuming several other amounts of power absorbed by a facility containing such a two-turn coil, as listed in Table 5-9, a displacement from the center of the coil may be found at which the force generated is equal and opposite to the external forces given in Table 5-9.

5.3.7 CUSP COIL

Two 2-turn coils, each having radius = 1.8 cm, separated by 3.5 cm (i.e. wound on a 5.0 cm dia. sphere).

Conductor diameter = 0.25 inch = 0.64 cm
Frequency = 100 KHz
Resistance = 0.0010 ohm

In Figure 5-20 the axial force exerted upon a 2.0 cm dia. sphere of large x-parameter on the axis of a cusp coil such as that described above, is given for a current of 100 amperes. Such a current requires the dissipation of 10 watts in the coil. The data in Table 5-10 were then calculated in the same manner as was done for the baseball coil.

5.3.8 SIX COIL CUBE

Six 3-turn coils each of 1.25 cm radius with coils which are opposite one another 4.3 cm apart (i.e. wound on the surface of a 5.0 cm dia. sphere).

Conductor diameter = 0.125 inch = 0.32 cm
Frequency = 100 KHz
Resistance = 0.0011 ohm (each coil)

The force each coil exerts upon a 2.0 cm dia. sphere may be written as

$$F = \frac{1}{4}a^3 G(x) \text{ grad } H^2 = \frac{1}{4}\text{grad } H^2 = \frac{1}{4}\text{grad}\left(\frac{H}{I}\right)^2 \frac{P}{R} \quad \text{(here R = coil resistance)}$$

$$= 228 \text{ grad}\left(\frac{H}{I}\right)^2 P \qquad (5.3.8\text{-}1)$$

where G(x) is taken to be unity, P is the power in watts dissipated in each coil, H is in oersteds, I in amperes and F in dynes. It may be assumed that the external force acts parallel to and on the axis of one pair of coils. Let it also be assumed that, in order to increase positioning stiffness, the coil which opposes it may draw up to one-half the total power absorbed by the six coils and the four neighboring coils share the other half. Again assuming the power conversion circuitry to be 50% efficient, this means that that one coil may draw up to one-quarter the total power to the facility.

The position of the 2.0 cm dia. sphere will be determined by the servo-control system which detects the position of the sphere and then "turns on" the opposing coil in proportion to the displacement Δ from the center of the coil system. We assume the power supplied to the coil to increase linearly with displacement of the sphere toward the coil, varying from zero at the center of the set of six coils to the maximum allotted power for a displacement of the sphere of 1.0 cm. Thus

Table 5-9

Stiffness of Baseball Coil

Total Power to Facility	Displacement from Center for F = 5 dynes	10 dynes	50 dynes
1000 watts	0.1 cm	0.2 cm	0.4 cm
500	0.2	0.3	0.5
250	0.3	0.4	0.8
100	0.4	0.5	1.1
50	0.5	0.8	*

*Coil unable to contain sphere

Table 5-10

Stiffness of Cusp Coil

Total Power to Facility	Displacement from Center for F = 5 dynes	10 dynes	50 dynes
1000 watts	0.0005 cm	0.001 cm	0.005 cm
500	0.0009	0.002	0.009
250	0.002	0.003	0.02
100	0.005	0.01	0.05
50	0.009	0.02	0.09

Table 5-11

Stiffness of Six-Coil Cube

Total Power to Facility	Displacement from Center for F = 5 dynes	10 dynes	50 dynes
1000 watts	0.01 cm	0.02 cm	0.08 cm
500	0.02	0.04	0.12
250	0.04	0.07	0.23
100	0.09	0.15	0.42
50	0.15	0.24	0.58

$$P = \frac{1}{4} \frac{\Delta}{1.0 \text{ cm}} P(\max) \qquad (5.3.8\text{-}2)$$

and, combining this with the force equation above.

$$F = 57\ \Delta \operatorname{grad}\left(\frac{H}{I}\right)^2 P(\max) \qquad (5.3.8\text{-}3)$$

Values of $\operatorname{grad}\left(\frac{H}{I}\right)^2$ were obtained from Section 5.2.3 and values of Δ were calculated as given in Table 5-11.

Comparison of the data of Tables 5-9, 5-10 and 5-11 shows that the "stiffness" of the particular cusp coil studied exceeds by about an order of magnitude the stiffness of even the 6-coil cube system in which unequal excitation of opposing coils is employed. The particular cusp coil selected for study here is one which has somewhat more axial stiffness than the configuration giving equal axial and radial gradients referred to previously. It is believed that such a choice would be appropriate when high power electron beams are employed in order to minimize displacement of the specimen being heated. Thus the cusp appears to be a logical choice to be made for those situations in which electron beam heating is employed at high powers and rather rigid control of specimen position is required.

5.3.9 RELATIVE EFFICIENCY FOR RF INDUCTION HEATING

5.3.9.1 Computations of Induction Heating Efficiency

From the detailed results which are available for magnetic field distributions and coil losses including proximity effect, it is possible to compute the fraction of total coil power which is transferred to the specimen. These evaluations are important not only to estimate total power requirements for heating and melting various specimens but also are important in determining feasibility for electromagnetic position sensing which depends upon appreciable changes in

specimen power absorption as the specimen position changes. Figure 5-29 shows results of computations for a specific baseball winding at several frequencies as a function of specimen resistivity. It is seen that the heating efficiency increases with specimen resistivity up to a maximum value which depends upon the operating frequency. In the limit of very high facility frequencies the heating efficiency increases continuously with specimen resistivity until an asymptote is reached.

Computations and measurements were made for heating efficiency of a 5.0 cm diameter baseball winding, versus frequency, with 2.50 cm diameter specimens of resistivities corresponding to that of aluminum and steel. These results are shown in Figure 5-30 as the solid curves. Figure 5-31 gives corresponding calculational data for a cusp coil of dimensions as illustrated in that figure. The equation given previously

$$P = 3\pi F(x) a \rho H^2 \quad \text{(MKS)} \qquad (5.3.9\text{-}1)$$

was used for values of frequency ranging from 1 KHz to 300 KHz and resistivity values of 4×10^{-6} ohm/cm and 74×10^{-6} ohm/cm. The latter were chosen to represent the electrical resistivity of the aluminum and steel spheres used in experimental measurements about to be described. The heating efficiencies were obtained by dividing the computed power dissipated in the specimen by the sum of that power and the power dissipated in the coil. The value of H^2 which was used in these calculations was neither the value of H^2 found at the center of the coil nor the value of H^2 averaged over the specimen's volume. This was because, in the cases considered, the skin depth is relatively small and the values of H^2 which most directly contribute to the generation of induced current in the specimen lie near the surface of the sphere in the vicinity of the axis or axes of symmetry. No attempt was made to make an exact computation of the best value of H^2 to be used but an average value of H^2 over the regions concerned was estimated from computer calculations of H^2 for several points in, or near, those regions.

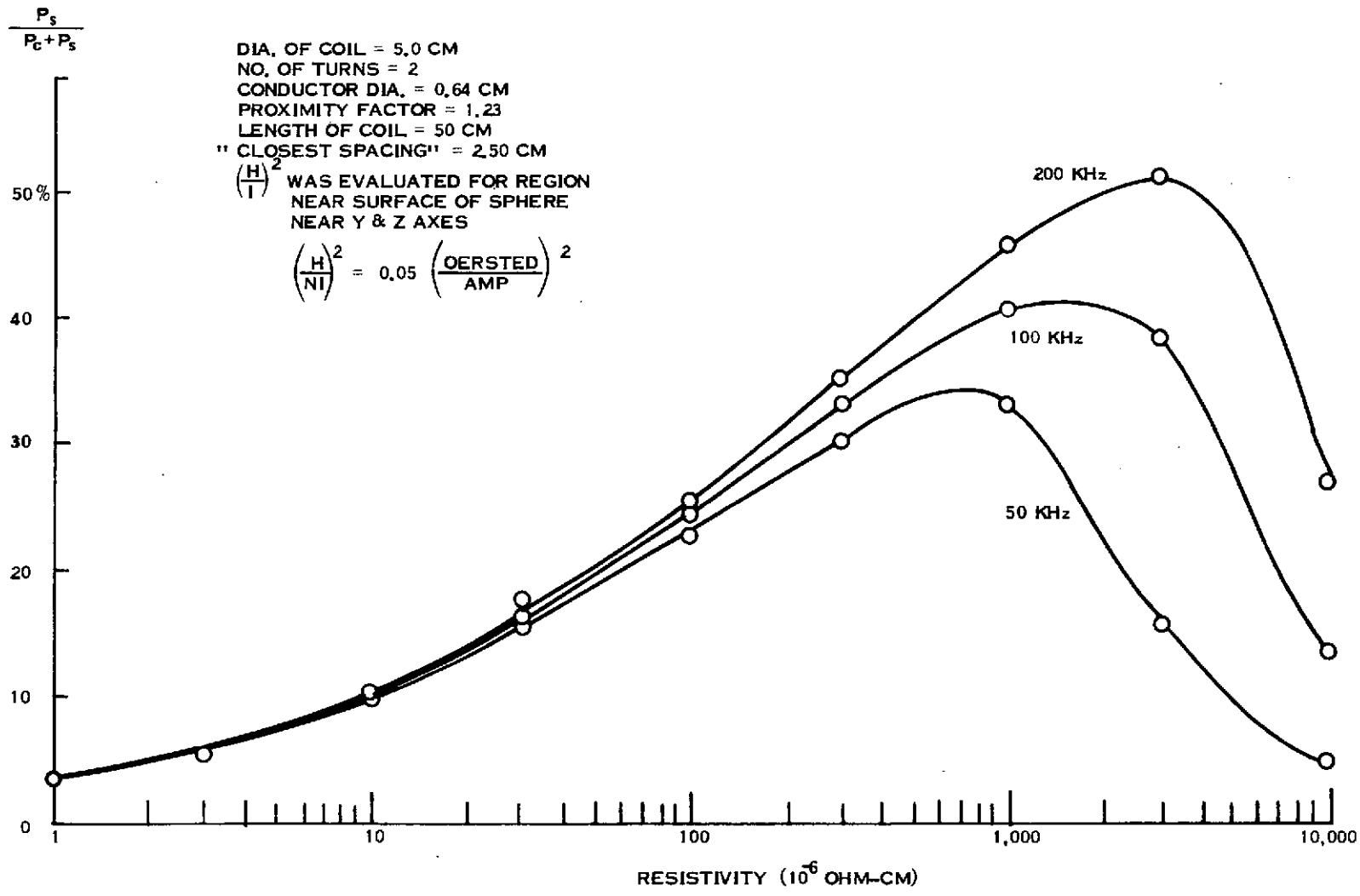

Figure 5-29. Efficiency of Heating a Specimen vs. Resistivity for a Baseball Coil

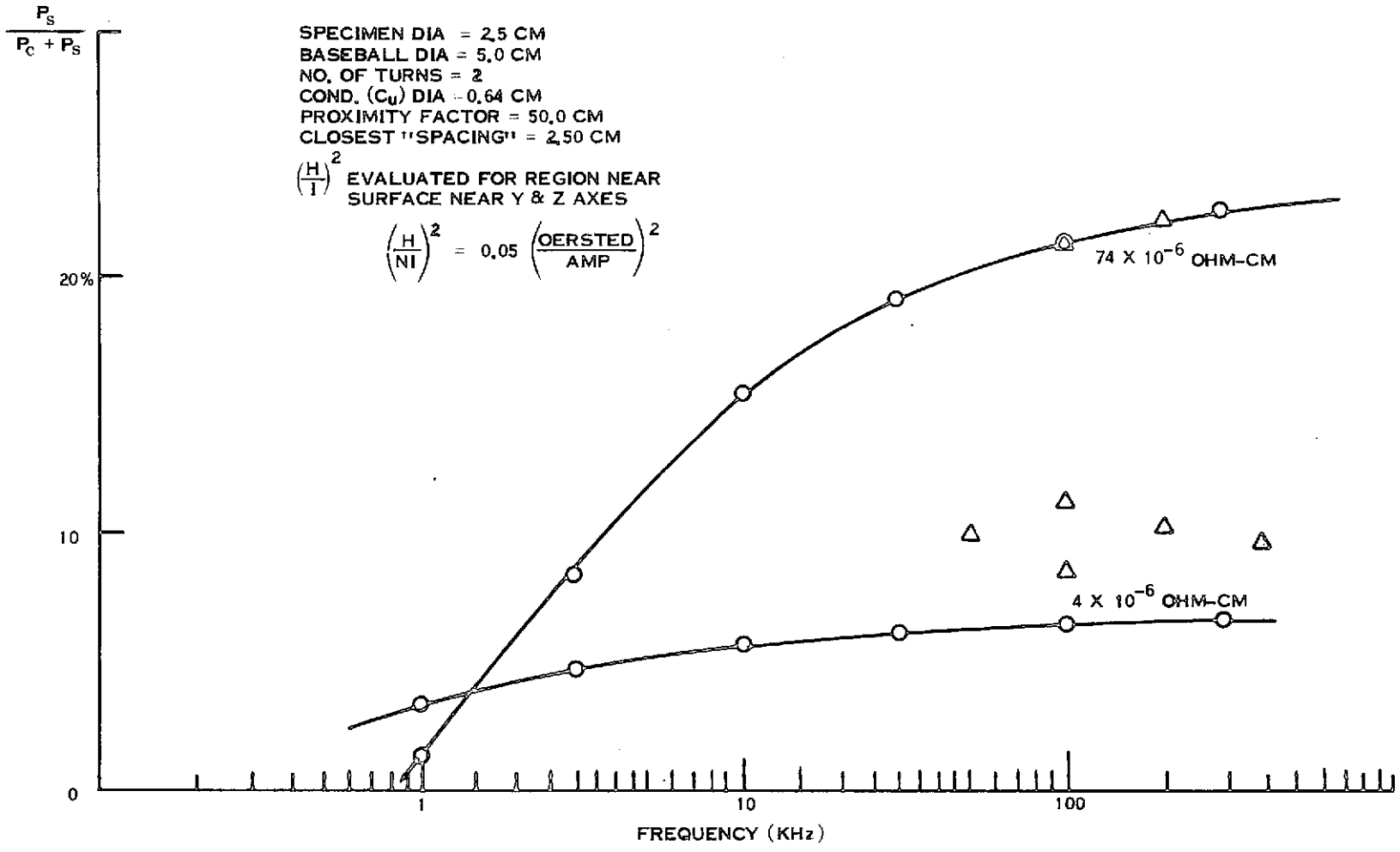

Figure 5-30. Efficiency of Heating a Specimen in a Baseball Coil

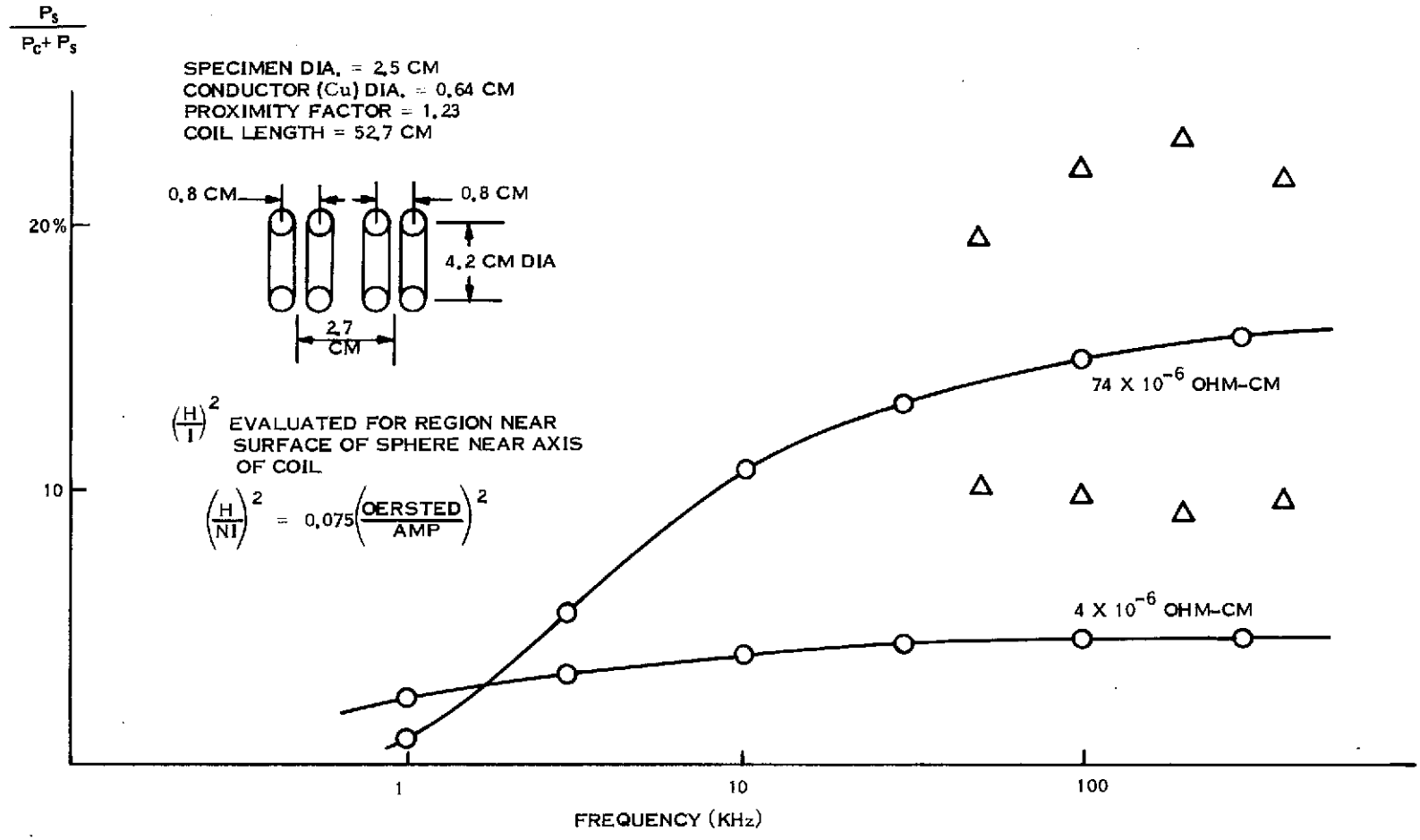

Figure 5-31. Efficiency of Heating a Specimen in a Cusp Coil

5.3.9.2 Measurements of Heating Efficiency

Measurements of heating efficiency have been performed by two different methods. The first method involves the measurement of the Q for the resonant tank circuit coupled to the field producing coil (see sketch) with and without the

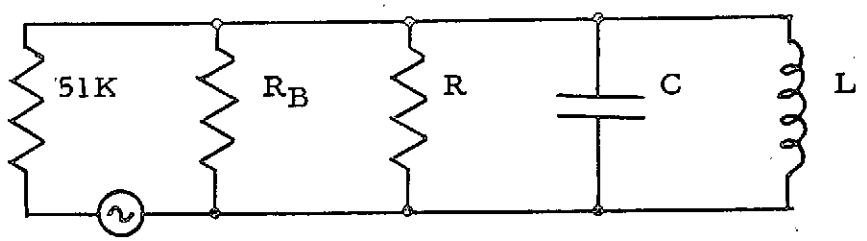

specimen placed in the field producing coil. The inductance and capacitance are furnished by the tank circuit. R represents the equivalent loss resistance furnished by copper losses and transformer losses. R_B represents the equivalent loss resistance introduced when the conducting ball representing the specimen is placed into the field producing coil. The voltage source represents the signal generator used in the experiments and the 51K resistor used to couple the generator to the circuit. It may be shown that, for relatively low coupling efficiencies and for the case in which the change in resonant frequency when the ball is introduced is small, the heating efficiency is given approximately by

$$\eta = R_L/R_B = 1 - \frac{Q_L}{Q_U}. \qquad (5.3.9\text{-}2)$$

R_L represents the resistance of the parallel combination 51K, R_B and R. Q_L is the measured Q of the loaded circuit with specimen in place and Q_U the measured Q of the unloaded circuit with specimen removed. When account is taken, with higher efficiencies of the change $\delta\omega$ in resonant frequency with the specimen in place, an additional term in the efficiency expression appears equal to $\delta\omega/\omega_L$ where ω_L is the resonant frequency for the loaded situation, i.e. with the specimen in the coil.

A second method for computation of heating efficiency is as follows. The diagram shows the circuit comprising the tank circuit, coil and specimen as

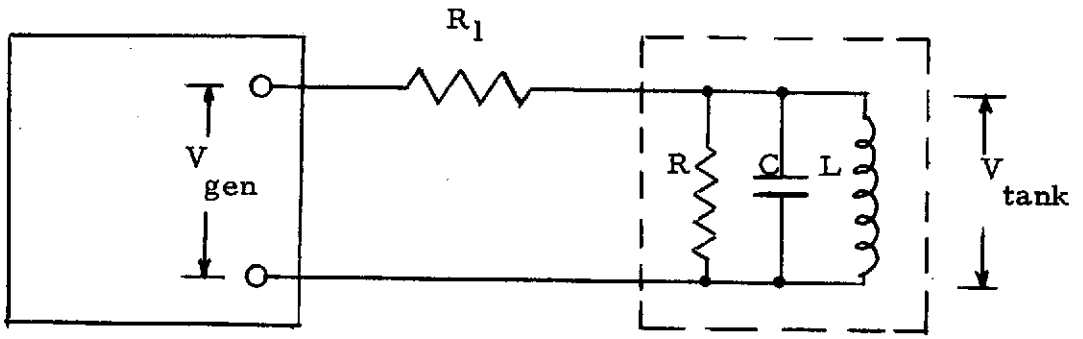

an equivalent RLC circuit. To measure absorbed power, the signal generator frequency is adjusted so that there is no phase shift between V_{gen} and V_{tank}. This means that the equivalent circuit is pure resistance and this resistance R represents the power absorbed by the tank circuit, capacitor, core, coil and specimen if one is present. This resistance is simply calculated when V_{gen}, V_{tank} and R_1 are measured. Because the current is the same in both resistors,

$$\frac{V_{gen} - V_{tank}}{R_1} = \frac{V_{tank}}{R} \quad \text{and} \quad R = \frac{R_1 V_{tank}}{V_{gen} - V_{tank}} \qquad (5.3.9\text{-}3)$$

To determine absorbed power in the specimen, R is determined without the specimen present (unloaded) and again with the specimen present (loaded). The specimen equivalent resistance when paralleled with the unloaded resistance gives the loaded resistance so the specimen equivalent resistance is readily calculated, and therefore its fraction of the incoming power is determined as

$$\eta = \frac{\text{Loaded Resistance}}{\text{Specimen Resistance}} . \qquad (5.3.9\text{-}4)$$

Comparison of the two methods of measurement of heating efficiency shows that they generally give results differing by only a few percent. Scatter in the experimental values can also fluctuate by a few percent.

Measured heating efficiency values utilizing the Q measurement method for both the baseball (shown in Figure 5-33, d.) and cusp coil configurations are plotted as the triangles in Figures 5-30 and 5-31 respectively. It can be seen that although agreement in the case of the baseball is reasonable, the measured efficiencies in the cusp are consistently higher than those calculated. This difference is attributed to too small a value for H^2 having been selected for the calculation.

The measured heating efficiencies show a drop-off (Figures 5-30 and 5-31) from those computed for the field producing coil losses alone beginning at about 100 KHz and becoming significant at 400 KHz with a standard available ferrite core material - designation 3E2A (Ref. 5-6). Analysis showed that this additional loss was proportional to frequency and indicated that loss in the ferrite core might be responsible. Analysis of available data for these commercially available cores used in the coupling transformers verified this suspicion. Experiments were therefore carried out with lower loss ferrite core materials (3C8 designation). These measurements for a 2.5 cm sphere of either aluminum or steel in a 5 cm diameter cusp coil are shown in Figure 5-32. It can be seen that losses at 400 KHz are very greatly reduced with the use of the 3C8 material.

Low loss core materials are available for use at even higher frequencies but are not presently fabricated into cores of the type required in these experiments. This indicates an area of presently non-commercially available components required for the Space Lab facility. The use of ferrite cores in the HF frequency regime greatly reduces copper losses due to the resulting compactness of the transformer windings. Utilization of air core transformers would produce increased copper loss. Since transformer and tank circuit efficiency are important

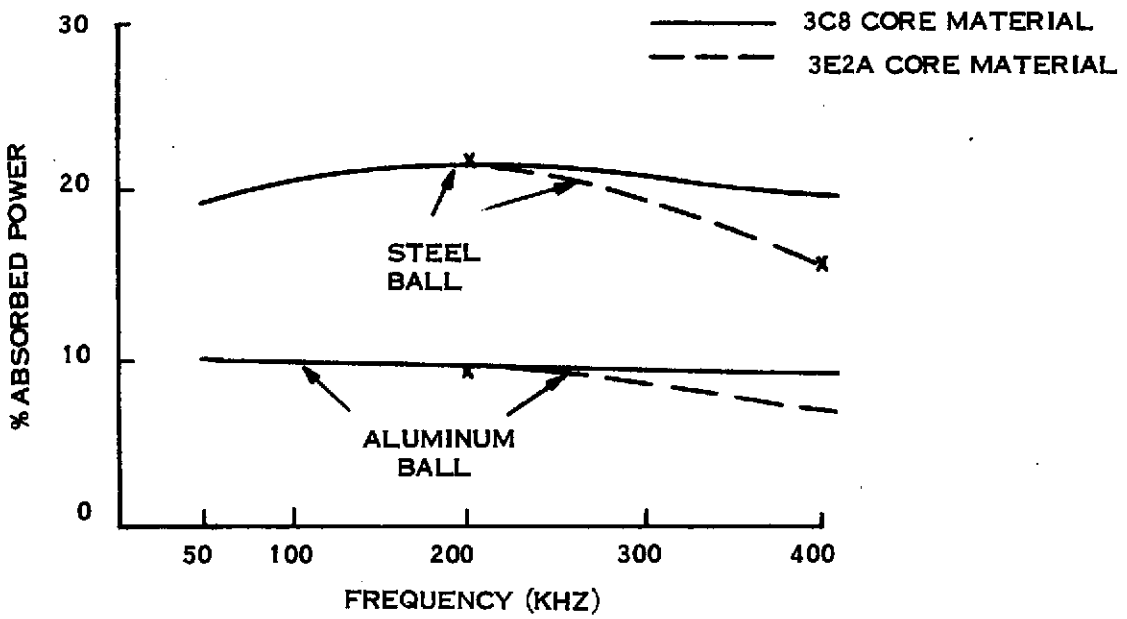

Figure 5-32. Measured Heating Efficiency with Two Specimens and Two Transformer Core Materials

in determining total facility power requirements this indicates desirability for an early detailed study in this area.

5.3.10 EFFICIENCY CONSIDERATIONS FOR RELATING INPUT POWER TO COIL-SPECIMEN REQUIREMENTS

Once the amount of power required by the coil has been established, it is necessary to know the efficiency of the equipment back to the input energy source in order to specify the overall power of the facility. The equipment considered in the estimation of overall efficiency is as follows.

a. Impedance Transformer - Tank Circuit

b. Working Coil Transmission Line

c. RF Generator or Amplifier

d. Power Conditioning Equipment

The efficiency of each of the above will be somewhat dependent on the specific process and possibly to a severe extent on imposed specifications of weight and volume limits. Another potentially significant factor affecting efficiency may be facility imposed by the need to observe, handle and store specimens, monitor temperature, accommodate an electron beam installation and environment control, plumbing such as vacuum ports, coolant equipment, etc.

It is obvious that overall mission considerations not known or within control at present make a definite determination of efficiency impossible but estimates can be made based on common commercial practice with modifications where called for.

5.3.10.1 Impedance Matching Transformer - Tank Circuit

This device's function is to match the RF power source impedance to the working coil impedance. This normally is a transformer accompanied by a capacitor whose function is to provide power factor correction. The transformer has an appropriate ferrite core which will weigh about 1.5 KG per KW at 10 KHz, less at higher frequencies. In the range 10-100 KHz, its efficiency can be made about 95%. The capacitor may be any high quality paper or plastic insulation unit. Commercial practice uses aluminum plates with a synthetic chlorinated oil impregnant.

At frequencies of 100 KHz to 1 MHz the transformer uses a low loss high frequency ferrite core and the capacitors are usually mica insulated aluminum plate units. The transformers are not so big or heavy, weighing about 0.5 KG per KW to about 0.2 KG per KW with the lighter units being those intended for operation at 1 MHz.

At frequencies from 1 MHz to about 30 MHz the transformer may be either ferrite or air core. Commercial transformer practice at high power and over 100 KHz is exclusively air core. Ferrites are available with

permeabilities of about 150 at 10 MHz and only a detailed design will show whether anything will be gained using them. Air core transformers used commercially regularly have efficiencies of 70% to 80%. Using ferrite cores this may possibly be raised to 85% or 90%.

Capacitors at these frequencies are air insulated with plates that are silver or gold plated.

5.3.10.2 Work Coil Transmission Line

Losses in the transmission line connecting the tank circuit and the work coil are directly proportional to length. Therefore the transformer is usually very near the work coil. Indeed, for small coils of about two turns the coil should be supported by the transformer secondary thereby eliminating the line. When the transformer cannot be physically placed adjacent to the coil an allowance must be made for its loss. At distances of two or three coil diameters an efficiency of 85% seems reasonable and will vary as its length changes.

5.3.10.3 RF Power Amplifier or Oscillator

When the device used is within its normal frequency range whether it is an inverter, amplifier or oscillator, its efficiency at optimum conditions is about 70% and it is likely that conditions will prevent an efficiency over 60%. Only unusual conditions would cause the efficiency to drop to 50% and anything under 50% would probably have to be justified by a particularly adverse process requirement, such as operation over a large range of absorbed power, impedance match switching devices being denied for some reason, etc.

5.3.10.4 Power Conditioning Equipment

The use of semiconductors would allow operation directly from batteries. Semiconductor devices capable of operating at frequencies of about 1 MHz or less

are available. Operation at higher frequencies and at the higher power levels will probably require vacuum tubes of the types used in industrial heaters and broadcast transmitters. These tubes generally require plate voltages of 5 KV to 10 KV. Normally, to obtain high voltage from batteries it is necessary to use an inverter with step-up of voltage and high voltage rectification. The efficiency of these inverter-rectifier systems vary from 70% to 90% depending on weight, voltage regulation, and Electromagnetic Interference requirements.

It is felt therefore that the following efficiencies, though not exact, are represen tative values for estimating power requirements.

a.	Transformer and Tank Circuit	70% to 95%
b.	Working Coil Transmission Line	85%
c.	RF Generator or Amplifier	50% to 70%
d.	Power Conditioning Equipment	70% to 90%

The efficiency figures quoted here were determined by our own experience with designs of lower power and by reference to published data and calculations.

Figure 5-33 consists of photographs of several of the laboratory test setups used for heating efficiency and force measurements. Figures 5-33 (a) and (c) show neutral buoyancy test setups used at low power with the baseball and cusp configurations, respectively. Figure 5-33 (b) shows the levitation in air of a 1 cm diameter aluminum sphere using a single hemispherical configuration coil with an operating position control and damping circuit. The sphere was melted and superheated to approximately 1000^{o}C using less than 200 watts total input power to the RF coil. Figure 5-33 (d) shows the scaled baseball coil utilized in the heating efficiency and force measurements referred to. In Section 6 of this report, it is considered that the overall coil dimensions and conductor tubing diameter would both scale in proportion for larger facilities

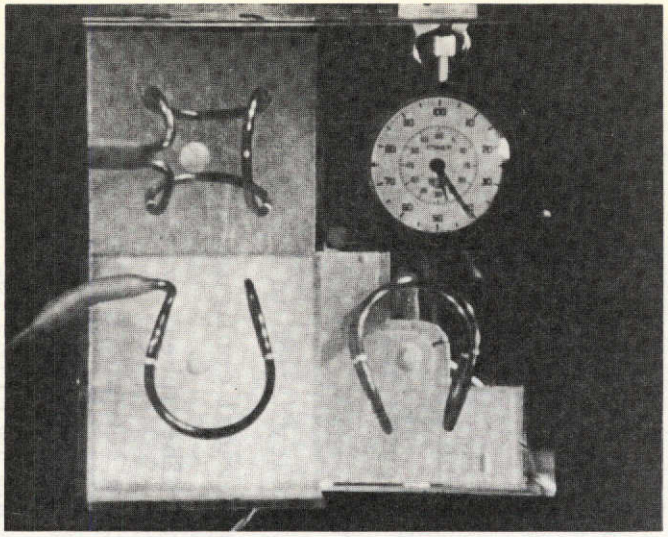

(a) One Turn Baseball Coil

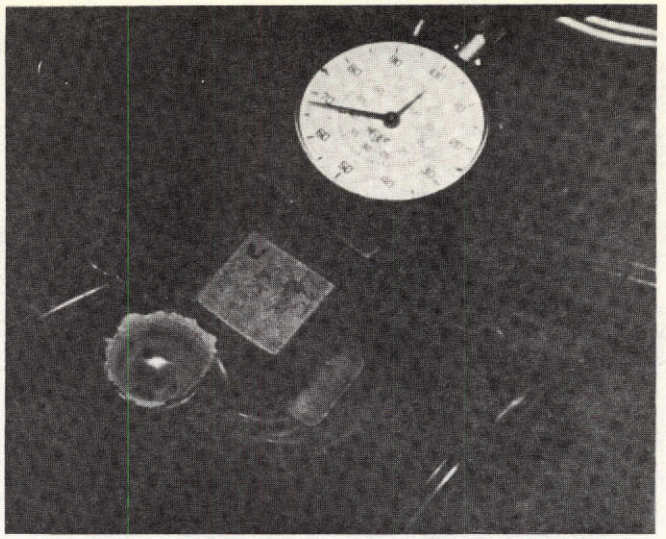

(b) Cup Coil with Levitated, Molten Aluminum 1 cm dia. sphere

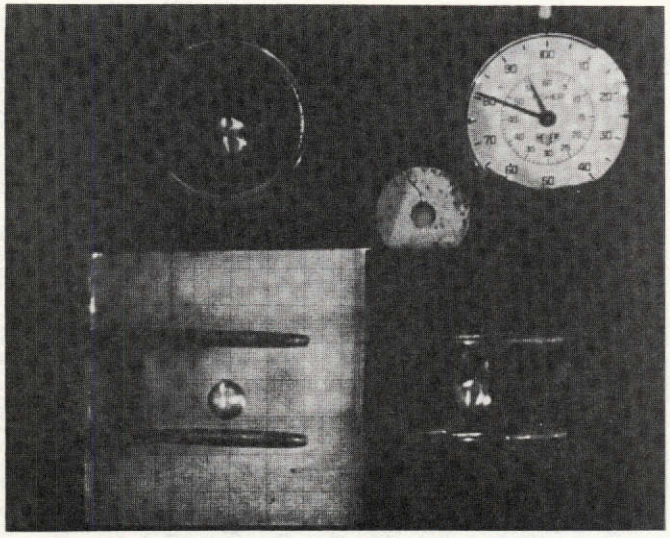

(c) One Turn Cusp Coil

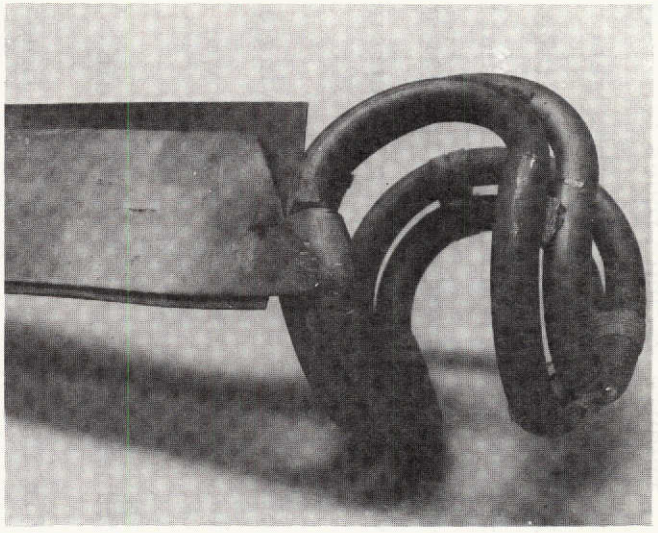

(d) Two Turn Baseball Coil

Figure 5-33. Photographs of Coils Used in Laboratory Tests and Demonstrations (Note that in (a) & (c) two mirrors are present which provide top and side views)

for maximum efficiency of operation. The transmission line consists of two closely spaced flat bus bars. Since the baseball and cusp windings and their transmission line have very small inductance, external field amplitudes requiring EMI shielding are minimized.

The above considerations formed the basis for the efficiency assumptions utilized in the Facilities Capabilities section below. In Section 6.0 maximum specimen size is derived as a function of specimen melting temperature for several assumed fixed levels of power available for use in the Containerless Processing Facility.

5.4 RECOMMENDED COIL CONFIGURATIONS FOR EARLY SPACE LABORATORY ELECTROMAGNETIC CONTAINERLESS PROCESSING FACILITY

In the preceding sections, intercomparison of the various electromagnetic field configurations eliminated some candidate coil configurations on the basis of suitability of the position control force field on an equal size and power basis. Evaluation of several engineering factors such as accessibility, compatibility with the simplest electromagnetic position servo and adaptability to significant thrusts caused by electron beam heating, further narrowed the list of most promising candidates. The two systems which appear from an overall engineering point of view as the best, based on all of the above considerations, appear to be the baseball and cusp arrangements. RF heating efficiency measurements for relatively large specimens do not serve to markedly distinguish between these two types of coil. For specimens whose size is small compared to the coil dimensions, however, the baseball heating efficiency will obviously be greater than that for the cusp coil because of the field null at the center of the latter. However, the cusp coil shows a much greater "stiffness" to maintain the specimen accurately at an electron beam focus than the baseball. Since, as will appear in the sequel below, both types of specimen heating and melting should be considered in a facility having the widest capability for processing

materials of various melting temperatures, it is recommended that the facility for Space Lab be designed to accommodate either type of coil interchangeably. For maximum power efficiency for both positioning or for induction heating, when the latter is used, exchangeable modular coils of sizes commensurate with the specimen size being processed should be considered, just as in the case of terrestrial levitation work. For the higher melting temperature specimens, conservation of total facility power will not allow the low efficiencies customary in terrestrial work when a coil size far from optimum is employed. The consideration of two types of coil configuration is compatible with the consideration of an interchangeable set of coils of various sizes. In the following section, the facility capability for handling the various materials and processes considered in Section 3 are delineated. Both electron beam heating and induction heating are considered.

5.5 REFERENCES

5-1 Okress, E. C., Wroughton, D. C. m Comenetz, G., Brace, P. H. and Kelly, J. C. R., "Electromagnetic Levitation of Solid and Molten Metals," Jrnl of App. Phy., 23, No. 5, p. 545-, May, 1952, Vol. 23, No. 12, p. 1413, Dec., 1952.

5-2 Price, E. G., Thesis, School of Metallurgy, Univ. of New South Wales, Australia, 1961.

5-3 Smith, W. E., "Electromagnetic Levitation Forces and Effective Inductances in Axially Symmetric Systems," Brit. Jrnl of App. Phys., 16, p. 377, 1965.

5-4 Brisley, W. and Thornton, B. S., "Electromagnetic Levitation Calculations for Axially Symmetric Systems," Brit. Jrnl of App. Phys., 14, p. 682, 1963.

5-5 Peirce, B. O., A Short Table of Integrals, Ginn & Co., Boston et al, 1929.

5-6 Linear Ferrite Materials & Components, Ferroxcube Corp., Saugerties, N. Y.

SECTION 6

SPACE LABORATORY FACILITY CAPABILITIES AS FUNCTION OF AVAILABLE POWER

6.1 INTRODUCTION

This final section summarizes the results of calculations performed to indicate the largest sizes of specimens, for fixed total power, which may be suspended in a cusp coil facility and melted either by electromagnetic induction or by some other source of heat, such as an electron beam. Because of the similarity of efficiency of the baseball for RF heating for larger specimens, which represents the main factor determining required facility power, these capability estimates can also be taken as typical of a baseball facility. These calculations have been performed from the consideration of power dissipated at or near the specimen's melting point, do not account for limitations in the dissipation and removal of large amounts of heat in very small coils and have been based upon laboratory data for which forces acting upon and power dissipated in actual specimens were measured. These laboratory data permit calculation of constants relating magnetic field strength and gradient averages to coil current, actually geometrical relationships, which were then used to calculate the behavior of the coil-specimen system for a range of specimen resistivities, sizes, and optimum frequencies.

6.2 LABORATORY DATA FOR 5.0 CM DIAMETER CUSP COIL

The force measuring apparatus described in Section 5.2.2 and the "second method" of computation of heating efficiency described in Section 5.2.9 were used to obtain data for this section. The characteristics of the aluminum sphere and of the copper cusp coil were as follows

aluminum sphere

diameter = 2.54 cm

resistivity = 4×10^{-6} ohm-cm

copper cusp coil

diameter (spherical)	=	5.0 cm
spacing between loops	=	2.7 cm, center-center
number of turns	=	2
diameter of conductor, d	=	0.64 cm
length of conductor, ℓ	=	53 cm
coil proximity factor	=	1.2

With a frequency of approximately 100 KHz for both force and heating efficiency measurements and a current of 67 amperes rms for the force measurements, the following were measured.

force: 100 dynes, 0.5 cm from center of coil, both on axis and on central plane

heating efficiency: 10%, at center of coil

Then, using the equations (5.1.3-3) and (5.3.9-1) given previously

$$F = \frac{1}{4}\, a^3\, G(x)\, \text{grad}\left(\frac{H}{I}\right)^2 I^2 \quad \text{CGS} \tag{6.2-1}$$

$$P_{\text{specimen}} = 3\pi\, F(x)\, a\rho \left(\frac{H}{I}\right)^2 I^2 \quad \text{MKS} \tag{6.2-2}$$

values of the desired constants were obtained, viz.

$$\text{grad}\left(\frac{H}{I}\right)^2, \text{ (0.5 cm from coil center)} = 0.49 \text{ oersteds}^2/\text{amp}^2\text{cm}$$

$$\left(\frac{H}{I}\right)^2, \text{ (at coil center)} = 0.28 \text{ oersteds}^2/\text{amp}^2 \tag{6.2-3}$$

6.3 SELECTION OF OPTIMUM FREQUENCIES

The efficiency of heating an electrically conducting sphere rises continuously with increasing frequency but the rate of increase is relatively slow for values of x greater than 3 and has virtually attained its asymptotic value for values of x greater than 20. The force exerted upon such a sphere per unit power is at a maximum at a value of x of about 3. It decreases rapidly for values less than 3 and less rapidly for values greater than 3. Thus, in general, it is desirable to operate a free suspension system with values of x greater than 3, and no great disadvantage is incurred when operating at values of x not greatly in excess of 20.

Because the cusp coil used in the laboratory was operated with no difficulty at 400 KHz, because a value of x of 3 or greater is attained with 400 KHz for resistivities less than 3×10^{-3} ohm-cm and because the force per unit power changes little with resistivities less than 3×10^{-3} ohm-cm at 400 KHz, 400 KHz was chosen to be the nominal operating frequency corresponding to the laboratory size coil in the calculations for 10^{-5} and 10^{-3} ohm-cm. For calculations at 10^{-1} ohm-cm a frequency of 15 MHz was selected because $x = 3$ with this combination. For 1 ohm-cm the same frequency, 15 MHz, was used despite a resulting value of x of 1, because it is at frequencies greater than 15 MHz that losses in the auxiliary circuits are expected to become noticeable by decreasing the efficiency of conveying power into the coil.

6.4 EXTENSION TO COILS OF DIFFERENT SIZES

In following sections, the power required by a cusp coil to position and to melt specimens of varying properties is calculated for the 5.0 cm dia. coil described above and for a 2.5 cm dia. specimen. Then, to determine the maximum size the specimens may have, for a particular limiting value of available power, it is necessary to examine how the power absorbed by the coil and the power absorbed by the specimen vary with the size of the specimen and coil.

This section establishes the basis for the "scaling" of the power as the physical dimensions of the system are "scaled."

Let a scale factor K be defined by the relation

$$K \equiv \frac{a}{1.25 \text{ cm}} \tag{6.4-1}$$

where a is the specimen radius so that any specimen of radius a is K times greater than the sphere used in the laboratory. Also, let all physical dimensions of the coil have the same scale factor relationship with the corresponding dimension used in the laboratory. Because the magnetic field intensity in the central region created by current flowing in a coil is inversely proportional to the size of the coil, for constant current, it may be seen that $\left(\frac{H}{I}\right)^2$ is proportional to K^{-2} and grad $\left(\frac{H}{I}\right)^2$ is proportional to K^{-3}.

Once the operating frequency has been selected for the 5.0 cm dia. coil the resulting value of x must be maintained near optimum with scaling of the coil. This means that the frequency is a function of K. The ratio of sphere radius to skin depth is x, the sphere radius is proportional to K and the skin depth is proportional to the reciprocal of the square root of frequency. Thus if x is to be kept constant, the frequency must be proportional to K^{-2}.

The resistance of the coil is

$$R_{coil} = \frac{\rho_{coil}\, \ell_{coil}}{\pi \delta_{coil}(d-\delta_{coil})} \tag{6.4-2}$$

If $d \gg \delta_{coil}$, as is true in all of the calculations in this section, the resistance is proportional to $\frac{\ell}{\delta d}$, which is proportional to $\frac{K}{f^{-1/2}K} = f^{1/2}$, which is proportional to K^{-1}. Thus R_{coil} is proportional to K^{-1}, when x is kept constant.

In summary,

$$\left(\frac{H}{I}\right)^2 \text{ is proportional to } K^{-2}$$

$$\text{grad}\left(\frac{H}{I}\right)^2 \text{ is proportional to } K^{-3} \qquad (6.4\text{-}3)$$

$$f \text{ is proportional to } K^{-2}$$

$$R_{coil} \text{ is proportional to } K^{-1}$$

The application of these relationships is in the scaling of several equations used in sections following.

6.5 INDUCTION HEATING

6.5.1 LABORATORY BASE CASE

The power, P_{spec}, required to melt and superheat specimens with melting points of 1000, 2000 and 3000°C was assumed to be 1.2 times the power required to maintain the specimen (with emissivity of 0.8) at 1000, 2000 and 3000°C. From equation 6.2-2 and $P_{coil} = I^2 R_{coil}$, the power dissipated in the coil was calculated for several values of resistivity, ρ, using

$$P_{coil} = \frac{P_{spec} R_{coil}}{3\pi F(x)\, a\, \rho \left(\frac{H}{I}\right)^2 (0.63)} \qquad (6.5.1\text{-}1)$$

(the factor 0.63 being required to use the equation for P_{spec} with cgs units except for P measured in watts). The sum of the total power consumed by the coil and specimen, $P_{coil} + P_{spec}$, was then calculated and, assuming efficiencies of power conversion as described in Section 5.3.11, this sum was multiplied by 2 to obtain the total maximum power required of such a free suspension system. The factor 2 assumes 50 percent for the combined efficiency of power amplifier

and power conditioning equipment. The 10 percent heating efficiency already discussed as the base measurement which was scaled for frequency and resistivity already included the transformer, tank circuit and transmission line losses. A product of RF generator and power conditioning efficiency of 50 percent will be conservative for low and intermediate frequencies where solid state devices can be used and operated directly from batteries. For the case of the smallest, highest resistivity specimens, which require the highest frequencies, vacuum tube amplifiers must be used so that 50 percent would not be conservative for the overall power amp/power conditioner. On the other hand, a 20 percent power margin was assumed and it is considered inappropriate in the present study to complicate the data given in this section by varying the assumed power amplifier and source efficiency with scaling.

P_{coil} was made subject to one restriction concerning its magnitude. As power is dissipated in the specimen a force acts upon it, the magnitude of which depends upon the displacement of the specimen from the center of the coil. In order to account for the need for the coil to supply a restraining force to the specimen it was assumed that a force of the form $F = ka^3$ is required which means $k = \frac{4}{3}\pi\sigma\alpha$, where σ is the density of the specimen and α is the acceleration of the specimen resulting from the application of the force. Assuming an acceleration of 1 cm sec^{-2} (10^{-3} g) and a density of 10 gm/cm^3, a value of 40 was selected for k. Thus

$$F = 40\, a^3 \qquad (6.5.1\text{-}2)$$

in which F is in dynes if a is in cm. This yields a force of 40 dynes for a specimen radius of 1 cm, which is considered adequate as discussed in Section 4.7.1. We shall henceforth drop the density variable in order to facilitate an

overview of facility capabilities. Acceleration minimums will thus be higher than 10^{-3} g for materials whose density is less than 10 gm cm^3. Provision of accelerations considerably above 10^{-3} g even for density 10 requires little additional power for most cases considered here. By combining equations 6.2-1 and 6.4-2, a value of minimum allowed P_{coil} required for positioning alone may be calculated.

$$P_{coil}(min) = \frac{160\, R_{coil}}{G(x)\, grad\left(\frac{H}{I}\right)^2} \qquad (6.5.1\text{-}3)$$

Whenever the value of P_{coil} calculated by equation (6.5.1-1) fell below $P_{coil}(min)$, the value used in obtaining the total power required by the system was $P_{coil}(min)$ in place of P_{coil} and with P_{spec} increased a proportionate amount. (They are proportional, one to the other, by equation 6.5.1-1.)

6.5.2 CALCULATION OF MAXIMUM RADII

The power radiated by a spherical surface is proportional to the square of its radius, hence P_{spec} is proportional to K^2. By application of the scaling relationships of section 6.4 to equation (6.5.1-1), P_{coil} is proportional to $\frac{P_{spec} R_{coil}}{a\left(\frac{H}{I}\right)^2}$ which is proportional to $\frac{K^2 K^{-1}}{K\, K^{-2}} = K^2$. Thus $(P_{coil} + P_{spec})$ and the total power required by the facility is proportional to K^2.

To calculate the radius of the largest meltable specimen at 5000 watts available peak power, the ratio of 5000 watts to the power required for a 2.5 cm dia. specimen was set equal to K^2 and a(max) calculated from 1.25 K cm. Higher peak powers of 10 and 20 kW were also assumed. Section 3 has indicated that peak powers are normally required for times not exceeding a few minutes, which makes consideration of battery furnished peak powers practical. Thus the data for Figure 6-1 and Table 6-1 were obtained.

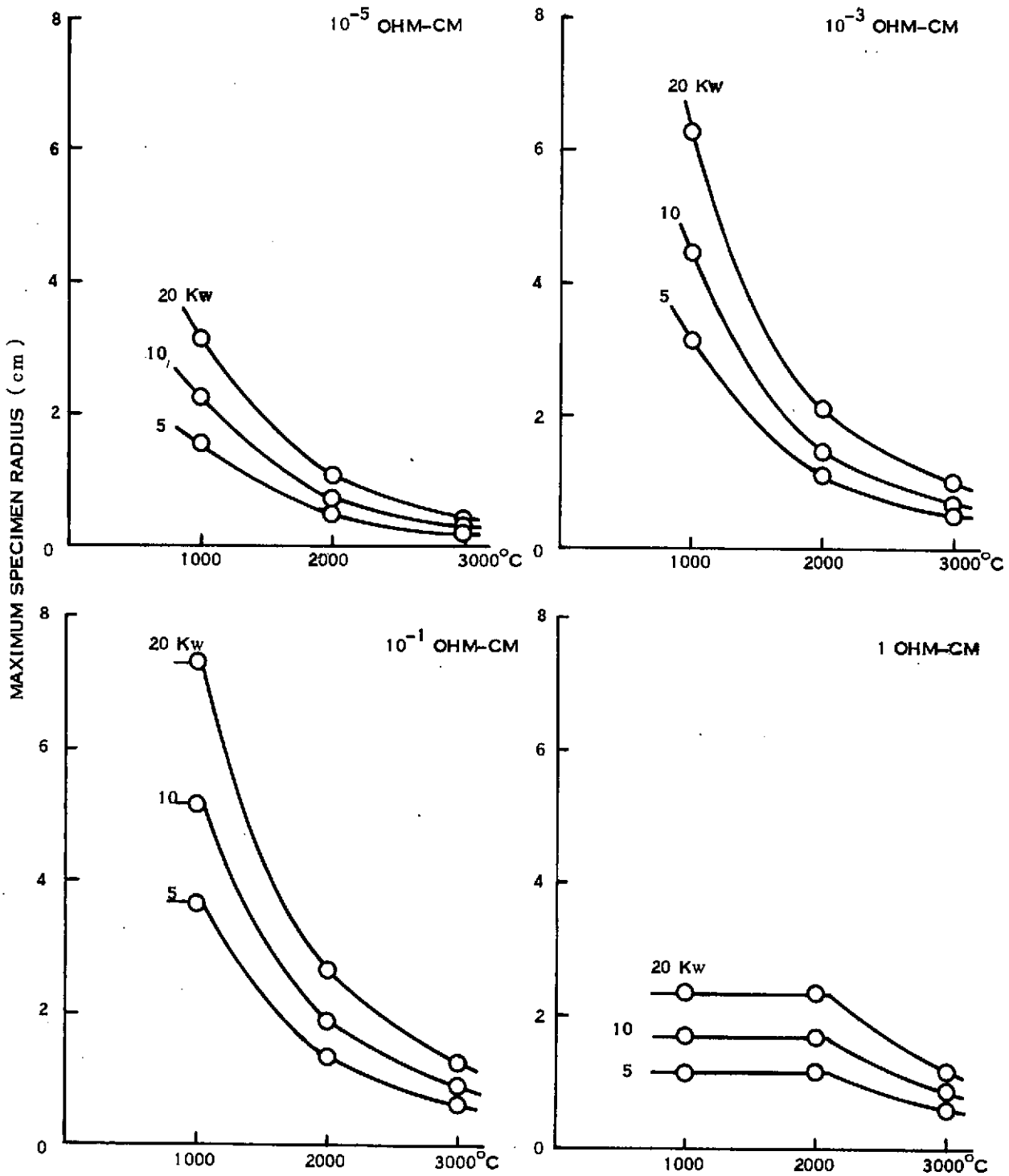

Figure 6-1. Maximum Radii of Specimens for Various Melting Temperatures and Assumed Total Facility Powers, RF Induction Heating

Table 6-1

Power Dissipation for Induction Heating

		1000°C			2000°C			3000°C		
Resistivity	Total Power Required	Maximum Radius (cm)	P_{coil} (watt)	P_{spec} (watt)	Maximum Radius (cm)	P_{coil} (watt)	P_{spec} (watt)	Maximum Radius (cm)	P_{coil} (watt)	P_{spec} (watt)
10^{-5} Ω-cm	5 Kw	1.6	2,100	400	0.5	2,100	400	0.3	2,100	400
	10	2.3	4,300	700	0.8	4,300	700	0.4	4,300	700
	20	3.2	8,500	1,500	1.1	8,500	1,500	0.5	8,500	1,500
10^{-3} Ω-cm	5 Kw	3.1	1,000	1,500	1.1	1,000	1,500	0.5	1,000	1,500
	10	4.4	2,100	2,900	1.5	2,100	2,900	0.7	2,100	2,900
	20	6.3	4,200	5,800	2.1	4,200	5,800	1.0	4,200	5,800
10^{-1} Ω-cm	5 Kw	3.6	200	2,300	1.3	200	2,300	0.6	200	2,300
	10	5.1	400	4,600	1.9	400	4,600	0.9	400	4,600
	20	7.3	800	9,200	2.7	800	9,200	1.3	800	9,200
1 Ω-cm	5 Kw	1.2	500	2,000	1.2	500	2,000	0.6	500	2,000
	10	1.6	900	4,100	1.6	900	4,100	0.8	900	4,100
	20	2.3	1,900	8,100	2.3	1,900	8,100	1.2	1,900	8,100

6.6 ELECTRON BEAM HEATING

6.6.1 LABORATORY BASE CASE

The sum of the power dissipated in the specimen by electromagnetic induction and the power conveyed to the specimen by an electron beam, i.e. $P_{spec} + P_{eb}$, was set equal to the power required to melt and superheat specimens with melting points of 1000, 2000 and 3000°C which was assumed, as in the preceding section, to be 1.2 times the power required to maintain the specimen (with emissivity of 0.8) at 1000, 2000 and 3000°C. During application of this power it was assumed that sufficient current was made to flow through the coil, that the force given by equation 6.5.1-2 was acting continuously. Thus $P_{coil} = P_{coil}(min)$ and the corresponding P_{spec} is given by equation 6.2-2 in the form

$$P_{spec} = 3\pi F(x)\, a\rho \left(\frac{H}{I}\right)^2 \frac{P_{coil}(min)}{R_{coil}}, \quad \text{(MKS)} \qquad (6.6.1\text{-}1)$$

6.6.2 CALCULATION OF MAXIMUM RADII

The power radiated by a spherical surface is proportional to the square of its radius, hence $P_{spec} + P_{eb}$ is proportional to K^2. From equation (6.6.1-1)

$P_{spec} \sim \frac{a\,(H/I)^2 P_{coil}(min)}{R_{coil}}$ which is proportional to $\frac{a\,(H/I)^2}{\text{grad}\,(H/I)^2}$ which is

$\frac{K\,K^{-2}}{K^{-3}} = K^2$. Thus, again the total power required of the system is proportional to K^2 and the maximum specimen radii, for induction heating, were calculated as indicated above. The results of these calculations are given in Figure 6-2 and Table 6-2.

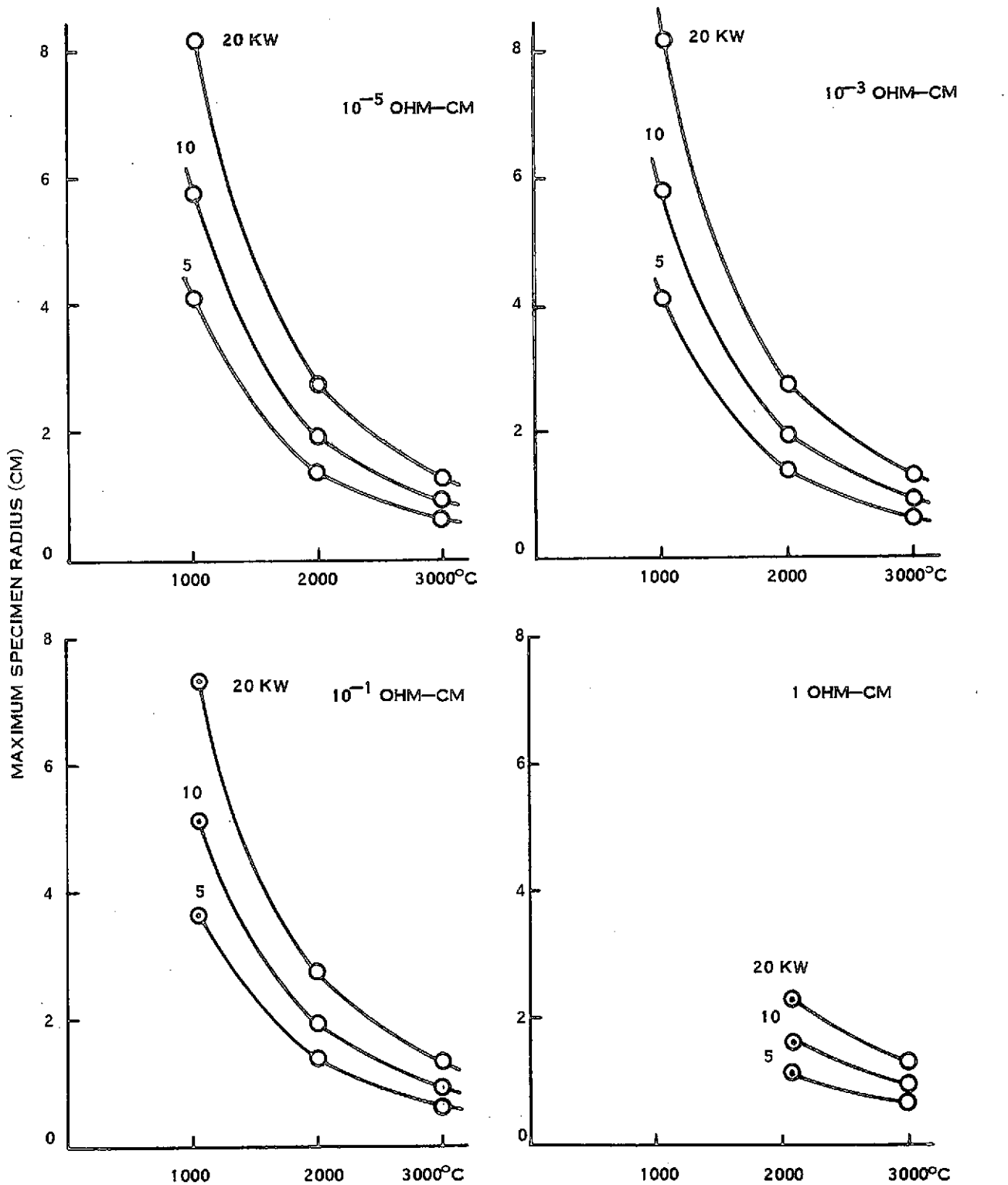

Figure 6-2. Maximum Radii of Specimens for Various Melting Temperatures and Assumed Total Facility Powers, Electron Beam Heating

Table 6-2

Power Dissipation for Electron Beam Heating

		1000°C				2000°C				3000°C			
Resistivity	Total Power Required	Max. Radius (cm)	P_{coil} (watt)	P_{spec} (watt)	P_{eb} (watt)	Max. Radius (cm)	P_{coil} (watt)	P_{spec} (watt)	P_{eb} (watt)	Max. Radius (cm)	P_{coil} (watt)	P_{spec} (watt)	P_{eb} (watt)
$10^{-5}\Omega$-cm	5 Kw	4.1	20	3	2,500	1.4	2	0.4	2,500	0.7	0.5	0.1	2,500
	10	5.8	40	7	5,000	2.0	5	0.8	5,000	0.9	1.0	0.2	5,000
	20	8.2	80	15	9,900	2.8	10	1.7	10,000	1.3	2.0	0.4	10,000
$10^{-3}\Omega$-cm	5 Kw	4.1	30	40	2,400	1.4	3	5	2,500	0.7	0.7	1.0	2,500
	10	5.6	60	80	4,900	2.0	7	10	5,000	0.9	1.5	2.0	5,000
	20	8.2	120	170	9,700	2.8	13	20	10,000	1.3	3.0	4.0	10,000
$10^{-1}\Omega$-cm	5 Kw					1.4	30	330	2,100	0.7	6	70	2,400
	10		*			1.9	50	660	4,300	0.9	12	150	4,800
	20					2.8	110	1,300	8,600	1.3	24	300	9,700
1 Ω-cm	5 Kw									0.6	140	600	1,800
	10		*				*			0.9	280	1,200	3,500
	20									1.3	560	2,400	7,000

*Maximum induction heating power exceeds power required to melt.

6.7 DISCUSSION OF RESULTS

Figures 6-1 and 6-2 should not be mistaken for a description of a continuum of possible specimen sizes, all obtainable with a single coil. It must be remembered that these figures were drawn for a specific, optimized ratio of specimen to coil size for specific optimized frequencies, and for a specific force for each size specimen and for a series of several different coil sizes as identified on the ordinate as a series of specimen sizes. One way Figures 6-1 and 6-2 are readily used is by selecting the size of specimen to be processed and then reading to the right to determine the maximum melting temperature that can be attained for the amount of power which is available.

In Figure 6-1, on the graph for 1 ohm-cm, it may be seen that each of the curves becomes horizontal at its left end. This indicates a region on the graph for which the available power results in insufficient force to meet the minimum force requirement for specimen sizes greater than those indicated by the horizontal line. For systems operating on such a horizontal line, the power dissipated in the specimen, as a result of meeting the minimum force requirement, is in excess of the quantity deemed necessary, in Section 4.1, to heat and melt specimens. If operation on a horizontal line is considered, it will necessitate operating the Containerless Processing Facility at full power only a fraction of the time such that the desired temperature is attained without severe superheating. In view of the considerations of accelerations to be encountered in a Space Laboratory, given in Section 4.7-1, the minimum acceleration requirements of 1 cm/sec^2 may be conservative with 0.1 cm/sec^2 perhaps more likely. If the required minimum acceleration were reduced, the horizontal lines in Figure 6-1 would rise to higher values of specimen radius.

In Figure 6-2, the regions described immediately above are left blank because the excess induction heating due to the minimum force requirement renders the electron beam unnecessary. The points, in Figure 6-2, at which the induction heating just equals the power radiated are marked by large dots inside the data points.

It should be noted that additional consideration must be given to the feasibility for processing the largest size specimens indicated in Figure 6-1. For specimen radii exceeding several centimeters, hydrodynamic stability of the molten mass whose integrity is maintained solely by surface tension forces must be considered. Elementary estimates by a method given in Ref. (6-1) indicate that positioning forces will lead to only moderate shape distortions for the largest sizes indicated in Figure 6-1. Another important physical consideration for these larger size specimens is heat transfer mechanisms within the specimen which will have a major effect upon the time required for melting and may indicate heating power margins other than the 20 percent assumed here to optimize the trade-off between facility peak power and duration of demand for peak power. It is expected that the distribution in depth of joule heating obtained with the higher resistivity specimens and stirring due to electromagnetic Lorentz forces will be important factors to be exploited.